ESAIM: M2AN 51 (2017) 2093–2126
DOI: 10.1051/m2an/2017022

ESAIM: Mathematical Modelling and Numerical Analysis
www.esaim-m2an.org

SEMI-DISCRETE ERROR ESTIMATES AND IMPLEMENTATION OF A MIXED METHOD FOR THE STEFAN PROBLEM *

Ch.B. Davis[1] and Sh.W. Walker[2]

Abstract. We analyze a dual formulation and finite element method for simulating the Stefan problem with surface tension (originally presented in [C.B. Davis and S.W. Walker, *Int. Free Bound.* **17** (2015) 427–464]). The method uses a mixed form of the heat equation in the solid and liquid (bulk) domains, and imposes a weak formulation of the interface motion law (on the solid-liquid interface) as a constraint. The computational method uses a conforming mesh approach to accurately capture the jump conditions across the interface. Preliminary error estimates are derived, under reduced regularity assumptions, for the difference between the time semi-discrete solution and the fully discrete solution over one time step. Moreover, details of the implementation are discussed including mesh generation issues. Several simulations of interface growth (in two dimensions) are presented to illustrate the method.

Mathematics Subject Classification. 65M60, 35K20.

Received July 29, 2016. Revised January 19, 2017. Accepted April 20, 2017.

1. Introduction

The Stefan problem describes a solidifying (or melting) interface and is a classic problem in phase transitions. It consists of time-dependent heat diffusion in the solid and liquid phases, with surface tension effects at the interface modeled by the Gibbs-Thomson relation with kinetic undercooling [44,45,61]. Derivation of the model can be found in [32]. Applications range from modeling the freezing (or melting) of water to the solidification of crystals from a melt and dendritic growth [17,33,39,53,54,60]. The mathematical theory of the Stefan problem can be found in [14,27,37,41,47–50] as well as for the related Mullins-Sekerka problem [20,23,26,42,51].

Many numerical schemes have been proposed to simulate the Stefan problem, such as phase-field methods [7,36,57] and level set methods [13,25,46,56]. The method we present uses a parametric approach where the interface parametrization conforms to a surrounding bulk mesh. Other parametric methods for the Stefan problem have also been given [2,5,35,36,52–55].

Our paper presents a mixed formulation of the Stefan problem, including the bulk heat equations [9], *i.e.* the problem is formulated in a saddle-point framework, where the heat equation is in mixed form, and the

Keywords and phrases. Stefan problem, mixed method, energy stability, error estimate; interface motion, semi-implicit scheme, re-meshing, conforming mesh.

* *This work was supported by the NSF under contract No. DMS-1418994.*

[1] Department of Mathematics, Tennessee Tech University, 1 William L Jones Dr, Cookeville, TN 38505, USA. cbdavis@tntech.edu

[2] Department of Mathematics, Louisiana State University, Baton Rouge, LA 70803-4918, USA. walker@math.lsu.edu

Article published by EDP Sciences

interface motion law appears as a constraint in the system of equations with a balancing Lagrange multiplier that represents the interface temperature. Our work recently appeared in [16], where we showed that our method satisfies an *a priori* energy bound for the time semi-discrete and fully discrete cases. It also satisfies a conservation law for the thermal energy.

In our method, the interface is represented by a surface triangulation that conforms to the bulk mesh and deforms with the interface. Thus, we must do occasional re-meshing with the method in [64]. We emphasize that we do *not* need to compute the intersection of meshes at adjacent time steps to transfer solution variables from one mesh to the next (*e.g.* for computing L^2 projections from one mesh to another). This is facilitated by a special ALE (Arbitrary-Lagrangian−Eulerian) mapping procedure (see Sect. 4.1.3).

The purpose of the current paper is to give more details on the implementation of the method in [16], as well as derive preliminary (semi-discrete) error estimates between the time semi-discrete and fully discrete solutions over one time step. We discuss the difficulties in obtaining a full error analysis at the beginning of Section 6. A noteworthy aspect of the error analysis is that the interface geometry does not have to be smooth and the solution variables may have *low regularity*.

In Section 2, we describe the governing equations. Section 3 gives basic background information. Section 4 describes our weak formulation for the time semi-discrete Stefan problem and explains how the interface motion is handled. We then do the same for the fully-discrete formulation (Sect. 5). Preliminary semi-discrete error estimates and regularity assumptions are described in Section 6. Details on the implementation of the method are given in Section 7 with numerical simulations in Section 8.

2. Model for the Stefan problem with surface tension

The particular mathematical model we consider can be found in [6, 16, 32]. In this section, we present the strong form of the Stefan problem in non-dimensional form.

2.1. Notation

Let Ω be a fixed domain in $\mathbb{R}^d$ (for $d = 2, 3$), with outer boundary $\partial\Omega$, that contains two phases, liquid (Ω_l) and solid (Ω_s), *i.e.* $\Omega = \mathrm{int}(\overline{\Omega_\mathrm{l}} \cup \overline{\Omega_\mathrm{s}})$ and $\Omega_\mathrm{l} \cap \Omega_\mathrm{s} = \emptyset$ (see Fig. 1). Furthermore, $\partial\Omega$ partitions as $\partial\Omega = \overline{\partial_\mathrm{D}\Omega} \cup \overline{\partial_\mathrm{N}\Omega}$ such that $\partial_\mathrm{D}\Omega \cap \partial_\mathrm{N}\Omega = \emptyset$ and $|\partial_\mathrm{D}\Omega| > 0$.

The solid-liquid interface is denoted $\Gamma = \overline{\Omega_\mathrm{l}} \cap \overline{\Omega_\mathrm{s}}$ (a closed surface). The domains Ω_l, Ω_s, and Γ are time-dependent, and we assume that $\Gamma(t) \subset \Omega$ for all t. For convenience in writing the strong form of the Stefan problem (Sect. 2.2), we assume $\Gamma(t)$ is smooth and let $\mathbf{X}(t)$ denote a parametrization of $\Gamma(t)$:

$$\mathbf{X}(\cdot, t) : \mathcal{M} \to \mathbb{R}^d, \quad \text{where } \mathcal{M} \subset \mathbb{R}^d \text{ is a given reference manifold,} \tag{2.1}$$

i.e. $\Gamma(t) = \mathbf{X}(\mathcal{M}, t)$. Furthermore, we introduce *fixed* reference domains $\widehat{\Omega}_\mathrm{l}$, $\widehat{\Omega}_\mathrm{s}$ for the liquid and solid domains such that $\Omega = \mathrm{int}(\overline{\widehat{\Omega}_\mathrm{l}} \cup \overline{\widehat{\Omega}_\mathrm{s}})$ and $\mathcal{M} = \overline{\widehat{\Omega}_\mathrm{l}} \cap \overline{\widehat{\Omega}_\mathrm{s}}$. We can extend $\mathbf{X}$ to all of Ω and such that $\Omega_\mathrm{l}(t) = \mathbf{X}(\widehat{\Omega}_\mathrm{l}, t)$ and $\Omega_\mathrm{s}(t) = \mathbf{X}(\widehat{\Omega}_\mathrm{s}, t)$. This is useful later when specifying the function spaces.

The surface Γ has a unit normal vector $\boldsymbol{\nu}$ that is assumed to point into Ω_l (see Fig. 1). For quantities q in Ω_l (Ω_s), we append a subscript: q_l (q_s). The symbol κ represents the *summed* curvature of the interface Γ (sum of the principle curvatures), and we assume the convention that κ is *positive* when Ω_s is convex.

Table 1 summarizes the notation we use for the physical domain and the physical variables (*e.g.* temperature, *etc.*). The non-dimensional parameters we use in the simulations are given in Table 2.

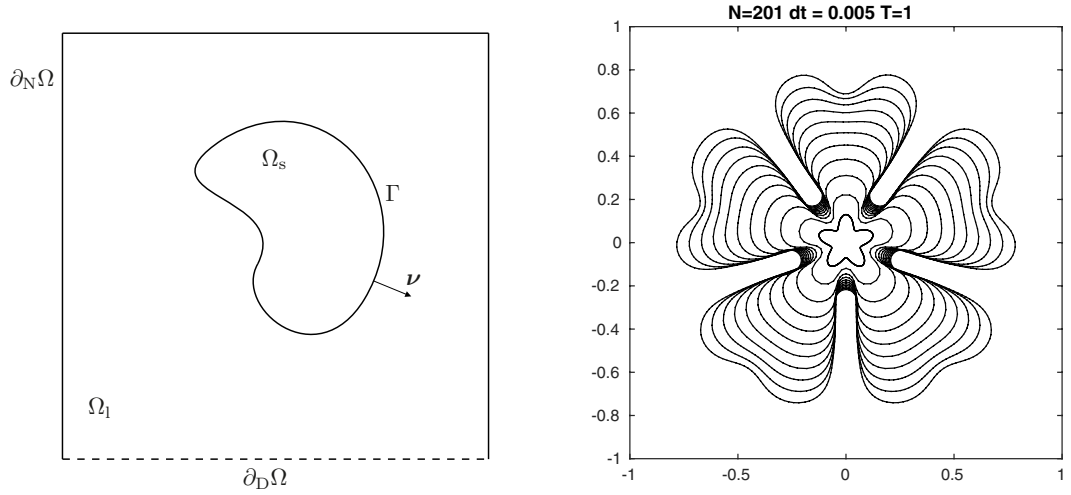

FIGURE 1. *Left*: Domains in the Stefan problem. The entire "box" is $\Omega = \mathrm{int}(\overline{\Omega_l} \cup \overline{\Omega_s})$ (containing two phases Ω_l, Ω_s) with Dirichlet boundary $\partial_D\Omega$ denoted by the dashed line. A Neumann condition is applied on the remaining sides $\partial_N\Omega$. The interface between the phases is $\Gamma = \overline{\Omega_l} \cap \overline{\Omega_s}$ with unit normal vector $\boldsymbol{\nu}$ pointing into Ω_l. *Right*: Simulation using the method developed in this paper (isotropic surface tension). Several time-lapses are shown to illustrate the evolution with initial interface having a "star" shape. See Section 8 for more simulations.

TABLE 1. General notation and symbols.

Symbol	Name	Units
Ω, Ω_l, Ω_s	Bulk Domains: Entire, Liquid, Solid	–
$\partial\Omega$	Boundary of Ω	–
$\partial_D\Omega$, $\partial_N\Omega$	Partition of $\partial\Omega = \overline{\partial_D\Omega} \cup \overline{\partial_N\Omega}$	–
Γ	Interface between Ω_l and Ω_s phases	–
$\mathbf{X}$, $\mathbf{V}$	Interface (Γ) Parametrization and Velocity	m, $\mathrm{m\,s^{-1}}$
u_l, u_s	Temperature in Ω_l and Ω_s	K (deg. Kelvin)
f_l, f_s	Heat sources in Ω_l and Ω_s	$\mathrm{J\,m^{-3}\,s^{-1}}$
∇_Γ, Δ_Γ	Surface Gradient and Laplace-Beltrami Operator	$\mathrm{m^{-1}}$, $\mathrm{m^{-2}}$
$\boldsymbol{\nu}$	Unit Normal Vector of Γ	–
$\nabla_\Gamma \mathbf{X} := \mathbf{I} - \boldsymbol{\nu} \otimes \boldsymbol{\nu}$	Projection onto Tangent Space of Γ	–
κ, $\kappa\boldsymbol{\nu} := -\Delta_\Gamma \mathbf{X}$	Summed Curvature and Curvature Vector of Γ	$\mathrm{m^{-1}}$

TABLE 2. Nondimensional parameters.

Symbol	Name	Value
$\widehat{S}$	Entropy coefficient	2
$\widehat{\beta}_0$	Mobility coefficient	0.01
$\widehat{\beta}$	Mobility function	–
$\widehat{K_l}$	Liquid conductivity	1
$\widehat{K_s}$	Solid conductivity	1
$\widehat{\alpha}$	Surface tension coefficient	0.0005

2.2. Non-dimensional strong form

The Stefan problem is as follows. Find $u : \Omega \times [0,T] \to \mathbb{R}$ and interface $\Gamma(t) \subset \Omega$ for all $t \in (0,T]$, such that $u|_{\Omega_\mathrm{l}} = u_\mathrm{l}$, $u|_{\Omega_\mathrm{s}} = u_\mathrm{s}$, and the following bulk conditions hold:

$$\begin{aligned} \partial_t u_\mathrm{l} - \widehat{K_\mathrm{l}} \Delta u_\mathrm{l} &= f_\mathrm{l}, && \text{in} && \Omega_\mathrm{l}(t), \\ \partial_t u_\mathrm{s} - \widehat{K_\mathrm{s}} \Delta u_\mathrm{s} &= f_\mathrm{s}, && \text{in} && \Omega_\mathrm{s}(t), \\ \boldsymbol{\nu}_\Omega \cdot \nabla u &= 0, && \text{on} && \partial_\mathrm{N}\Omega, \\ u &= u_\mathrm{D}, && \text{on} && \partial_\mathrm{D}\Omega, \\ u(\cdot,0) &= u_0, && \text{in} && \Omega, \end{aligned} \tag{2.2}$$

where u_0 is the initial temperature, and the following interface conditions hold:

$$\begin{aligned} u_\mathrm{l} - u_\mathrm{s} &= 0, \ \text{on } \Gamma(t), \\ \boldsymbol{\nu} \cdot (\widehat{K_\mathrm{l}} \nabla u_\mathrm{l} - \widehat{K_\mathrm{s}} \nabla u_\mathrm{s}) + \widehat{S}\, \partial_t \mathbf{X} \cdot \boldsymbol{\nu} &= 0, && \text{on} && \Gamma(t), \\ \frac{1}{\widehat{\beta}(\boldsymbol{\nu})} \partial_t \mathbf{X} \cdot \boldsymbol{\nu} + \widehat{\alpha}\kappa + \widehat{S}\, u &= 0, && \text{on} && \Gamma(t), \\ \mathbf{X}(\cdot,0) - \mathbf{X}_0(\cdot) &= \mathbf{0}, && \text{on} && \mathcal{M}, \\ \Gamma(0) &= \Gamma_0, && \text{in} && \Omega, \end{aligned} \tag{2.3}$$

where Γ_0 is the initial interface (parameterized by $\mathbf{X}_0$) and $\mathbf{X}(\cdot,t)$ parameterizes $\Gamma(t)$. Note that $u = T - T_\mathrm{M}$, where T is the temperature in degrees Kelvin and T_M is the melting temperature at the interface Γ, and that u is continuous across the interface. We assume throughout the paper that the non-dimensional coefficients satisfy

$$\infty > \widehat{K_\mathrm{l}}, \widehat{K_\mathrm{s}}, \widehat{\alpha}, \widehat{S} > 0, \quad \infty \geq \widehat{\beta}(\boldsymbol{\nu}) \geq \widehat{\beta}_- > 0, \quad \text{where } \widehat{\beta}_- \text{ is a constant.}$$

3. Preliminaries

3.1. Function spaces

Since the domain and interface deform in time, we define the function spaces using a reference domain [6]. For simplicity, we shall assume that $\partial\Omega \cap \partial\Omega_\mathrm{l} = \partial\Omega$ (see Fig. 1); thus, $\overline{\Omega_\mathrm{s}} \subset \Omega$. We use standard notation for denoting Sobolev spaces [1, 58], *e.g.* $L^2(\Omega)$ is the space of square integrable functions on Ω. For any vector-valued function $\boldsymbol{\eta}$, if we write $\boldsymbol{\eta} \in L^2(\Omega)$, we mean each component of $\boldsymbol{\eta}$ is in $L^2(\Omega)$. Continuing, we have $H^1(\Omega) = \{u \in L^2(\Omega) : \nabla u \in L^2(\Omega)\}$ and $H(\mathrm{div}, \Omega) = \{\boldsymbol{\eta} \in L^2(\Omega) : \nabla \cdot \boldsymbol{\eta} \in L^2(\Omega)\}$. The norms on these spaces are defined in the obvious way, *i.e.* $\|u\|^2_{L^2(\Omega)} = \int_\Omega |u|^2$, $\|u\|^2_{H^1(\Omega)} = \|u\|^2_{L^2(\Omega)} + \|\nabla u\|^2_{L^2(\Omega)}$, $\|\boldsymbol{\eta}\|^2_{H(\mathrm{div},\Omega)} = \|\boldsymbol{\eta}\|^2_{L^2(\Omega)} + \|\nabla \cdot \boldsymbol{\eta}\|^2_{L^2(\Omega)}$.

For a general function $f : \Omega \to \mathbb{R}$, we denote its *trace* (or restriction) to a sub-domain $\Sigma \subset \Omega$ (of co-dimension 1) by $f|_\Sigma$. The trace of a function in $H^1(\Omega)$ is well-defined; for a function in $L^2(\Omega)$, the trace is *not* well-defined. Moreover, the trace of all functions (on $\Sigma \subset \Omega$) in $H^1(\Omega)$ spans a Hilbert space, denoted $H^{1/2}(\Sigma)$, which is a proper dense subspace of $L^2(\Sigma)$. Referring to ([8], p. 48), the norm for $H^{1/2}(\partial\Omega)$ is defined by

$$\|v\|_{H^{1/2}(\partial\Omega)} := \inf_{\substack{w \in H^1(\Omega) \\ w|_{\partial\Omega} = v}} \|w\|_{H^1(\Omega)} = \|\bar{v}\|_{H^1(\Omega)}, \tag{3.1}$$

where $\bar{v}$ is the unique weak solution of $-\Delta\bar{v} + \bar{v} = 0$ in Ω, with $\bar{v} = v$ on $\partial\Omega$. We also have $H^{-1/2}(\partial\Omega)$, *i.e.* the dual space of $H^{1/2}(\partial\Omega)$ with the dual norm,

$$\|\varrho\|_{H^{-1/2}(\partial\Omega)} := \sup_{v \in H^{1/2}(\partial\Omega)} \frac{\langle \varrho, v \rangle_{\partial\Omega}}{\|v\|_{H^{1/2}(\partial\Omega)}}, \tag{3.2}$$

where $\langle \cdot, \cdot \rangle_{\partial\Omega}$ denotes the duality pairing between $H^{-1/2}(\partial\Omega)$ and $H^{1/2}(\partial\Omega)$.

It is well known ([28], Thm. 1.7, [8], Lem. 2.1.1) that $\boldsymbol{\eta}\cdot\boldsymbol{\nu}|_{\partial\Omega}$ is in $H^{-1/2}(\partial\Omega)$ for all $\boldsymbol{\eta}$ in $H(\mathrm{div},\Omega)$ ($\boldsymbol{\nu}_\Omega$ is the unit normal vector on $\partial\Omega$). In fact, by ([28], (1.44)), we have that

$$\|\boldsymbol{\eta}\cdot\boldsymbol{\nu}\|_{H^{-1/2}(\partial\Omega)} \le \|\boldsymbol{\eta}\|_{H(\mathrm{div},\Omega)}, \text{ for all } \boldsymbol{\eta}\in H(\mathrm{div},\Omega). \tag{3.3}$$

With this, one can show that $\|v\|_{H^{1/2}(\partial\Omega)}$ has a dual norm realization.

Proposition 3.1.

$$\|v\|_{H^{1/2}(\partial\Omega)} = \sup_{\boldsymbol{\eta}\in H(\mathrm{div},\Omega)} \frac{\langle \boldsymbol{\eta}\cdot\boldsymbol{\nu}, v\rangle_{\partial\Omega}}{\|\boldsymbol{\eta}\|_{H(\mathrm{div},\Omega)}}.$$

Enforcing boundary conditions requires the trace. To this end, let $H^1_{0,D}(\Omega) = \{u\in H^1(\Omega) : u|_{\partial_{\mathrm{D}}\Omega} = 0\}$. On the reference domains $\widehat{\Omega}_{\mathrm{l}}$ and $\widehat{\Omega}_{\mathrm{s}}$, we introduce:

$$\begin{aligned}
&\mathbb{V} = H(\mathrm{div},\Omega), \quad && \mathbb{V}(g) = \{\boldsymbol{\eta}\in\mathbb{V} : \langle \boldsymbol{\eta}\cdot\boldsymbol{\nu}_\Omega - g, q\rangle_{\partial\Omega} = 0,\ \forall q\in H^1_{0,D}(\Omega)\},\\
&\mathbb{V}_{\mathrm{l}} = H(\mathrm{div},\widehat{\Omega}_{\mathrm{l}}), \quad && \mathbb{V}_{\mathrm{l}}(g) = \{\boldsymbol{\eta}\in\mathbb{V}_{\mathrm{l}} : \langle \boldsymbol{\eta}\cdot\boldsymbol{\nu}_\Omega - g, q\rangle_{\partial\Omega} = 0,\ \forall q\in H^1_{0,D}(\Omega)\},\\
&\mathbb{V}_{\mathrm{s}} = H(\mathrm{div},\widehat{\Omega}_{\mathrm{s}}),
\end{aligned} \tag{3.4}$$

where g is in $H^{-1/2}(\partial\Omega)$ (see [8], Rem. 2.1.3). We also have the spaces

$$\mathbb{Q} = L^2(\Omega), \quad \mathbb{Q}_{\mathrm{l}} = L^2(\widehat{\Omega}_{\mathrm{l}}), \quad \mathbb{Q}_{\mathrm{s}} = L^2(\widehat{\Omega}_{\mathrm{s}}). \tag{3.5}$$

On the reference manifold $\mathcal{M}$, we define [1]

$$\mathbb{M} = H^{1/2}(\mathcal{M},\mathbb{R}), \qquad \mathbb{Y} = H^1(\mathcal{M},\mathbb{R}^d), \tag{3.6}$$

The norm for $\mathbb{Y}$ is $\|\mathbf{V}\|^2_{H^1(\Gamma)} = \int_\Gamma |\mathbf{V}|^2 + \int_\Gamma |\nabla_\Gamma \mathbf{V}|^2$ (see Sect. 3.2 for ∇_Γ).

We use the following abuse of notation, similar to [6]. We identify functions $\boldsymbol{\eta}_{\mathrm{l}}$ in $\mathbb{V}_{\mathrm{l}}$ with $\boldsymbol{\eta}_{\mathrm{l}}\circ\mathbf{X}^{-1}$ defined on $\Omega_{\mathrm{l}}(t)$ (recall $\Omega_{\mathrm{l}}(t) = \mathbf{X}(\widehat{\Omega}_{\mathrm{l}},t)$), and denote both functions simply as $\boldsymbol{\eta}_{\mathrm{l}}$; similar considerations are made for functions $\boldsymbol{\eta}_{\mathrm{s}}$ in $\mathbb{V}_{\mathrm{s}}$. Likewise, we identify $\mathbf{V}$ in $\mathbb{Y}$ with $\mathbf{V}\circ\mathbf{X}^{-1}$ defined on $\Gamma(t)$, and denote both functions as $\mathbf{V}$; similar considerations are made for functions μ in $\mathbb{M}$. Along these lines, we have $\mathbb{V}_{\mathrm{l}} \simeq H(\mathrm{div},\Omega_{\mathrm{l}})$, $\mathbb{V}_{\mathrm{s}} \simeq H(\mathrm{div},\Omega_{\mathrm{s}})$, $\mathbb{Q}_{\mathrm{l}} \simeq L^2(\Omega_{\mathrm{l}})$, $\mathbb{Q}_{\mathrm{s}} \simeq L^2(\Omega_{\mathrm{s}})$, $\mathbb{M} \simeq H^{1/2}(\Gamma)$, $\mathbb{Y} \simeq H^1(\Gamma)$, provided the mapping $\mathbf{X}$ is not degenerate.

For technical reasons, we need two versions of the $H^{1/2}(\Gamma)$ norm related to Ω_{l} and Ω_{s}. Define

$$\|v\|_{H^{1/2}_{\mathrm{l}}(\Gamma)} := \sup_{\boldsymbol{\eta}_{\mathrm{l}}\in\mathbb{V}_{\mathrm{l}}(0)} \frac{\langle \boldsymbol{\eta}_{\mathrm{l}}\cdot\boldsymbol{\nu}, v\rangle_\Gamma}{\|\boldsymbol{\eta}_{\mathrm{l}}\|_{H(\mathrm{div},\Omega_{\mathrm{l}})}}, \quad \|v\|_{H^{1/2}_{\mathrm{s}}(\Gamma)} := \sup_{\boldsymbol{\eta}_{\mathrm{s}}\in\mathbb{V}_{\mathrm{s}}} \frac{\langle \boldsymbol{\eta}_{\mathrm{s}}\cdot\boldsymbol{\nu}, v\rangle_\Gamma}{\|\boldsymbol{\eta}_{\mathrm{s}}\|_{H(\mathrm{div},\Omega_{\mathrm{s}})}} \tag{3.7}$$

Basically, these norms are related to the "side" of Γ on which we take the trace. We also define the $H^{1/2}$ and $H^{-1/2}$ norm on Γ by

$$\|v\|_{H^{1/2}(\Gamma)} := \frac{1}{2}\left(\|v\|_{H^{1/2}_{\mathrm{l}}(\Gamma)} + \|v\|_{H^{1/2}_{\mathrm{s}}(\Gamma)}\right), \qquad \|\varrho\|_{H^{-1/2}(\Gamma)} := \sup_{v\in H^{1/2}(\Gamma)} \frac{\langle \varrho, v\rangle_\Gamma}{\|v\|_{H^{1/2}(\Gamma)}}, \tag{3.8}$$

To conclude this section, we define the dual norm for $H^{-1}(\Gamma)$:

$$\|\varrho\|_{H^{-1}(\Gamma)} := \sup_{v\in H^1(\Gamma)} \frac{\langle \varrho, v\rangle_\Gamma}{\|v\|_{H^1(\Gamma)}}, \tag{3.9}$$

where $\langle \varrho, v\rangle_\Gamma$ is understood to be the duality pairing between $H^{-1}(\Gamma)$ and $H^1(\Gamma)$.

3.2. Curvature

We review some differential geometry and surface derivatives [19,38,65]. Given a function $\omega : \Gamma \to \mathbb{R}$, defined on a smooth surface Γ, we can *extend* it to a tubular neighborhood [18,65] that contains Γ and define the tangential gradient (or surface gradient) as $\nabla_\Gamma \omega = \nabla\omega - [(\boldsymbol{\nu}\cdot\nabla)\omega]\boldsymbol{\nu}$. Given $\mathbf{Y} : \Gamma \to \mathbb{R}^3$, we have $\nabla_\Gamma \mathbf{Y} = (\nabla_\Gamma Y_1, \nabla_\Gamma Y_2, \nabla_\Gamma Y_3)$ (a 3×3 matrix). Moreover, we have the tangential divergence $\nabla_\Gamma \cdot \mathbf{Y} := \text{trace}(\nabla_\Gamma \mathbf{Y})$ and the Laplace-Beltrami operator: $\Delta_\Gamma \omega = \nabla_\Gamma \cdot \nabla_\Gamma \omega$.

When Γ is a one-dimensional curve with oriented unit tangent vector $\boldsymbol{\tau}$, we have $\nabla_\Gamma \equiv \boldsymbol{\tau}\partial_s$ and $\Delta_\Gamma \equiv \partial_s^2$, where ∂_s is the derivative with respect to arc-length. Therefore, taking $\mathbf{X}(\cdot,t)$ to be a local parameterization of $\Gamma(t)$, the vector curvature $\kappa\boldsymbol{\nu}$ of $\Gamma(t)$ [19,38,65] is given by $-\Delta_\Gamma \mathbf{X} = \kappa\boldsymbol{\nu}$, where κ is the sum of the principle curvatures.

In the rest of the paper, we take advantage of a weak formulation of the vector curvature [3,21,24,67]. If Γ is a closed C^2 manifold, then the following integration by parts relation is true:

$$\int_\Gamma \kappa\boldsymbol{\nu}\cdot\mathbf{Y} = \int_\Gamma \nabla_\Gamma \mathbf{X} : \nabla_\Gamma \mathbf{Y}, \quad \text{for all } \mathbf{Y} \text{ in } \mathbb{Y}, \tag{3.10}$$

where $\nabla_\Gamma \mathbf{X}$ is a symmetric matrix that represents the projection operator onto the tangent space of Γ, *i.e.* $\nabla_\Gamma \mathbf{X} = \mathbf{I} - \boldsymbol{\nu}\otimes\boldsymbol{\nu}$. We use (3.10) in order to write the curvature term appearing in (2.3) in the weak form (4.6).

4. Time Semi-Discrete formulation

We now partition the time interval $(0,T)$ into subintervals of size Δt. We use a superscript i to denote a time dependent quantity at time t_i. Furthermore, let $(\cdot,\cdot)_\Sigma$ denote the L^2 inner product on the generic domain Σ. For a general domain Σ, let $\langle\cdot,\cdot\rangle_\Sigma$ denote the duality pairing on Σ between $H^{-1/2}(\Sigma)$ and $H^{1/2}(\Sigma)$ or between $H^{-1}(\Sigma)$ and $H^1(\Sigma)$ (the context will make it clear).

4.1. Domain velocity

4.1.1. Map Γ^i to Γ^{i+1}

We introduce the interface velocity $\mathbf{V} := \partial_t \mathbf{X}$ as a new variable. Thus, we approximate the interface position at time t_{i+1} by a backward Euler scheme:

$$\mathbf{X}^{i+1} = \mathbf{X}^i + \Delta t\, \mathbf{V}^{i+1}, \quad \text{where } \mathbf{V}^{i+1} : \Gamma^i \to \mathbb{R}^3. \tag{4.1}$$

Thus, knowing $\mathbf{V}^{i+1}$ and $\mathbf{X}^i$ we can update the parametrization of the interface and obtain the interface Γ^{i+1} at t_{i+1}. Note that $\mathbf{X}^i(\cdot) \equiv \text{id}_{\Gamma^i}(\cdot)$ (the identity map) on Γ^i.

Remark 4.1. We shall assume throughout this paper that $\mathbf{V}^{i+1}$ (for all i) is at least in $W^{1,\infty}(\Gamma^i)$ in order for the update (4.1) to make sense.

4.1.2. Map Ω_1^i, Ω_s^i to Ω_1^{i+1}, Ω_s^{i+1}

Clearly, the bulk domains Ω_1, Ω_s follow the interface Γ. Given $\mathbf{V}^{i+1}$ on Γ^i, it can be extended to the entire domain Ω by a harmonic extension [24,67], *i.e.* if $\mathbf{V}_E^{i+1}$ denotes the extension, then

$$\mathbf{V}_E^{i+1} \in H^1(\Omega): \quad -\Delta \mathbf{V}_E^{i+1} = \mathbf{0}, \text{ in } \Omega_1^i \cup \Omega_s^i, \quad \mathbf{V}_E^{i+1} = \mathbf{V}^{i+1}, \quad \text{on} \quad \Gamma^i, \quad \mathbf{V}_E^{i+1} = \mathbf{0}, \quad \text{on} \quad \partial\Omega, \tag{4.2}$$

In the following, we drop the E subscript and use $\mathbf{V}^{i+1}$ to denote the extension. This induces a map $\Phi_{i+1} : \Omega^i \to \Omega^{i+1}$ for "updating" the domain:

$$\Phi_{i+1}(\mathbf{x}) = \text{id}_{\Omega^i}(\mathbf{x}) + \Delta t \mathbf{V}^{i+1}(\mathbf{x}), \quad \text{for all } \mathbf{x} \in \Omega^i. \tag{4.3}$$

See [30,31] for similar constructions in an ALE (Arbitrary-Lagrangian−Eulerian) context.

Note that Φ_{i+1} is defined over both Ω_{l}^i and Ω_{s}^i, and $\Omega_{\mathrm{l}}^{i+1} := \Phi_{i+1}(\Omega_{\mathrm{l}}^i)$, $\Omega_{\mathrm{s}}^{i+1} := \Phi_{i+1}(\Omega_{\mathrm{s}}^i)$ conform to Γ^{i+1}. Similarly as for (4.1), we assume $\mathbf{V}^{i+1}$ (on Ω^i) is at least in $W^{1,\infty}(\Omega^i)$. Furthermore, we assume Φ_{i+1} is a bijective map and $\det([\nabla_{\mathbf{x}}\Phi_{i+1}(\mathbf{x})]) > 0$. We note the following properties satisfied by Φ_{i+1} [34,59].

- If $\mathbf{y} = \Phi_{i+1}(\mathbf{x})$, then $(\nabla_{\mathbf{y}}\Phi_{i+1}^{-1} \circ \Phi_{i+1})(\mathbf{x}) = [\nabla_{\mathbf{x}}\Phi_{i+1}(\mathbf{x})]^{-1}$.
- If $f : \Omega^{i+1} \to \mathbb{R}$, then $\int_{\Omega^{i+1}} f(\mathbf{y})\, d\mathbf{y} = \int_{\Omega^i} f(\Phi_{i+1}(\mathbf{x})) \det([\nabla_{\mathbf{x}}\Phi_{i+1}(\mathbf{x})])\, \mathrm{d}\mathbf{x}$.

We use the map Φ_{i+1} to transform the functions u_{l}^{i+1}, u_{s}^{i+1} on Ω^i to new functions on Ω^{i+1} in order to advance the solution to the next time step (see (4.7)).

Remark 4.2 (Time step restriction)**.** In order for (4.3) to remain bijective, Δt cannot be too large. In fact, it depends on $\|\nabla \mathbf{V}^{i+1}\|_{L^\infty(\Omega)}$ because $\det(\nabla \Phi_{i+1})$ depends on $\nabla \mathbf{V}^{i+1}$.

4.1.3. Time derivative: Eulerian vs. Lagrangian

Similar to (4.1), we use a backward Euler method to discretize the temperature time derivatives at each time step:

$$(\partial_t u_{\mathrm{l}})^{i+1} \approx \frac{u_{\mathrm{l}}^{i+1} - u_{\mathrm{l}}^i}{\Delta t}, \quad (\partial_t u_{\mathrm{s}})^{i+1} \approx \frac{u_{\mathrm{s}}^{i+1} - u_{\mathrm{s}}^i}{\Delta t}.$$

But, because the domain is changing, u_j^{i+1}, u_j^i ($j = \mathrm{l}, \mathrm{s}$) are defined on different domains (Ω_j^i, Ω_j^{i-1}, respectively; see next section). This means u_j^i must be *transferred* to the new domain in order to compute the (discrete) Eulerian time derivative. The transference can be accomplished by an L^2 projection, for instance, but is not so convenient for a numerical method.

Therefore, we make use of the material derivative [59]. Using the standard formula $\dot{u}_j = \partial_t u_j + \mathbf{V} \cdot \nabla u_j$, and introducing the flux variables $\boldsymbol{\sigma}_{\mathrm{l}} := -\widehat{K_{\mathrm{l}}} \nabla u_{\mathrm{l}}$, $\boldsymbol{\sigma}_{\mathrm{s}} := -\widehat{K_{\mathrm{s}}} \nabla u_{\mathrm{s}}$, we have $\dot{u}_j = \partial_t u_j - \widehat{K_{\mathrm{l}}}^{-1} \mathbf{V} \cdot \boldsymbol{\sigma}_j$ for $j = \mathrm{l}, \mathrm{s}$. Thus, we adopt the following discretization of $\partial_t u_{\mathrm{l}}$ and $\partial_t u_{\mathrm{s}}$:

$$(\partial_t u_j)^{i+1} \approx \frac{u_j^{i+1} - u_j^i \circ \Phi_i^{-1}}{\Delta t} + \frac{1}{\widehat{K_j}} \left(\boldsymbol{\sigma}_j^i \cdot \mathbf{V}^i\right) \circ \Phi_i^{-1}, \text{ for } j = \mathrm{l}, \mathrm{s}. \tag{4.4}$$

Note that we have treated the convective term explicitly, and (formally) taking $\Delta t \to 0$ recovers the standard material derivative formula. The advantage here is that computing $u_j^i \circ \Phi_i^{-1}$ and $\left(\boldsymbol{\sigma}_j^i \cdot \mathbf{V}^i\right) \circ \Phi_i^{-1}$ ($j = \mathrm{l}, \mathrm{s}$), in the fully discrete method, is straightforward (see (5.3) and the discussion in Sect. 5.1.1).

4.2. Weak formulation

We give the time semi-discrete weak formulation of (2.2), (2.3) which was originally presented in our previous work [16]. Let $u_{\mathrm{D}}(\cdot, t)$ in $H^1_{0,N}(\Omega) = \{u \in H^1(\Omega) : u|_{\partial_{\mathrm{N}}\Omega} = 0\}$. Next, suppose the input data $f_{\mathrm{l}}(\cdot, t)$, $f_{\mathrm{s}}(\cdot, t)$ in $H^1(\Omega)$, and initial data $\mathbf{X}(\cdot, 0) = \mathbf{X}_0$, $u_{\mathrm{s}}(\cdot, 0) = u_{\mathrm{s},0}$, $u_{\mathrm{l}}(\cdot, 0) = u_{\mathrm{l},0}$.

The derivation of (4.5), (4.6) follows by using the flux variables and multiplying by a test function and integrating by parts on the current domain Ω^i, Γ^i, *i.e.* all L^2 inner products and duality pairings are written on the current domain. However, the solution variables are posed at the next time step t_{i+1} (*i.e.* a semi-implicit method). Moreover, we apply (4.1) and (4.4) and set $u_{\mathrm{D}}^{i+1} = u_{\mathrm{D}}(\cdot, t_{i+1})$, $f_{\mathrm{l}}^{i+1} = f_{\mathrm{l}}(\cdot, t_{i+1})$, and $f_{\mathrm{s}}^{i+1} = f_{\mathrm{s}}(\cdot, t_{i+1})$ (the details can be found in [16]). Thus, we arrive at the following. At time t_i, find $\boldsymbol{\sigma}_{\mathrm{l}}^{i+1}$ in $\mathbb{V}_{\mathrm{l}}^i(0)$, $\boldsymbol{\sigma}_{\mathrm{s}}^{i+1}$ in $\mathbb{V}_{\mathrm{s}}^i$, $\mathbf{V}^{i+1}$ in $\mathbb{Y}^i$, u_{l}^{i+1} in $\mathbb{Q}_{\mathrm{l}}^i$, u_{s}^{i+1} in $\mathbb{Q}_{\mathrm{s}}^i$, λ^{i+1} in $\mathbb{M}^i$ such that

$$\begin{aligned}
&\frac{1}{\widehat{K_{\mathrm{l}}}}(\boldsymbol{\sigma}_{\mathrm{l}}^{i+1}, \boldsymbol{\eta}_{\mathrm{l}})_{\Omega_{\mathrm{l}}^i} - (u_{\mathrm{l}}^{i+1}, \nabla \cdot \boldsymbol{\eta}_{\mathrm{l}})_{\Omega_{\mathrm{l}}^i} - \langle \boldsymbol{\eta}_{\mathrm{l}} \cdot \boldsymbol{\nu}^i, \lambda^{i+1} \rangle_{\Gamma^i} = -\langle \boldsymbol{\eta}_{\mathrm{l}} \cdot \boldsymbol{\nu}_\Omega, u_{\mathrm{D}}^{i+1} \rangle_{\partial\Omega}, \quad \text{for all} \quad \boldsymbol{\eta}_{\mathrm{l}} \in \mathbb{V}_{\mathrm{l}}^i(0), \\
&-(\nabla \cdot \boldsymbol{\sigma}_{\mathrm{l}}^{i+1}, q_{\mathrm{l}})_{\Omega_{\mathrm{l}}^i} - \frac{1}{\Delta t}(u_{\mathrm{l}}^{i+1}, q_{\mathrm{l}})_{\Omega_{\mathrm{l}}^i} + \frac{1}{\Delta t}(\overline{u_{\mathrm{l}}}^i, q_{\mathrm{l}})_{\Omega_{\mathrm{l}}^i} = -(f_{\mathrm{l}}^{i+1}, q_{\mathrm{l}})_{\Omega_{\mathrm{l}}^i}, \quad \text{for all} \quad q_{\mathrm{l}} \in \mathbb{Q}_{\mathrm{l}}^i, \\
&\frac{1}{\widehat{K_{\mathrm{s}}}}(\boldsymbol{\sigma}_{\mathrm{s}}^{i+1}, \boldsymbol{\eta}_{\mathrm{s}})_{\Omega_{\mathrm{s}}^i} - (u_{\mathrm{s}}^{i+1}, \nabla \cdot \boldsymbol{\eta}_{\mathrm{s}})_{\Omega_{\mathrm{s}}^i} + \langle \boldsymbol{\eta}_{\mathrm{s}} \cdot \boldsymbol{\nu}^i, \lambda^{i+1} \rangle_{\Gamma^i} = 0, \quad \text{for all} \quad \boldsymbol{\eta}_{\mathrm{s}} \in \mathbb{V}_{\mathrm{s}}^i, \\
&-(\nabla \cdot \boldsymbol{\sigma}_{\mathrm{s}}^{i+1}, q_{\mathrm{s}})_{\Omega_{\mathrm{s}}^i} - \frac{1}{\Delta t}(u_{\mathrm{s}}^{i+1}, q_{\mathrm{s}})_{\Omega_{\mathrm{s}}^i} + \frac{1}{\Delta t}(\overline{u_{\mathrm{s}}}^i, q_{\mathrm{s}})_{\Omega_{\mathrm{s}}^i} = -(f_{\mathrm{s}}^{i+1}, q_{\mathrm{s}})_{\Omega_{\mathrm{s}}^i}, \quad \text{for all} \quad q_{\mathrm{s}} \in \mathbb{Q}_{\mathrm{s}}^i,
\end{aligned} \tag{4.5}$$

$$(\widehat{\beta}^{-1}(\boldsymbol{\nu}^i)\mathbf{V}^{i+1}\cdot\boldsymbol{\nu}^i, \mathbf{Y}\cdot\boldsymbol{\nu}^i)_{\Gamma^i} + \Delta t\widehat{\alpha}(\nabla_{\Gamma^i}\mathbf{V}^{i+1}, \nabla_{\Gamma^i}\mathbf{Y})_{\Gamma^i} + \widehat{S}(\mathbf{Y}\cdot\boldsymbol{\nu}^i, \lambda^{i+1})_{\Gamma^i} = -\widehat{\alpha}(\nabla_{\Gamma^i}\mathbf{X}^i, \nabla_{\Gamma^i}\mathbf{Y})_{\Gamma^i}, \quad \text{for all} \quad \mathbf{Y}\in\mathbb{Y}^i,$$
$$\widehat{S}(\mathbf{V}^{i+1}\cdot\boldsymbol{\nu}^i, \mu)_{\Gamma^i} - \langle\boldsymbol{\sigma}_{\mathrm{l}}^{i+1}\cdot\boldsymbol{\nu}^i, \mu\rangle_{\Gamma^i} + \langle\boldsymbol{\sigma}_{\mathrm{s}}^{i+1}\cdot\boldsymbol{\nu}^i, \mu\rangle_{\Gamma^i} = 0, \quad \text{for all} \quad \mu\in\mathbb{M}^i, \tag{4.6}$$

where the function spaces are defined over the current (known) domain Ω^i, Γ^i. Then we use (4.1) to obtain the new interface position, which induces a map $\Phi_{i+1}:\Omega^i\to\Omega^{i+1}$. Because of (4.4), the temperature from the previous time index, $u_j^i:\Omega_j^{i-1}\to\mathbb{R}$, is mapped onto Ω_j^i by

$$\overline{u_j}^i := u_j^i\circ\Phi_i^{-1} - \Delta t\frac{1}{\widehat{K}_j}\left(\boldsymbol{\sigma}_j^i\cdot\mathbf{V}^i\right)\circ\Phi_i^{-1}, \text{ for } j=\mathrm{l},\mathrm{s}. \tag{4.7}$$

Iterating this procedure gives a time semi-discrete approximation of (2.2), (2.3).

Remark 4.3 (How to start the method)**.** From (4.7), it is clear we need $\mathbf{V}^0$ to compute $\overline{u_{\mathrm{l}}}^0$, $\overline{u_{\mathrm{s}}}^0$. However, we start solving (4.5), (4.6) at $i=0$, which only gives $\mathbf{V}^1$. Hence, we must do one of the following. (i) specify $\mathbf{V}^0$, $\boldsymbol{\sigma}_{\mathrm{l}}^0$, $\boldsymbol{\sigma}_{\mathrm{s}}^0$; (ii) set $\mathbf{V}^0=\boldsymbol{\sigma}_{\mathrm{l}}^0=\boldsymbol{\sigma}_{\mathrm{s}}^0=\mathbf{0}$ (*i.e.* choose $\overline{u_{\mathrm{l}}}^0$, $\overline{u_{\mathrm{s}}}^0$ directly); (iii) or apply (ii) with a small time step to obtain an approximation of $\mathbf{V}^0$, $\boldsymbol{\sigma}_{\mathrm{l}}^0$, $\boldsymbol{\sigma}_{\mathrm{s}}^0$.

4.3. Abstract formulation

In order to simplify notation, we shall drop the time index notation and remember that we are solving for all variables on the current known domain $\Omega\equiv\Omega^i$, $\Gamma\equiv\Gamma^i$ with the current known normal vector $\boldsymbol{\nu}\equiv\boldsymbol{\nu}^i$. In particular, we take

$$\boldsymbol{\sigma}_{\mathrm{l}}^{i+1}\equiv\boldsymbol{\sigma}_{\mathrm{l}},\quad \boldsymbol{\sigma}_{\mathrm{s}}^{i+1}\equiv\boldsymbol{\sigma}_{\mathrm{s}},\quad \mathbf{V}^{i+1}\equiv\mathbf{V},\quad u_{\mathrm{l}}^{i+1}\equiv u_{\mathrm{l}},\quad u_{\mathrm{s}}^{i+1}\equiv u_{\mathrm{s}},\quad \lambda^{i+1}\equiv\lambda,$$
$$f_{\mathrm{l}}^{i+1}\equiv f_{\mathrm{l}},\quad f_{\mathrm{s}}^{i+1}\equiv f_{\mathrm{s}},\quad u_{\mathrm{D}}^{i+1}\equiv u_{\mathrm{D}},\quad \overline{u_{\mathrm{l}}}^i\equiv\overline{u_{\mathrm{l}}},\quad \overline{u_{\mathrm{s}}}^i\equiv\overline{u_{\mathrm{s}}},\quad \mathbf{X}^i\equiv\overline{\mathbf{X}},\quad \nabla_{\Gamma^i}\equiv\nabla_\Gamma.$$

4.3.1. Bilinear and Linear forms

The bilinear forms are defined as follows:

$$a((\boldsymbol{\eta}_{\mathrm{l}},\boldsymbol{\eta}_{\mathrm{s}},\mathbf{Y}),(\boldsymbol{\sigma}_{\mathrm{l}},\boldsymbol{\sigma}_{\mathrm{s}},\mathbf{V})) = \frac{1}{\widehat{K}_{\mathrm{l}}}(\boldsymbol{\eta}_{\mathrm{l}},\boldsymbol{\sigma}_{\mathrm{l}})_{\Omega_{\mathrm{l}}} + \frac{1}{\widehat{K}_{\mathrm{s}}}(\boldsymbol{\eta}_{\mathrm{s}},\boldsymbol{\sigma}_{\mathrm{s}})_{\Omega_{\mathrm{s}}} + (\widehat{\beta}^{-1}(\boldsymbol{\nu})\mathbf{Y}\cdot\boldsymbol{\nu},\mathbf{V}\cdot\boldsymbol{\nu})_\Gamma + \Delta t\widehat{\alpha}(\nabla_\Gamma\mathbf{Y},\nabla_\Gamma\mathbf{V})_\Gamma, \tag{4.8}$$

$$b((\boldsymbol{\eta}_{\mathrm{l}},\boldsymbol{\eta}_{\mathrm{s}},\mathbf{Y}),(q_{\mathrm{l}},q_{\mathrm{s}},\mu)) = -(\nabla\cdot\boldsymbol{\eta}_{\mathrm{l}},q_{\mathrm{l}})_{\Omega_{\mathrm{l}}} - (\nabla\cdot\boldsymbol{\eta}_{\mathrm{s}},q_{\mathrm{s}})_{\Omega_{\mathrm{s}}} - \langle\boldsymbol{\eta}_{\mathrm{l}}\cdot\boldsymbol{\nu},\mu\rangle_\Gamma + \langle\boldsymbol{\eta}_{\mathrm{s}}\cdot\boldsymbol{\nu},\mu\rangle_\Gamma + \widehat{S}\,(\mathbf{Y}\cdot\boldsymbol{\nu},\mu)_\Gamma, \tag{4.9}$$

$$c((q_{\mathrm{l}},q_{\mathrm{s}},\mu),(u_{\mathrm{l}},u_{\mathrm{s}},\lambda)) = \frac{1}{\Delta t}(q_{\mathrm{l}},u_{\mathrm{l}})_{\Omega_{\mathrm{l}}} + \frac{1}{\Delta t}(q_{\mathrm{s}},u_{\mathrm{s}})_{\Omega_{\mathrm{s}}}. \tag{4.10}$$

The linear forms are given by

$$\chi(\boldsymbol{\eta}_{\mathrm{l}},\boldsymbol{\eta}_{\mathrm{s}},\mathbf{Y}) = -\left(\langle\boldsymbol{\eta}_{\mathrm{l}}\cdot\boldsymbol{\nu}_\Omega,u_{\mathrm{D}}\rangle_{\partial\Omega} + \widehat{\alpha}(\nabla_\Gamma\overline{\mathbf{X}},\nabla_\Gamma\mathbf{Y})_\Gamma\right),$$
$$\psi(q_{\mathrm{l}},q_{\mathrm{s}},\mu) = -\left((f_{\mathrm{l}},q_{\mathrm{l}})_{\Omega_{\mathrm{l}}} + (f_{\mathrm{s}},q_{\mathrm{s}})_{\Omega_{\mathrm{s}}} + \frac{1}{\Delta t}(\overline{u_{\mathrm{l}}},q_{\mathrm{l}})_{\Omega_{\mathrm{l}}} + \frac{1}{\Delta t}(\overline{u_{\mathrm{s}}},q_{\mathrm{s}})_{\Omega_{\mathrm{s}}}\right). \tag{4.11}$$

4.3.2. Saddle-point formulation

Define the primal space by

$$\mathbb{Z} = \mathbb{V}_{\mathrm{l}}(0) \times \mathbb{V}_{\mathrm{s}} \times \mathbb{Y}, \tag{4.12}$$

and the multiplier space by

$$\mathbb{T} = \mathbb{Q}_{\mathrm{l}} \times \mathbb{Q}_{\mathrm{s}} \times \mathbb{M}. \tag{4.13}$$

Next, we define appropriate norms for $\mathbb{Z}$ and $\mathbb{T}$. The norm on $\mathbb{Z}$ is given by

$$\begin{aligned}\|(\boldsymbol{\eta}_{\mathrm{l}}, \boldsymbol{\eta}_{\mathrm{s}}, \mathbf{Y})\|_{\mathbb{Z}}^2 = &\frac{1}{\widehat{K_{\mathrm{l}}}}\|\boldsymbol{\eta}_{\mathrm{l}}\|_{H(\mathrm{div},\Omega_{\mathrm{l}})}^2 + \frac{1}{\widehat{K_{\mathrm{s}}}}\|\boldsymbol{\eta}_{\mathrm{s}}\|_{H(\mathrm{div},\Omega_{\mathrm{s}})}^2 + \|\widehat{\beta}^{-1/2}\mathbf{Y}\cdot\boldsymbol{\nu}\|_{L^2(\Gamma)}^2 \\ &+ \|\mathbf{Y}\cdot\boldsymbol{\nu}\|_{H^{-1/2}(\Gamma)}^2 + \Delta t\widehat{\alpha}\|\nabla_\Gamma \mathbf{Y}\|_{L^2(\Gamma)}^2.\end{aligned} \tag{4.14}$$

The choice of $\|\mathbf{Y}\cdot\boldsymbol{\nu}\|_{H^{-1/2}(\Gamma)}^2$ is to control the constant part of $\mathbf{Y}$, which follows by:

Proposition 4.4. *Let Γ be a Lipschitz or polyhedral manifold. Define:*

$$|||\mathbf{Y}|||^2 = \|\mathbf{Y}\cdot\boldsymbol{\nu}\|_{H^{-1/2}(\Gamma)}^2 + \|\nabla_\Gamma \mathbf{Y}\|_{L^2(\Gamma)}^2.$$

Then, $|||\mathbf{Y}||| \approx \|\mathbf{Y}\|_{H^1(\Gamma)}$, with constants that only depend on the domain.

Proof. See [16]. □

The norm on $\mathbb{T}$ is given by

$$\|(q_{\mathrm{l}}, q_{\mathrm{s}}, \mu)\|_{\mathbb{T}}^2 = \|\tilde{q}_{\mathrm{l}}\|_{L^2(\Omega_{\mathrm{l}})}^2 + \|\tilde{q}_{\mathrm{s}}\|_{L^2(\Omega_{\mathrm{s}})}^2 + \|\mu - \hat{q}_{\mathrm{l}}\|_{H_{\mathrm{l}}^{1/2}(\Gamma)}^2 + \|\mu - \hat{q}_{\mathrm{s}}\|_{H_{\mathrm{s}}^{1/2}(\Gamma)}^2 + \widehat{S}\|\mu\boldsymbol{\nu}\|_{H^{-1}(\Gamma)}^2, \tag{4.15}$$

where we introduced the mean value: $\hat{q}_i := \frac{1}{|\Omega_i|}\int_{\Omega_i} q_i$, and $\tilde{q}_i := q_i - \hat{q}_i$ (for $i = \mathrm{l}, \mathrm{s}$). We also define the mean value on Γ: $\hat{\mu} := \frac{1}{|\Gamma|}\int_\Gamma \mu$, and $\tilde{\mu} := \mu - \hat{\mu}$.

With the above notation, the formulation (4.5), (4.6) can be written as a saddle-point problem.

Variational formulation 4.5. *Find $(\boldsymbol{\sigma}_{\mathrm{l}}, \boldsymbol{\sigma}_{\mathrm{s}}, \mathbf{V})$ in $\mathbb{V}_{\mathrm{l}}(0) \times \mathbb{V}_{\mathrm{s}} \times \mathbb{Y}$ and $(u_{\mathrm{l}}, u_{\mathrm{s}}, \lambda)$ in $\mathbb{Q}_{\mathrm{l}} \times \mathbb{Q}_{\mathrm{s}} \times \mathbb{M}$ such that*

$$\begin{aligned}&a((\boldsymbol{\eta}_{\mathrm{l}}, \boldsymbol{\eta}_{\mathrm{s}}, \mathbf{Y}), (\boldsymbol{\sigma}_{\mathrm{l}}, \boldsymbol{\sigma}_{\mathrm{s}}, \mathbf{V})) + b((\boldsymbol{\eta}_{\mathrm{l}}, \boldsymbol{\eta}_{\mathrm{s}}, \mathbf{Y}), (u_{\mathrm{l}}, u_{\mathrm{s}}, \lambda)) = \chi(\boldsymbol{\eta}_{\mathrm{l}}, \boldsymbol{\eta}_{\mathrm{s}}, \mathbf{Y}), \\ &+ b((\boldsymbol{\sigma}_{\mathrm{l}}, \boldsymbol{\sigma}_{\mathrm{s}}, \mathbf{V}), (q_{\mathrm{l}}, q_{\mathrm{s}}, \mu)) - c((q_{\mathrm{l}}, q_{\mathrm{s}}, \mu), (u_{\mathrm{l}}, u_{\mathrm{s}}, \lambda)) = \psi(q_{\mathrm{l}}, q_{\mathrm{s}}, \mu),\end{aligned} \tag{4.16}$$

for all $(\boldsymbol{\eta}_{\mathrm{l}}, \boldsymbol{\eta}_{\mathrm{s}}, \mathbf{Y})$ in $\mathbb{V}_{\mathrm{l}}(0) \times \mathbb{V}_{\mathrm{s}} \times \mathbb{Y}$, and $(q_{\mathrm{l}}, q_{\mathrm{s}}, \mu)$ in $\mathbb{Q}_{\mathrm{l}} \times \mathbb{Q}_{\mathrm{s}} \times \mathbb{M}$. The temperatures u_{l}, u_{s} are Lagrange multipliers as well as the interface temperature λ.

The formulation (4.16) was shown to be well-posed, by verifying coercivity and inf-sup conditions [10, 12], in our previous work [16] with the chosen norms (4.14), (4.15). Furthermore, we showed that the semi-discrete system (4.5), (4.6) satisfies both an *a priori* stability bound in time and a conservation law [16].

5. Fully discrete formulation

5.1. Discretization

5.1.1. Formulation

Let $\boldsymbol{\nu}_h$ denote the unit normal vector on Γ_h and $\partial\Omega_h$. We approximate the domains Ω_{l}^i, Ω_{s}^i by three dimensional triangulations $\Omega_{\mathrm{l},h}^i$, $\Omega_{\mathrm{s},h}^i$ such that $\Gamma_h^i = \overline{\Omega_{\mathrm{l},h}^i} \cap \overline{\Omega_{\mathrm{s},h}^i}$ is an embedded polyhedral surface contained in the faces of the mesh. A standard Galerkin approximation of equations (4.5), (4.6) follows by replacing the function

spaces with finite dimensional approximations, *i.e.* find $\boldsymbol{\sigma}_{\mathrm{l},h}^{i+1}$ in $\mathbb{V}_{\mathrm{l},h}^i(0)$, $\boldsymbol{\sigma}_{\mathrm{s},h}^{i+1}$ in $\mathbb{V}_{\mathrm{s},h}^i$, $\mathbf{V}_h^{i+1}$ in $\mathbb{Y}_h^i$, $u_{\mathrm{l},h}^{i+1}$ in $\mathbb{Q}_{\mathrm{l},h}^i$, $u_{\mathrm{s},h}^{i+1}$ in $\mathbb{Q}_{\mathrm{s},h}^i$, λ_h^{i+1} in $\mathbb{M}_h^i$ such that for all $\boldsymbol{\eta}_\mathrm{l} \in \mathbb{V}_{\mathrm{l},h}^i(0)$, $\boldsymbol{\eta}_\mathrm{s} \in \mathbb{V}_{\mathrm{s},h}^i$, $q_\mathrm{l} \in \mathbb{Q}_{\mathrm{l},h}^i$, $q_\mathrm{s} \in \mathbb{Q}_{\mathrm{s},h}^i$, $\mathbf{Y} \in \mathbb{Y}_h^i$, $\mu \in \mathbb{M}_h^i$,

$$
\begin{aligned}
&\frac{1}{\widehat{K}_\mathrm{l}}(\boldsymbol{\sigma}_{\mathrm{l},h}^{i+1}, \boldsymbol{\eta}_\mathrm{l})_{\Omega_{\mathrm{l},h}^i} - (u_{\mathrm{l},h}^{i+1}, \nabla\cdot\boldsymbol{\eta}_\mathrm{l})_{\Omega_{\mathrm{l},h}^i} - \langle \boldsymbol{\eta}_\mathrm{l}\cdot\boldsymbol{\nu}_h^i, \lambda_h^{i+1}\rangle_{\Gamma_h^i} = -\langle \boldsymbol{\eta}_\mathrm{l}\cdot\boldsymbol{\nu}_h^i, u_\mathrm{D}^{i+1}\rangle_{\partial\Omega_h},\\
&-(\nabla\cdot\boldsymbol{\sigma}_{\mathrm{l},h}^{i+1}, q_\mathrm{l})_{\Omega_{\mathrm{l},h}^i} - \frac{1}{\Delta t}(u_{\mathrm{l},h}^{i+1}, q_\mathrm{l})_{\Omega_{\mathrm{l},h}^i} + \frac{1}{\Delta t}(\overline{u_{\mathrm{l},h}}^i, q_\mathrm{l})_{\Omega_{\mathrm{l},h}^i} = -(f_\mathrm{l}^{i+1}, q_\mathrm{l})_{\Omega_{\mathrm{l},h}^i},\\
&\frac{1}{\widehat{K}_\mathrm{s}}(\boldsymbol{\sigma}_{\mathrm{s},h}^{i+1}, \boldsymbol{\eta}_\mathrm{s})_{\Omega_{\mathrm{s},h}^i} - (u_{\mathrm{s},h}^{i+1}, \nabla\cdot\boldsymbol{\eta}_\mathrm{s})_{\Omega_{\mathrm{s},h}^i} + \langle \boldsymbol{\eta}_\mathrm{s}\cdot\boldsymbol{\nu}_h^i, \lambda_h^{i+1}\rangle_{\Gamma_h^i} = 0,\\
&-(\nabla\cdot\boldsymbol{\sigma}_{\mathrm{s},h}^{i+1}, q_\mathrm{s})_{\Omega_{\mathrm{s},h}^i} - \frac{1}{\Delta t}(u_{\mathrm{s},h}^{i+1}, q_\mathrm{s})_{\Omega_{\mathrm{s},h}^i} + \frac{1}{\Delta t}(\overline{u_{\mathrm{s},h}}^i, q_\mathrm{s})_{\Omega_{\mathrm{s},h}^i} = -(f_\mathrm{s}^{i+1}, q_\mathrm{s})_{\Omega_{\mathrm{s},h}^i},
\end{aligned}
\tag{5.1}
$$

$$
\begin{aligned}
&(\widehat{\beta}^{-1}(\boldsymbol{\nu}_h^i)\mathbf{V}_h^{i+1}\cdot\boldsymbol{\nu}_h^i, \mathbf{Y}\cdot\boldsymbol{\nu}_h^i)_{\Gamma_h^i} + \Delta t\widehat{\alpha}(\nabla_\Gamma\mathbf{V}_h^{i+1}, \nabla_\Gamma\mathbf{Y})_{\Gamma_h^i}\\
&\qquad\qquad + \widehat{S}(\mathbf{Y}\cdot\boldsymbol{\nu}_h^i, \lambda_h^{i+1})_{\Gamma_h^i} = -\widehat{\alpha}(\nabla_\Gamma\mathbf{X}^i, \nabla_\Gamma\mathbf{Y})_{\Gamma_h^i},\\
&\widehat{S}(\mathbf{V}_h^{i+1}\cdot\boldsymbol{\nu}_h^i, \mu)_{\Gamma_h^i} - \langle \boldsymbol{\sigma}_{\mathrm{l},h}^{i+1}\cdot\boldsymbol{\nu}_h^i, \mu\rangle_{\Gamma_h^i} + \langle \boldsymbol{\sigma}_{\mathrm{s},h}^{i+1}\cdot\boldsymbol{\nu}_h^i, \mu\rangle_{\Gamma_h^i} = 0,
\end{aligned}
\tag{5.2}
$$

where the discrete spaces are defined over the current (known) domain Ω_h^i, Γ_h^i. We then use the space discrete version of (4.1) to compute the new interface Γ_h^{i+1}, followed by the space discrete version of (4.2), (4.3) to compute the map $\Phi_{i+1,h} : \Omega_h^i \to \Omega_h^{i+1}$.

Remark 5.1 (Finite element space for domain velocity)**.**

The extension (4.2) of $\mathbf{V}_h^{i+1}$ to all of Ω_h^i is computed by solving a discrete Laplace equation using a finite element space $\mathbb{L}_h^i$ on Ω_h^i whose restriction to Γ_h^i contains $\mathbb{Y}_h^i$. Because of (4.1), (4.3), the shape of the tetrahedral elements T in Ω_h^i must be representable by functions in $\mathbb{L}_h^i$, *i.e.* the parametrization of T must be expressed as a linear combination of basis functions in the local finite element space of $\mathbb{L}_h^i$. For example, this is achieved when $\mathbb{L}_h^i$ is piecewise linear and Ω_h^i consists of affine tetrahedra.

The space discrete version of the temperature update formula (4.7) is then given by

$$
\overline{u_{j,h}}^i := \left[u_{j,h}^i - \Delta t\frac{1}{\widehat{K}_j}\Pi_{\mathbb{Q}_{j,h}^i}\left(\boldsymbol{\sigma}_{j,h}^i\cdot\mathcal{I}_{\mathring{\mathbb{V}}_h^i}\mathbf{V}_h^i\right)\right]\circ\Phi_{i,h}^{-1}, \qquad \text{for} \quad j = \mathrm{l},\mathrm{s},
\tag{5.3}
$$

where $\Pi_{\mathbb{Q}_{j,h}^i} : L^2(\Omega_{j,h}^i) \to \mathbb{Q}_{j,h}^i$ is the standard L^2 projection onto $\mathbb{Q}_{j,h}^i$ and $\mathcal{I}_{\mathring{\mathbb{V}}_h^i} : H_0^1(\Omega_h^i) \to \mathring{\mathbb{V}}_h^i$ is a suitable interpolant; see Section 5.2 for a description of these operators. They are needed to ensure that the fully discrete scheme inherits the *a priori* bound and conservation law of the semi-discrete scheme (see [16] for more details). Iterating this procedure gives the fully discrete approximation of (2.2), (2.3).

Using a Lagrangian approach (5.3) *avoids* having to compute the intersection of the mesh from one time step to the next (*i.e.* the L^2 projections (5.12) are computed on the previous domains $\Omega_{\mathrm{l},h}^{i-1}$, $\Omega_{\mathrm{s},h}^{i-1}$). The alternative would have been to compute the L^2 projection (for $j = \mathrm{l},\mathrm{s}$) of $u_{j,h}^i$ from $\Omega_{j,h}^{i-1}$ to $\Omega_{j,h}^i$, but this requires computing the intersection of the meshes representing $\Omega_{j,h}^{i-1}$ and $\Omega_{j,h}^i$.

Just as in Section 4.3, **we drop the time index notation** when considering (5.1), (5.2) at a single time step. This leads to a fully discrete version of (4.16).

Variational formulation 5.2. *Find* $(\boldsymbol{\sigma}_{\mathrm{l},h}, \boldsymbol{\sigma}_{\mathrm{s},h}, \mathbf{V}_h)$ *in* $\mathbb{Z}_h$ *and* $(u_{\mathrm{l},h}, u_{\mathrm{s},h}, \lambda_h)$ *in* $\mathbb{T}_h$ *such that*

$$
\begin{aligned}
&a_h((\boldsymbol{\eta}_\mathrm{l}, \boldsymbol{\eta}_\mathrm{s}, \mathbf{Y}), (\boldsymbol{\sigma}_{\mathrm{l},h}, \boldsymbol{\sigma}_{\mathrm{s},h}, \mathbf{V}_h)) + b_h((\boldsymbol{\eta}_\mathrm{l}, \boldsymbol{\eta}_\mathrm{s}, \mathbf{Y}), (u_{\mathrm{l},h}, u_{\mathrm{s},h}, \lambda_h)) = \chi_h(\boldsymbol{\eta}_\mathrm{l}, \boldsymbol{\eta}_\mathrm{s}, \mathbf{Y}),\\
&+b_h((\boldsymbol{\sigma}_{\mathrm{l},h}, \boldsymbol{\sigma}_{\mathrm{s},h}, \mathbf{V}_h), (q_\mathrm{l}, q_\mathrm{s}, \mu)) - c_h((q_\mathrm{l}, q_\mathrm{s}, \mu), (u_{\mathrm{l},h}, u_{\mathrm{s},h}, \lambda_h)) = \psi_h(q_\mathrm{l}, q_\mathrm{s}, \mu),
\end{aligned}
\tag{5.4}
$$

for all $(\boldsymbol{\eta}_\mathrm{l}, \boldsymbol{\eta}_\mathrm{s}, \mathbf{Y})$ *in* $\mathbb{Z}_h$*, and* $(q_\mathrm{l}, q_\mathrm{s}, \mu)$ *in* $\mathbb{T}_h$*.*

The discrete version of the forms in Section 4.3.1 are defined in the obvious way. The discrete product spaces are defined similar to (4.12), (4.13): $\mathbb{Z}_h = \mathbb{V}_{\mathrm{l},h}(0) \times \mathbb{V}_{\mathrm{s},h} \times \mathbb{Y}_h$, $\mathbb{T}_h = \mathbb{Q}_{\mathrm{l},h} \times \mathbb{Q}_{\mathrm{s},h} \times \mathbb{M}_h$.

5.1.2. Norms

The discrete multiplier norm is slightly different from the continuous case. We first introduce a discrete version of the $H^{1/2}(\Gamma_h)$ norm. For any $\mu \in H^{1/2}(\Gamma_h)$, define the discrete version of (3.7):

$$\|\mu\|_{H^{1/2}_{\mathrm{l},h}(\Gamma_h)} := \sup_{\boldsymbol{\eta}_\mathrm{l}\in\mathbb{V}_{\mathrm{l},h}(0)} \frac{\langle \boldsymbol{\eta}_\mathrm{l}\cdot\boldsymbol{\nu}_h,\mu\rangle_{\Gamma_h}}{\|\boldsymbol{\eta}_\mathrm{l}\|_{H(\mathrm{div},\Omega_{\mathrm{l},h})}}, \quad \|\mu\|_{H^{1/2}_{\mathrm{s},h}(\Gamma_h)} := \sup_{\boldsymbol{\eta}_\mathrm{s}\in\mathbb{V}_{\mathrm{s},h}} \frac{\langle \boldsymbol{\eta}_\mathrm{s}\cdot\boldsymbol{\nu}_h,\mu\rangle_{\Gamma_h}}{\|\boldsymbol{\eta}_\mathrm{s}\|_{H(\mathrm{div},\Omega_{\mathrm{s},h})}}. \tag{5.5}$$

Clearly, for $j=\mathrm{l},\mathrm{s}$, $\|\mu\|_{H^{1/2}_{j,h}(\Gamma_h)} \le \|\mu\|_{H^{1/2}_{j}(\Gamma_h)}$ and $\langle \boldsymbol{\eta}\cdot\boldsymbol{\nu}_h,\mu\rangle_{\Gamma_h} \le \|\boldsymbol{\eta}\|_{H(\mathrm{div},\Omega_{j,h})}\|\mu\|_{H^{1/2}_{j,h}(\Gamma_h)}$ (discrete Schwarz inequality). We shall also use a discrete version of the $H^{-1}(\Gamma_h)$ norm to control the mean value of $\mu\in\mathbb{M}_h$. For all $\mathbf{v}$ in $H^{-1}(\Gamma_h)$, define

$$\|\mathbf{v}\|_{H^{-1}_h(\Gamma_h)} := \sup_{\mathbf{Y}\in\mathbb{Y}_h} \frac{\langle \mathbf{v},\mathbf{Y}\rangle_{\Gamma_h}}{\|\mathbf{Y}\|_{H^1(\Gamma_h)}}, \tag{5.6}$$

which also satisfies $\|\mathbf{v}\|_{H^{-1}_h(\Gamma_h)} \le \|\mathbf{v}\|_{H^{-1}(\Gamma_h)}$ and $\langle \mathbf{v},\mathbf{Y}\rangle_{\Gamma_h} \le \|\mathbf{v}\|_{H^{-1}_h(\Gamma_h)}\|\mathbf{Y}\|_{H^1(\Gamma_h)}$ (discrete Schwarz inequality). Then the discrete version of $\|(q_\mathrm{l},q_\mathrm{s},\mu)\|^2_{\mathbb{T}^\diamond}$ is $\|(q_\mathrm{l},q_\mathrm{s},\mu)\|^2_{\mathbb{T}^\diamond_h} = \|q_\mathrm{l}\|^2_{L^2(\Omega_{\mathrm{l},h})} + \|q_\mathrm{s}\|^2_{L^2(\Omega_{\mathrm{s},h})} + \|\mu\|^2_{H^{1/2}_h(\Gamma_h)}$, where

$$\|\mu\|_{H^{1/2}_h(\Gamma_h)} := \frac{1}{2}\left(\|\mu\|_{H^{1/2}_{\mathrm{l},h}(\Gamma_h)} + \|\mu\|_{H^{1/2}_{\mathrm{s},h}(\Gamma_h)}\right). \tag{5.7}$$

and the discrete version of (4.15) is

$$\begin{aligned}\|(q_\mathrm{l},q_\mathrm{s},\mu)\|^2_{\mathbb{T}_h} =& \|\tilde{q}_\mathrm{l}\|^2_{L^2(\Omega_{\mathrm{l},h})} + \|\tilde{q}_\mathrm{s}\|^2_{L^2(\Omega_{\mathrm{s},h})} \\ &+ \|\mu-\hat{q}_\mathrm{l}\|^2_{H^{1/2}_{\mathrm{l},h}(\Gamma_h)} + \|\mu-\hat{q}_\mathrm{s}\|^2_{H^{1/2}_{\mathrm{s},h}(\Gamma_h)} + \widehat{S}\|\mu\boldsymbol{\nu}_h\|^2_{H^{-1}_h(\Gamma_h)}.\end{aligned} \tag{5.8}$$

The discrete version of the primal norm (4.14) is also slightly different. It requires a discrete version of the $H^{-1/2}(\Gamma_h)$ norm to control the mean value of $\mathbf{Y}\cdot\boldsymbol{\nu}_h$ for $\mathbf{Y}\in\mathbb{Y}_h$. For any $\mathbf{Y}\cdot\boldsymbol{\nu}_h \in H^{-1/2}(\Gamma_h)$, define

$$\|\mathbf{Y}\cdot\boldsymbol{\nu}_h\|_{H^{-1/2}_h(\Gamma_h)} := \sup_{\mu_h\in\mathbb{M}_h} \frac{\langle \mathbf{Y}\cdot\boldsymbol{\nu}_h,\mu_h\rangle_{\Gamma_h}}{\|\mu_h\|_{H^{1/2}_h(\Gamma_h)}}, \tag{5.9}$$

Clearly, $\langle \mathbf{Y}\cdot\boldsymbol{\nu}_h,\mu_h\rangle_{\Gamma_h} \le \|\mathbf{Y}\cdot\boldsymbol{\nu}_h\|_{H^{-1/2}_h(\Gamma_h)}\|\mu_h\|_{H^{1/2}_h(\Gamma_h)}$ (discrete Schwarz inequality). Then the discrete version of $\|(\boldsymbol{\eta}_\mathrm{l},\boldsymbol{\eta}_\mathrm{s},\mathbf{Y})\|^2_{\mathbb{Z}}$ is obtained by replacing $\|\mathbf{Y}\cdot\boldsymbol{\nu}\|_{H^{-1/2}(\Gamma)}$ with $\|\mathbf{Y}\cdot\boldsymbol{\nu}_h\|_{H^{-1/2}_h(\Gamma_h)}$. A discrete version of Proposition 4.4 also holds.

5.2. Space assumptions

Well-posedness of the discrete system follows by showing appropriate coercivity and inf-sup conditions. To facilitate this, we make the following general assumptions on the choice of finite dimensional subspaces (see Sect. 5.3 for the specific spaces used).

Let $\mathbb{V}_h$ be a conforming finite dimensional subspace, *i.e.* $\mathbb{V}_h \subset \mathbb{V} \equiv H(\mathrm{div},\Omega)$, and define

$$\mathring{\mathbb{V}}_h := \{\boldsymbol{\eta}\in\mathbb{V}_h : \boldsymbol{\eta}\cdot\boldsymbol{\nu}_h = 0, \text{ on } \partial\Omega_h\} \subset \{\boldsymbol{\eta}\in\mathbb{V} : \langle \boldsymbol{\eta}\cdot\boldsymbol{\nu}_h, q\rangle_{\partial\Omega_h} = 0,\ \forall q\in H^1_0(\Omega_h)\}.$$

Furthermore, assume that for any $\boldsymbol{\eta}$ in $\mathring{\mathbb{V}}_h$, we have $\boldsymbol{\eta}|_{\Omega_{\mathrm{l},h}} \in \mathbb{V}_{\mathrm{l},h}(0)$ and $\boldsymbol{\eta}|_{\Omega_{\mathrm{s},h}} \in \mathbb{V}_{\mathrm{s},h}$.

Next, take $\mathring{\mathbb{V}}_{\mathrm{l},h} = \{\boldsymbol{\eta}_\mathrm{l}\in\mathbb{V}_{\mathrm{l},h} : \boldsymbol{\eta}_\mathrm{l}\cdot\boldsymbol{\nu}_h = 0, \text{ on } \partial\Omega_{\mathrm{l},h}\}$ and $\hat{\mathbb{Q}}_{\mathrm{l},h} = \{q\in\mathbb{Q}_{\mathrm{l},h} : \int_{\Omega_{\mathrm{l},h}} q\,dx = 0\}$, and assume that $\nabla\cdot\mathbb{V}_{\mathrm{l},h} = \mathbb{Q}_{\mathrm{l},h}$, $\nabla\cdot\mathring{\mathbb{V}}_{\mathrm{l},h} = \hat{\mathbb{Q}}_{\mathrm{l},h}$, and $\mathbb{V}_{\mathrm{l},h}$ contains continuous piecewise linear functions on Γ_h. Analogous definitions are made for $\mathbb{V}_{\mathrm{s},h}$ and $\mathbb{Q}_{\mathrm{s},h}$. Moreover, assume $(\mathbb{V}_{\mathrm{l},h},\mathbb{Q}_{\mathrm{l},h})$ and $(\mathbb{V}_{\mathrm{s},h},\mathbb{Q}_{\mathrm{s},h})$ satisfy

$$\sup_{\boldsymbol{\eta}_\mathrm{l}\in\mathbb{V}_{\mathrm{l},h}} \frac{-(\nabla\cdot\boldsymbol{\eta}_\mathrm{l},q_\mathrm{l})_{\Omega_{\mathrm{l},h}}}{\|\boldsymbol{\eta}_\mathrm{l}\|_{H(\mathrm{div},\Omega_{\mathrm{l},h}))}} \ge c\|q_\mathrm{l}\|_{L^2(\Omega_{\mathrm{l},h})}, \qquad \sup_{\boldsymbol{\eta}_\mathrm{s}\in\mathbb{V}_{\mathrm{s},h}} \frac{-(\nabla\cdot\boldsymbol{\eta}_\mathrm{s},q_\mathrm{s})_{\Omega_{\mathrm{s},h}}}{\|\boldsymbol{\eta}_\mathrm{s}\|_{H(\mathrm{div},\Omega_{\mathrm{s},h}))}} \ge c\|q_\mathrm{s}\|_{L^2(\Omega_{\mathrm{s},h})}, \tag{5.10}$$

for all $q_{\mathrm{l}} \in \mathbb{Q}_{\mathrm{l},h}$, $q_{\mathrm{s}} \in \mathbb{Q}_{\mathrm{s},h}$, with c independent of h and that an analogous condition is satisfied for $(\mathring{\mathbb{V}}_{\mathrm{l},h}, \hat{\mathbb{Q}}_{\mathrm{l},h})$ and $(\mathring{\mathbb{V}}_{\mathrm{s},h}, \hat{\mathbb{Q}}_{\mathrm{s},h})$. This implies that we can solve the discrete mixed form of Laplace's equation. As for $\mathbb{Y}_h$ and $\mathbb{M}_h$, assume they are spaces of continuous functions.

Regarding (5.3), we have a "Fortin interpolant" [10,12] $\mathcal{I}_{\mathring{\mathbb{V}}_h} : H^1_0(\Omega_h) \to \mathring{\mathbb{V}}_h$ that satisfies for any $\mathbf{V} \in H^1_0(\Omega_h)$:

$$\|\mathcal{I}_{\mathring{\mathbb{V}}_h}\mathbf{V}\|_{L^2(\Omega_h)} \leq C\|\mathbf{V}\|_{H^1(\Omega_h)}, \text{ and } (q, \nabla\cdot\mathbf{V} - \nabla\cdot\mathcal{I}_{\mathring{\mathbb{V}}_h}\mathbf{V})_{\Omega_{j,h}} = 0, \ \forall\, q \in \mathbb{Q}_{j,h}, \text{ for } j = \mathrm{l},\mathrm{s}. \tag{5.11}$$

And the L^2 projections $\Pi_{\mathbb{Q}_{j,h}} : L^2(\Omega_{j,h}) \to \mathbb{Q}_{j,h}$ (for $j = \mathrm{l},\mathrm{s}$) satisfy for any $v \in L^2(\Omega_{j,h})$:

$$\|\Pi_{\mathbb{Q}_{j,h}}v\|_{L^2(\Omega_{j,h})} \leq \|v\|_{L^2(\Omega_{j,h})}, \text{ and } (q, v - \Pi_{\mathbb{Q}_{j,h}}v)_{\Omega_{j,h}} = 0, \ \forall\, q \in \mathbb{Q}_{j,h}, \text{ for } j = \mathrm{l},\mathrm{s}. \tag{5.12}$$

With the above considerations, we were able to prove well-posedness of the fully discrete system (5.1), (5.2), as well as obtain an *a priori* stability bound in time and conservation law [16].

5.3. Specific realization

The specific discrete spaces are as follows. Let $\mathcal{T}_h$ be a quasi-uniform, shape regular triangulation of $\overline{\Omega_h} = \overline{\Omega_{\mathrm{l},h}} \cup \overline{\Omega_{\mathrm{s},h}}$ consisting of affine tetrahedra T of maximum size $h \equiv h_T$ [11]. We choose the finite element spaces in the bulk to be $\mathbb{V}_{\mathrm{l},h} = \mathrm{BDM}_1 \subset H(\mathrm{div}, \Omega_{\mathrm{l},h})$, $\mathbb{V}_{\mathrm{s},h} = \mathrm{BDM}_1 \subset H(\mathrm{div}, \Omega_{\mathrm{s},h})$, *i.e.* the lowest order Brezzi–Douglas–Marini space of piecewise linear vector functions [8,28], and $\mathbb{Q}_{\mathrm{l},h}$, $\mathbb{Q}_{\mathrm{s},h}$ to be the set of piecewise constants.

Next, assume that Γ_h is represented by a conforming set of faces $\mathcal{F}_h$ in the triangulation $\mathcal{T}_h$, *i.e.* $\mathcal{F}_h$ is the surface triangulation obtained by restricting $\mathcal{T}_h$ to Γ_h. Then choose $\mathbb{M}_h$ to be the space of continuous piecewise linear functions over $\mathcal{F}_h$ and each of the three components of the space $\mathbb{Y}_h$ to be continuous piecewise linear functions over $\mathcal{F}_h$. Recalling Remark 5.1, we choose $\mathbb{L}_h$ to be the space of continuous piecewise linear functions over Ω_h.

These spaces satisfy the assumptions in Section 5.2. Indeed, it is possible to enforce zero boundary values point-wise with BDM_1. Moreover, we take $\mathcal{I}_{\mathring{\mathbb{V}}_h}$ in (5.11) to be the classic BDM_1 interpolant [8, 12]; the L^2 projections $\Pi_{\mathbb{Q}_{\mathrm{l},h}}$, $\Pi_{\mathbb{Q}_{\mathrm{s},h}}$ are standard [11]. This allows (5.3) to be computed *locally* (*i.e.* element-by-element).

6. Error estimates

In this section, we estimate the error between the time semi-discrete solution and the fully discrete solution over one time step. For convenience, we assume that the "true" domain $\Omega = \Omega_h$, $\Gamma = \Gamma_h$ is a polyhedral domain. Hence, we ignore the domain approximation error. Furthermore, we assume the solution from the previous time step is exact: $\overline{u_{\mathrm{l},h}} = \overline{u_{\mathrm{l}}}$, $\overline{u_{\mathrm{s},h}} = \overline{u_{\mathrm{s}}}$. So we do not consider the accumulated error over all time steps.

A complete error analysis for the time-dependent problem seems out of reach. In the following, we outline a procedure for analyzing the full problem, and point out the difficulties that must be overcome.

(1) One major hurdle is in (4.1), *i.e.* does the interface update formula make sense in the time semi-discrete formulation? In order for (4.1) to produce a well-defined interface Γ^{i+1} at the next time step, we (at least) need $\mathbf{V}^{i+1}$ in $W^{1,\infty}$. Hence, given a weak solution of (4.5), (4.6), a regularity estimate is needed to show that $\mathbf{V}^{i+1}$ is in $W^{1,\infty}$, which is not obvious. For instance, see [15] for a highly sophisticated mathematical analysis of a bending plate interacting with the Navier-Stokes equations.
In short, this is a major hang-up for any numerical method that handles geometric effects in a parametric way.

(2) Assuming we have an *a priori* estimate that says $\|\mathbf{V}^{i+1}\|_{W^{1,\infty}(\Gamma^i)}$ is bounded by data, we then proceed to derive an error estimate between the semi-discrete (4.5), (4.6) and fully discrete formulations (5.1), (5.2) for a single time-step. This is essentially what we do in the following sections, with the following caveat: we assume the discrete and continuous domains are *identical*. In particular, we assume the interface is polyhedral. Avoiding this assumption requires one to analyze the error in approximating the domain, *i.e.*

a variational crime [11, 40]. We believe this can be done in our setting, upon adding several technical arguments [4], if we assume the discrete domain approximates the continuous one in a well-defined way, *e.g.* if the discrete domain "interpolates" a given smooth domain.

(3) If the previous two issues are resolved, one then "stitches" together our single time step error estimate over many time steps to arrive at the full error estimate of the method. However, this introduces another serious issue. As the domains evolve (both continuous and discrete) they will begin to deviate from each other because of errors between the continuous and discrete solution (namely $\mathbf{V}^{i+1}$ and $\mathbf{V}_h^{i+1}$). After several time-steps, the continuous and discrete domains may only partially overlap, which raises the question: how to define the error? It seems reasonable to map one domain to another, but how is this map to be defined and how does it affect the error? To the best of our knowledge, this has not been considered at all by other parametric finite element methods for geometric problems. Because of this difficulty, we ignore the solution error from the previous time-step in our analysis.

(4) Furthermore, topological changes (of Γ) should be ignored to have any hope of deriving a full time-dependent error analysis.

We emphasize that one must also analyze the error between the *fully continuous* problem and the semi-discrete formulation, which introduces more difficulties. Therefore, we only give preliminary error estimates in the following sections, which is useful for showing the potential accuracy of the method.

6.1. Preliminaries

6.1.1. Domain regularity

The "smoothness" of Γ affects the error analysis because the normal vector $\boldsymbol{\nu}$ appears in the weak formulation. We use the following definition in Theorem 6.9 and Lemmas 6.13 and 6.14.

Definition 6.1 (γ regularity)**.** Let $\Gamma \subset \mathbb{R}^3$ be a polyhedral manifold with oriented unit normal vector $\boldsymbol{\nu}$; note that $\boldsymbol{\nu}$ is not defined on polyhedral edges and vertices because $\boldsymbol{\nu}$ has a jump discontinuity. We say Γ is γ regular if there exists a unit vector field $\boldsymbol{\nu}_\gamma : \Gamma \to \mathbb{R}^3$, and corresponding function $\gamma : \Gamma \to [0, 2]$, with the following properties.

- $\boldsymbol{\nu} \cdot \boldsymbol{\nu}_\gamma = 1 - \gamma$ on Γ.
- $\|\boldsymbol{\nu}_\gamma\|_{W^{1,\infty}(\Gamma)} \leq C_\gamma < \infty$, for some positive constant C_γ depending on Γ and γ.

Furthermore, let $\gamma_0 := \sup_{\mathbf{x}\in\Gamma} \gamma$. We call γ_0 the regularity coefficient and C_γ the $W^{1,\infty}(\Gamma)$ stability constant.

If *both* γ_0 and C_γ are small, then the angles (at an edge) of the polyhedral surface are close to 180°, *i.e.* the surface is almost flat across a corner or edge of the polyhedral surface. To see this, consider the following construction of $\boldsymbol{\nu}_\gamma$ using a continuous piecewise linear function $\mathbf{m}(\mathbf{x})$ over Γ (linear on each face). In other words, set the value at each node v, with vertex coordinates $\mathbf{x}$, to be

$$\boldsymbol{\nu}_\gamma(\mathbf{x}) := \mathbf{m}(\mathbf{x})/|\mathbf{m}(\mathbf{x})|, \text{ such that } \mathbf{m}(\mathbf{x}) := \sum_{F\in \mathrm{Star}(\mathbf{x})} \frac{|F|}{|\mathrm{Star}(\mathbf{x})|}\boldsymbol{\nu}_F, \quad \text{where } \boldsymbol{\nu}_F \text{ is the unit normal on } F, \tag{6.1}$$

i.e. this is the notion of weak normal vector given in [6], where $\mathrm{Star}(\mathbf{x})$ is the set of faces (triangles) in Γ that contain $\mathbf{x}$ as a vertex. If each star of faces is sufficiently flat, then $\boldsymbol{\nu} \cdot \boldsymbol{\nu}_F \geq 1 - \epsilon/2$ for all faces F, for some small $\epsilon > 0$. This implies that $\boldsymbol{\nu}(\mathbf{x}) \cdot \boldsymbol{\nu}_\gamma(\mathbf{x}) \geq 1 - \epsilon$, so then $\gamma_0 \leq \epsilon$; $C_\gamma < \infty$ because $\mathbf{m}$ is piecewise linear and $|\mathbf{m}| \geq c_0 > 0$.

Another example is if Γ is the piecewise linear interpolant of a C^2 manifold $\widetilde{\Gamma}$. Then, assuming Γ has sufficiently small faces, one can map $\boldsymbol{\nu}_{\tilde{\Gamma}}$ from $\widetilde{\Gamma}$ to Γ (using a closest point projection [22]) and set $\boldsymbol{\nu}_\gamma := \boldsymbol{\nu}_{\tilde{\Gamma}}$ with $\gamma_0 \leq \frac{1}{2}$. In this case, C_γ depends only on the curvature (and measure) of $\widetilde{\Gamma}$. Note that, for polyhedral surfaces, it is not possible to construct $\boldsymbol{\nu}_\gamma$ such that $\|\boldsymbol{\nu}_\gamma\|_{W^{1,\infty}(\Gamma)} < \infty$ *and* $\gamma_0 = 0$. The following result gives additional properties of $\boldsymbol{\nu}_\gamma$.

Lemma 6.2. *Let $\boldsymbol{\nu}_\gamma$ be given by Definition 6.1. Then,*

$$|\boldsymbol{\nu} - \boldsymbol{\nu}_\gamma| = \sqrt{2\gamma}, \text{ almost everywhere on } \Gamma. \tag{6.2}$$

If Γ is a polyhedral surface that interpolates a C^2 surface $\widetilde{\Gamma}$, and there exists a smooth bijective map $\Phi : \Gamma \to \widetilde{\Gamma}$, then $\boldsymbol{\nu}_\gamma := \tilde{\boldsymbol{\nu}} \circ \Phi$, where $\tilde{\boldsymbol{\nu}}$ is the unit normal of $\widetilde{\Gamma}$. In this case, on each face F (triangle) of Γ, we have

$$\gamma \leq C \left(\operatorname{diam}(F) K_0\right)^2, \text{ everywhere on } \Gamma, \tag{6.3}$$

where $C > 0$ is an independent constant, $K_0 = \max_{\mathbf{x} \in \Gamma} \tilde{\kappa} \circ \Phi(\mathbf{x})$, and $\tilde{\kappa}$ is the curvature of $\widetilde{\Gamma}$.

Proof. The first result follows easily by

$$|\boldsymbol{\nu} - \boldsymbol{\nu}_\gamma|^2 = \boldsymbol{\nu} \cdot \boldsymbol{\nu} - 2\boldsymbol{\nu} \cdot \boldsymbol{\nu}_\gamma + \boldsymbol{\nu}_\gamma \cdot \boldsymbol{\nu}_\gamma = 2(1 - \boldsymbol{\nu} \cdot \boldsymbol{\nu}_\gamma) = 2\gamma.$$

For the second result, we have $\gamma = 1 - \boldsymbol{\nu} \cdot \boldsymbol{\nu}_\gamma = 1 - \cos\varphi \leq \frac{1}{2}\varphi^2$, where φ is the angle between $\boldsymbol{\nu}$ and $\boldsymbol{\nu}_\gamma$. Because each facet is a linear approximation of the smooth surface $\widetilde{\Gamma}$, a Taylor expansion argument shows that $\varphi \leq C_0 \operatorname{diam}(F) \max_{\mathbf{x} \in F} \tilde{\kappa} \circ \Phi(\mathbf{x})$ (see [24,63], Lem. 6.1) for an example of this. □

Remark 6.3. By using Definition 6.1, we can avoid making too strong of an assumption on the polyhedral interface Γ. For instance, if Γ is a *piecewise* smooth manifold with a finite number of corners and edges (with no extreme angles at the edges), then it is possible to construct $\boldsymbol{\nu}_\gamma$ with $\gamma_0 \leq \frac{1}{2}$ in the following way. Take a triangulation of Γ, with mesh size h sufficiently small, such that the vertices and edges of the mesh conform to the corners and edges of Γ, then use the construction in (6.1).

6.1.2. Projection operators

We introduce standard projection operators for the spaces $\mathbb{V}_{\mathrm{l},h}$, $\mathbb{V}_{\mathrm{s},h}$ and $\mathbb{Q}_{\mathrm{l},h}$, $\mathbb{Q}_{\mathrm{s},h}$ that are useful for the error analysis [8,12]. Let $\boldsymbol{\sigma}_{\mathrm{l},I}$ ($\boldsymbol{\sigma}_{\mathrm{s},I}$) be the canonical projection of $\boldsymbol{\sigma}_{\mathrm{l}}$ ($\boldsymbol{\sigma}_{\mathrm{s}}$) into BDM_1, $u_{\mathrm{l},I}$ ($u_{\mathrm{s},I}$) the L^2 projection of u_{l} (u_{s}) into $\mathbb{Q}_{\mathrm{l},h}$ ($\mathbb{Q}_{\mathrm{s},h}$), λ_I the L^2 projection of λ into $\mathbb{M}_h$, and $\mathbf{V}_I$ the L^2 projection of $\mathbf{V}$ into $\mathbb{Y}_h$. Note that $\boldsymbol{\sigma}_{\mathrm{l},I}$, $\boldsymbol{\sigma}_{\mathrm{s},I}$ and $u_{\mathrm{l},I}$, $u_{\mathrm{s},I}$ satisfy

$$\int_F [\boldsymbol{\sigma}_j - \boldsymbol{\sigma}_{j,I}] \cdot \boldsymbol{\nu}\, z \,\mathrm{d}S = 0, \quad z \in \mathcal{P}_1(F), \qquad \int_T [u_j - u_{j,I}] \,\mathrm{d}\mathbf{x} = 0, \quad j = \mathrm{l}, \mathrm{s}, \tag{6.4}$$

for each face F of $\mathcal{F}_h$ and tetrahedron T of $\mathcal{T}_h$. For $\boldsymbol{\sigma}_j$ in $H^1(\Omega_j)$, we have the usual estimate

$$\|\boldsymbol{\sigma}_j - \boldsymbol{\sigma}_{j,I}\|_{L^2(\Omega_j)} \leq Ch \|\boldsymbol{\sigma}_j\|_{H^1(\Omega_j)}, \quad j = \mathrm{l}, \mathrm{s}. \tag{6.5}$$

The above projections and interpolants satisfy the following results.

Proposition 6.4. *For $j = \mathrm{l}, \mathrm{s}$, we have that*

$$(q, \nabla \cdot (\boldsymbol{\sigma}_j - \boldsymbol{\sigma}_{j,I}))_{\Omega_j} = 0, \ \forall q \in \mathbb{Q}_{j,h}, \qquad (u_j - u_{j,I}, \nabla \cdot \boldsymbol{\eta}_h)_{\Omega_j} = 0, \ \forall \boldsymbol{\eta}_h \in \mathbb{V}_{j,h},$$
$$\langle (\boldsymbol{\sigma}_j - \boldsymbol{\sigma}_{j,I}) \cdot \boldsymbol{\nu}, \mu \rangle_\Gamma = 0, \ \forall \mu \in \mathbb{M}_h.$$

Proposition 6.5. *Let $(\boldsymbol{\sigma}_{\mathrm{l}}, \boldsymbol{\sigma}_{\mathrm{s}}, \mathbf{V})$ in $\mathbb{V}_{\mathrm{l}}(0) \times \mathbb{V}_{\mathrm{s}} \times \mathbb{Y}$ and $(u_{\mathrm{l}}, u_{\mathrm{s}}, \lambda)$ in $\mathbb{Q}_{\mathrm{l}} \times \mathbb{Q}_{\mathrm{s}} \times \mathbb{M}$ be the solution of (4.16), and $(\boldsymbol{\sigma}_{\mathrm{l},h}, \boldsymbol{\sigma}_{\mathrm{s},h}, \mathbf{V}_h)$ in $\mathbb{Z}_h$ and $(u_{\mathrm{l},h}, u_{\mathrm{s},h}, \lambda_h)$ in $\mathbb{T}_h$ be the solution of (5.4). Then, we have*

$$-\nabla \cdot (\boldsymbol{\sigma}_{j,h} - \boldsymbol{\sigma}_{j,I}) = \Delta t^{-1} (u_{j,h} - u_{j,I}), \text{ for } j = \mathrm{l}, \mathrm{s}.$$

Proof. Note the projection properties (6.4). From (4.5), (5.1), and Proposition 6.4, one can show

$$(q, -\nabla \cdot (\boldsymbol{\sigma}_{j,h} - \boldsymbol{\sigma}_{j,I}))_{\Omega_j} = \Delta t^{-1} (q, u_{j,h} - u_{j,I})_{\Omega_j}, \forall q \in \mathbb{Q}_{j,h}, \text{ for } j = \mathrm{l}, \mathrm{s}.$$

Since $-\nabla \cdot (\boldsymbol{\sigma}_{j,h} - \boldsymbol{\sigma}_{j,I})$ and $u_{j,h} - u_{j,I}$ are in $\mathbb{Q}_{j,h}$, we get the assertion. □

6.1.3. Properties of the Piola transform

Each tetrahedron T in Ω is obtained by applying a linear bijective map $F_T : T^* \to T$ to the reference simplex T^*, *i.e.* $T = F_T(T^*)$. The Jacobian matrix of the transformation is denoted by ∇F_T. Scalar valued functions are mapped between T^* and T by composition with F_T, *i.e.* $q = q^* \circ F_T^{-1}$, where q is defined on T and q^* is defined on T^*.

Vector valued functions are mapped *via* the Piola transformation:

$$\boldsymbol{\sigma} = \left(\frac{1}{\det(\nabla F_T)} [\nabla F_T] \boldsymbol{\sigma}^* \right) \circ F_T^{-1},$$

where $\boldsymbol{\sigma}$ is defined on T and $\boldsymbol{\sigma}^*$ is defined on T^*. In particular, the local BDM_1 basis functions on T are obtained from applying the Piola transformation to the BDM_1 basis functions on T^*. The Piola transform satisfies the following properties [12]:

$$\int_T q \nabla \cdot \boldsymbol{\sigma} \, \mathrm{d}\mathbf{x} = \int_{T^*} q^* \nabla \cdot \boldsymbol{\sigma}^* \, \mathrm{d}\mathbf{x}^*, \qquad \int_F q \boldsymbol{\sigma} \cdot \boldsymbol{\nu} \mathrm{d}S(\mathbf{x}) = \int_{F^*} q^* \boldsymbol{\sigma}^* \cdot \boldsymbol{\nu}^* \mathrm{d}S(\mathbf{x}^*), \tag{6.6}$$

where F (F^*) is a face of ∂T (∂T^*).

6.1.4. Non-standard estimate

To the best of our knowledge, regularity estimates are not available for the formulation (4.16). Thus, we make a reduced regularity assumption in the error analysis. The following results are useful in this regard.

Proposition 6.6. *For all sufficiently regular functions, and $r \geq 0$, we have*

$$|\boldsymbol{\sigma}^*|_{H^r(T^*)} \leq C h_T^{r-1+d/2} |\boldsymbol{\sigma}|_{H^r(T)}, \qquad |q^*|_{H^r(F^*)} \leq C h_T^{r+1/2-d/2} |q|_{H^r(F)}, \tag{6.7}$$

where d is the dimension of T and h_T is the diameter of T.

Proof. Follows by standard scaling arguments [11, 12]. □

Lemma 6.7. *Fix r such that $0 < r \leq \frac{1}{2}$. Suppose $\boldsymbol{\sigma}_j \in H^{r+1/2}(\Omega_j)$ and $\boldsymbol{\sigma}_{j,I}$ is the* BDM_1 *interpolant of $\boldsymbol{\sigma}_j$ for $j = \mathrm{l}, \mathrm{s}$. Then,*

$$\|\boldsymbol{\sigma}_{j,I}\|_{L^2(\Omega_j)} \leq C \left(\|\boldsymbol{\sigma}_j\|_{L^2(\Omega_j)} + h^{r+1/2} |\boldsymbol{\sigma}_j|_{H^{r+1/2}(\Omega_j)} \right), \quad j = \mathrm{l}, \mathrm{s}. \tag{6.8}$$

Proof. We show this for $\boldsymbol{\sigma}_\mathrm{l}$ only. Given any tetrahedron T in Ω_l, we can write $\boldsymbol{\sigma}_{\mathrm{l},I}$ in terms of a local basis $\{\mathbf{v}_i\}_{i=1}^{12}$ on T such that $\boldsymbol{\sigma}_{\mathrm{l},I}(\mathbf{x}) = \sum_{i=1}^{12} \alpha_i \mathbf{v}_i(\mathbf{x})$. By the definition of the BDM_1 interpolant, the basis can be chosen such that

$$\alpha_i = \frac{1}{|F_i|} \int_{F_i} (\boldsymbol{\sigma}_\mathrm{l} \cdot \boldsymbol{\nu}) \phi_i,$$

where F_i is one of the (four) faces of T and ϕ_i is one of the (three) standard "hat" basis functions on the face F_i.

Next, note the following standard trace inequality [1, 58]:

$$\|\boldsymbol{\sigma}_\mathrm{l}^* \cdot \boldsymbol{\nu}^*\|_{H^r(F_i^*)} = \|\boldsymbol{\sigma}_\mathrm{l}^*\|_{H^r(F_i^*)} \leq \|\boldsymbol{\sigma}_\mathrm{l}^*\|_{H^r(\partial T^*)} \leq C \|\boldsymbol{\sigma}_\mathrm{l}^*\|_{H^{r+1/2}(T^*)}.$$

Thus, by (6.6) and (6.7), we have

$$\begin{aligned} \int_{F_i} (\boldsymbol{\sigma}_\mathrm{l} \cdot \boldsymbol{\nu}) \phi_i &= \int_{F_i^*} (\boldsymbol{\sigma}_\mathrm{l}^* \cdot \boldsymbol{\nu}^*) \phi_i^* \leq \|\boldsymbol{\sigma}_\mathrm{l}^* \cdot \boldsymbol{\nu}^*\|_{H^r(F_i^*)} \|\phi_i^*\|_{(H^r(F_i^*))^*} \\ &\leq C_0 \left(\|\boldsymbol{\sigma}_\mathrm{l}^*\|_{L^2(T^*)} + |\boldsymbol{\sigma}_\mathrm{l}^*|_{H^{r+1/2}(T^*)} \right) \\ &\leq C_1 h_T^{1/2} \left(\|\boldsymbol{\sigma}_\mathrm{l}\|_{L^2(T)} + h_T^{r+1/2} |\boldsymbol{\sigma}_\mathrm{l}|_{H^{r+1/2}(T)} \right), \end{aligned}$$

where $\|\phi_i^*\|_{(H^r(F_i^*))^*}$ is bounded by an independent constant because ϕ_i^* is a fixed polynomial on F_i^*.

Next, for any $T \subset \Omega_\mathrm{l}$ we have $\|\boldsymbol{\sigma}_{\mathrm{l},I}\|^2_{L^2(T)} \leq C_2|T|\sum_j \alpha_i^2$. So, by shape regularity of the triangulation and the above results, we get

$$\begin{aligned}\|\boldsymbol{\sigma}_{\mathrm{l},I}\|^2_{L^2(\Omega_\mathrm{l})} &\leq C_2 \sum_{T\subset\Omega_\mathrm{l}} |T| \sum_i \left(|F_i|^{-1}\int_{F_i}(\boldsymbol{\sigma}_\mathrm{l}\cdot\boldsymbol{\nu})\phi_i\right)^2 \leq C_3 \sum_{T\subset\Omega_\mathrm{l}} h_T^3 (h_T^2)^{-2} \sum_i \left(\int_{F_i}(\boldsymbol{\sigma}_\mathrm{l}\cdot\boldsymbol{\nu})\phi_i\right)^2 \\ &\leq C_4 \sum_{T\subset\Omega_\mathrm{l}} h_T^{-1}\left(C_1 h_T^{1/2}\left(\|\boldsymbol{\sigma}_\mathrm{l}\|_{L^2(T)} + h_T^{r+1/2}|\boldsymbol{\sigma}_\mathrm{l}|_{H^{r+1/2}(T)}\right)\right)^2 \\ &\leq C_5 \sum_{T\subset\Omega_\mathrm{l}} (\|\boldsymbol{\sigma}_\mathrm{l}\|^2_{L^2(T)} + h_T^{2r+1}|\boldsymbol{\sigma}_\mathrm{l}|^2_{H^{r+1/2}(T)}) = C_5(\|\boldsymbol{\sigma}_\mathrm{l}\|^2_{L^2(\Omega_\mathrm{l})} + h^{2r+1}|\boldsymbol{\sigma}_\mathrm{l}|^2_{H^{r+1/2}(\Omega_\mathrm{l})}),\end{aligned}$$

which is the assertion. □

The following lemma is analogous to a result in ([24], Lem. 6.3). However, the result in [24] only holds for two dimensional domains, where as Lemma 6.8 is true for three dimensional domains.

Lemma 6.8. *Assume the hypothesis of Lemma 6.7 and let s satisfy $r+\frac{1}{2} \leq s \leq 1$. Then,*

$$\|\boldsymbol{\sigma}_j - \boldsymbol{\sigma}_{j,I}\|_{L^2(\Omega_j)} \leq Ch^\theta \|\boldsymbol{\sigma}_j\|_{H^s(\Omega_j)}, \quad \theta = \frac{s-(r+1/2)}{1-(r+1/2)}, \quad \text{for } j = \mathrm{l},\mathrm{s}. \tag{6.9}$$

Proof. From (6.8), note that

$$\|\boldsymbol{\sigma}_j - \boldsymbol{\sigma}_{j,I}\|_{L^2(\Omega_j)} \leq C\|\boldsymbol{\sigma}_j\|_{H^{r+1/2}(\Omega_j)}.$$

Next, we interpolate between $H^{r+1/2}$ and H^1 so that we can "tune" our regularity assumption on $\boldsymbol{\sigma}_j$. From ([58], Chap. 34), we have

$$W^{s,p}(\Omega_j) = (W^{m_1,p}(\Omega_j), W^{m_2,p}(\Omega_j))_{\theta,p}, \quad s = (1-\theta)m_1 + \theta m_2,$$

In our case, $p=2$, $m_1 = r+1/2$, $m_2 = 1$, which implies $H^s(\Omega_j) = (H^{r+1/2}(\Omega_j), H^1(\Omega_j))_{\theta,2}$, with $\theta = \frac{s-(r+1/2)}{1-(r+1/2)}$. Then, we can combine (6.8) and (6.5) to get the error estimate (6.9) (see [58], Lem. 22.3). Note: if $s=1$, then $\theta = 1$, and if $s = r+1/2$, then $\theta = 0$. □

6.2. Primal error estimate

6.2.1. Main estimate

We start with an initial estimate.

Theorem 6.9. *Assume Γ is γ regular with $\gamma_0 \leq \frac{1}{2\sqrt{6}}$. Let $(\boldsymbol{\sigma}_\mathrm{l}, \boldsymbol{\sigma}_\mathrm{s}, \mathbf{V})$ in $\mathbb{V}_\mathrm{l}(0)\times\mathbb{V}_\mathrm{s}\times\mathbb{Y}$ and $(u_\mathrm{l}, u_\mathrm{s}, \lambda)$ in $\mathbb{Q}_\mathrm{l}\times\mathbb{Q}_\mathrm{s}\times\mathbb{M}$ be the solution of (4.16), and $(\boldsymbol{\sigma}_{\mathrm{l},h}, \boldsymbol{\sigma}_{\mathrm{s},h}, \mathbf{V}_h)$ in $\mathbb{Z}_h$ and $(u_{\mathrm{l},h}, u_{\mathrm{s},h}, \lambda_h)$ in $\mathbb{T}_h$ be the solution of (5.4). Then,*

$$\begin{aligned}&\|\boldsymbol{\sigma}_{\mathrm{l},h} - \boldsymbol{\sigma}_{\mathrm{l},I}\|^2_{H(\mathrm{div},\Omega_\mathrm{l})} + \|\boldsymbol{\sigma}_{\mathrm{s},h} - \boldsymbol{\sigma}_{\mathrm{s},I}\|^2_{H(\mathrm{div},\Omega_\mathrm{s})} + \|\widehat{\beta}^{-1/2}(\boldsymbol{\nu})(\mathbf{V}_h - \mathbf{V}_I)\cdot\boldsymbol{\nu}\|^2_{L^2(\Gamma)} \\ &\quad + \Delta t\|\nabla_\Gamma(\mathbf{V}_h - \mathbf{V}_I)\|^2_{L^2(\Gamma)} + \Delta t^{-2}\|u_h - u_I\|^2_{L^2(\Omega)} \\ &\quad \leq C\Big\{\|\boldsymbol{\sigma}_\mathrm{l} - \boldsymbol{\sigma}_{\mathrm{l},I}\|^2_{L^2(\Omega_\mathrm{l})} + \|\boldsymbol{\sigma}_\mathrm{s} - \boldsymbol{\sigma}_{\mathrm{s},I}\|^2_{L^2(\Omega_\mathrm{s})} + \|\widehat{\beta}^{-1/2}(\boldsymbol{\nu})(\mathbf{V} - \mathbf{V}_I)\cdot\boldsymbol{\nu}\|^2_{L^2(\Gamma)} \\ &\qquad + \Delta t\|\nabla_\Gamma(\mathbf{V} - \mathbf{V}_I)\|^2_{L^2(\Gamma)} + \left(1 + \frac{\Delta t}{h^2}\right)\|(\mathbf{V} - \mathbf{V}_I)\cdot\boldsymbol{\nu}\|^2_{L^2(\Gamma)} \\ &\qquad + \left(1 + \varpi\frac{\gamma_0}{\Delta t}\right)\|\lambda - \lambda_I\|^2_{L^2(\Gamma)} + \|\lambda - \lambda_I\|^2_{H^{1/2}(\Gamma)}\Big\},\end{aligned} \tag{6.10}$$

where the constant $C>0$ only depends on the physical constants and the domain geometry. If $\widehat{\beta}$ is unbounded, *then $\varpi = 1$ and C is independent of $\widehat{\beta}$; otherwise, $\varpi = 0$.*

Proof. For simplicity, we write $c((q_\mathrm{l},q_\mathrm{s},\mu),(u_\mathrm{l},u_\mathrm{s},\lambda)) = \Delta t^{-1}(q,u)_\Omega$, where $u|_{\Omega_j} = u_j$ and $q|_{\Omega_j} = q_j$ for $j = \mathrm{l},\mathrm{s}$. Then, by combining the continuous and discrete equations, we obtain the error equations

$$\begin{aligned}
&a((\boldsymbol{\eta}_\mathrm{l},\boldsymbol{\eta}_\mathrm{s},\mathbf{Y}),(\boldsymbol{\sigma}_{\mathrm{l},h}-\boldsymbol{\sigma}_{\mathrm{l},I},\boldsymbol{\sigma}_{\mathrm{s},h}-\boldsymbol{\sigma}_{\mathrm{s},I},\mathbf{V}_h-\mathbf{V}_I)) + b((\boldsymbol{\eta}_\mathrm{l},\boldsymbol{\eta}_\mathrm{s},\mathbf{Y}),(u_{\mathrm{l},h}-u_{\mathrm{l},I},u_{\mathrm{s},h}-u_{\mathrm{s},I},\lambda_h-\lambda_I)) =\\
&\quad a((\boldsymbol{\eta}_\mathrm{l},\boldsymbol{\eta}_\mathrm{s},\mathbf{Y}),(\boldsymbol{\sigma}_\mathrm{l}-\boldsymbol{\sigma}_{\mathrm{l},I},\boldsymbol{\sigma}_\mathrm{s}-\boldsymbol{\sigma}_{\mathrm{s},I},\mathbf{V}-\mathbf{V}_I)) + b((\boldsymbol{\eta}_\mathrm{l},\boldsymbol{\eta}_\mathrm{s},\mathbf{Y}),(u_\mathrm{l}-u_{\mathrm{l},I},u_\mathrm{s}-u_{\mathrm{s},I},\lambda-\lambda_I)),\\
&\quad b((\boldsymbol{\sigma}_{\mathrm{l},h}-\boldsymbol{\sigma}_{\mathrm{l},I},\boldsymbol{\sigma}_{\mathrm{s},h}-\boldsymbol{\sigma}_{\mathrm{s},I},\mathbf{V}_h-\mathbf{V}_I),(q_\mathrm{l},q_\mathrm{s},\mu)) - \Delta t^{-1}(q,u_h-u_I)_\Omega =\\
&\quad b((\boldsymbol{\sigma}_\mathrm{l}-\boldsymbol{\sigma}_{\mathrm{l},I},\boldsymbol{\sigma}_\mathrm{s}-\boldsymbol{\sigma}_{\mathrm{s},I},\mathbf{V}-\mathbf{V}_I),(q_\mathrm{l},q_\mathrm{s},\mu)) - \Delta t^{-1}(q,u-u_I)_\Omega,
\end{aligned}$$

for all $(\boldsymbol{\eta}_\mathrm{l},\boldsymbol{\eta}_\mathrm{s},\mathbf{Y})$ in $\mathbb{Z}_h$ and all $(q_\mathrm{l},q_\mathrm{s},\mu)$ in $\mathbb{T}_h$. Next, set the test functions: $\boldsymbol{\eta}_\mathrm{l} = \boldsymbol{\sigma}_{\mathrm{l},h}-\boldsymbol{\sigma}_{\mathrm{l},I}$, $\boldsymbol{\eta}_\mathrm{s} = \boldsymbol{\sigma}_{\mathrm{s},h}-\boldsymbol{\sigma}_{\mathrm{s},I}$, $\mathbf{Y} = \mathbf{V}_h-\mathbf{V}_I$, $q_\mathrm{l} = \Delta t^{-1}(u_{\mathrm{l},h}-u_{\mathrm{l},I})$, $q_\mathrm{s} = \Delta t^{-1}(u_{\mathrm{s},h}-u_{\mathrm{s},I})$, and $\mu = \lambda_h-\lambda_I$. Combining the error equations then yields

$$\begin{aligned}
&a((\boldsymbol{\eta}_\mathrm{l},\boldsymbol{\eta}_\mathrm{s},\mathbf{Y}),(\boldsymbol{\sigma}_{\mathrm{l},h}-\boldsymbol{\sigma}_{\mathrm{l},I},\boldsymbol{\sigma}_{\mathrm{s},h}-\boldsymbol{\sigma}_{\mathrm{s},I},\mathbf{V}_h-\mathbf{V}_I)) + \Delta t^{-1}(q,u_h-u_I)_\Omega = \Delta t^{-1}(q,u-u_I)_\Omega\\
&\quad + a((\boldsymbol{\eta}_\mathrm{l},\boldsymbol{\eta}_\mathrm{s},\mathbf{Y}),(\boldsymbol{\sigma}_\mathrm{l}-\boldsymbol{\sigma}_{\mathrm{l},I},\boldsymbol{\sigma}_\mathrm{s}-\boldsymbol{\sigma}_{\mathrm{s},I},\mathbf{V}-\mathbf{V}_I)) + b((\boldsymbol{\eta}_\mathrm{l},\boldsymbol{\eta}_\mathrm{s},\mathbf{Y}),(u_\mathrm{l}-u_{\mathrm{l},I},u_\mathrm{s}-u_{\mathrm{s},I},\lambda-\lambda_I))\\
&\quad - b((\boldsymbol{\sigma}_\mathrm{l}-\boldsymbol{\sigma}_{\mathrm{l},I},\boldsymbol{\sigma}_\mathrm{s}-\boldsymbol{\sigma}_{\mathrm{s},I},\mathbf{V}-\mathbf{V}_I),(q_\mathrm{l},q_\mathrm{s},\mu)),
\end{aligned}$$

which, after using Young's inequality and moving terms to the left-hand-side, becomes

$$\begin{aligned}
&\frac{1}{2}\Big[\widehat{K_\mathrm{l}}^{-1}\|\boldsymbol{\sigma}_{\mathrm{l},h}-\boldsymbol{\sigma}_{\mathrm{l},I}\|^2_{L^2(\Omega_\mathrm{l})} + \widehat{K_\mathrm{s}}^{-1}\|\boldsymbol{\sigma}_{\mathrm{s},h}-\boldsymbol{\sigma}_{\mathrm{s},I}\|^2_{L^2(\Omega_\mathrm{s})} + \|\widehat{\beta}^{-1/2}(\boldsymbol{\nu})(\mathbf{V}_h-\mathbf{V}_I)\cdot\boldsymbol{\nu}\|^2_{L^2(\Gamma)}\\
&\quad + \Delta t\widehat{\alpha}\|\nabla_\Gamma(\mathbf{V}_h-\mathbf{V}_I)\|^2_{L^2(\Gamma)}\Big] + \Delta t^{-2}\|u_h-u_I\|^2_{L^2(\Omega)}\\
&\le \frac{1}{2}\Big[\widehat{K_\mathrm{l}}^{-1}\|\boldsymbol{\sigma}_\mathrm{l}-\boldsymbol{\sigma}_{\mathrm{l},I}\|^2_{L^2(\Omega_\mathrm{l})} + \widehat{K_\mathrm{s}}^{-1}\|\boldsymbol{\sigma}_\mathrm{s}-\boldsymbol{\sigma}_{\mathrm{s},I}\|^2_{L^2(\Omega_\mathrm{s})} + \|\widehat{\beta}^{-1/2}(\boldsymbol{\nu})(\mathbf{V}-\mathbf{V}_I)\cdot\boldsymbol{\nu}\|^2_{L^2(\Gamma)}\\
&\quad + \Delta t\widehat{\alpha}\|\nabla_\Gamma(\mathbf{V}-\mathbf{V}_I)\|^2_{L^2(\Gamma)}\Big] + \Delta t^{-1}(q,u-u_I)_\Omega\\
&\quad - (\nabla\cdot(\boldsymbol{\sigma}_{\mathrm{l},h}-\boldsymbol{\sigma}_{\mathrm{l},I}),u_\mathrm{l}-u_{\mathrm{l},I})_{\Omega_\mathrm{l}} - (\nabla\cdot(\boldsymbol{\sigma}_{\mathrm{s},h}-\boldsymbol{\sigma}_{\mathrm{s},I}),u_\mathrm{s}-u_{\mathrm{s},I})_{\Omega_\mathrm{s}}\\
&\quad - \langle(\boldsymbol{\sigma}_{\mathrm{l},h}-\boldsymbol{\sigma}_{\mathrm{l},I})\cdot\boldsymbol{\nu},\lambda-\lambda_I\rangle_\Gamma + \langle(\boldsymbol{\sigma}_{\mathrm{s},h}-\boldsymbol{\sigma}_{\mathrm{s},I})\cdot\boldsymbol{\nu},\lambda-\lambda_I\rangle_\Gamma + \widehat{S}\,((\mathbf{V}_h-\mathbf{V}_I)\cdot\boldsymbol{\nu},\lambda-\lambda_I)_\Gamma\\
&\quad + \Delta t^{-1}(\nabla\cdot(\boldsymbol{\sigma}_\mathrm{l}-\boldsymbol{\sigma}_{\mathrm{l},I}),u_{\mathrm{l},h}-u_{\mathrm{l},I})_{\Omega_\mathrm{l}} + \Delta t^{-1}(\nabla\cdot(\boldsymbol{\sigma}_\mathrm{s}-\boldsymbol{\sigma}_{\mathrm{s},I}),u_{\mathrm{s},h}-u_{\mathrm{s},I})_{\Omega_\mathrm{s}}\\
&\quad + \langle(\boldsymbol{\sigma}_\mathrm{l}-\boldsymbol{\sigma}_{\mathrm{l},I})\cdot\boldsymbol{\nu},\lambda_h-\lambda_I\rangle_\Gamma - \langle(\boldsymbol{\sigma}_\mathrm{s}-\boldsymbol{\sigma}_{\mathrm{s},I})\cdot\boldsymbol{\nu},\lambda_h-\lambda_I\rangle_\Gamma - \widehat{S}\,((\mathbf{V}-\mathbf{V}_I)\cdot\boldsymbol{\nu},\lambda_h-\lambda_I)_\Gamma.
\end{aligned}$$

Using (6.4) and Proposition 6.4, we can eliminate several terms to get

$$\begin{aligned}
&\frac{1}{2}\Big[\widehat{K_\mathrm{l}}^{-1}\|\boldsymbol{\sigma}_{\mathrm{l},h}-\boldsymbol{\sigma}_{\mathrm{l},I}\|^2_{L^2(\Omega_\mathrm{l})} + \widehat{K_\mathrm{s}}^{-1}\|\boldsymbol{\sigma}_{\mathrm{s},h}-\boldsymbol{\sigma}_{\mathrm{s},I}\|^2_{L^2(\Omega_\mathrm{s})} + \|\widehat{\beta}^{-1/2}(\boldsymbol{\nu})(\mathbf{V}_h-\mathbf{V}_I)\cdot\boldsymbol{\nu}\|^2_{L^2(\Gamma)}\\
&\quad + \Delta t\widehat{\alpha}\|\nabla_\Gamma(\mathbf{V}_h-\mathbf{V}_I)\|^2_{L^2(\Gamma)}\Big] + \Delta t^{-2}\|u_h-u_I\|^2_{L^2(\Omega)}\\
&\le \frac{1}{2}\Big[\widehat{K_\mathrm{l}}^{-1}\|\boldsymbol{\sigma}_\mathrm{l}-\boldsymbol{\sigma}_{\mathrm{l},I}\|^2_{L^2(\Omega_\mathrm{l})} + \widehat{K_\mathrm{s}}^{-1}\|\boldsymbol{\sigma}_\mathrm{s}-\boldsymbol{\sigma}_{\mathrm{s},I}\|^2_{L^2(\Omega_\mathrm{s})} + \|\widehat{\beta}^{-1/2}(\boldsymbol{\nu})(\mathbf{V}-\mathbf{V}_I)\cdot\boldsymbol{\nu}\|^2_{L^2(\Gamma)}\\
&\quad + \Delta t\widehat{\alpha}\|\nabla_\Gamma(\mathbf{V}-\mathbf{V}_I)\|^2_{L^2(\Gamma)}\Big] - \langle(\boldsymbol{\sigma}_{\mathrm{l},h}-\boldsymbol{\sigma}_{\mathrm{l},I})\cdot\boldsymbol{\nu},\lambda-\lambda_I\rangle_\Gamma + \langle(\boldsymbol{\sigma}_{\mathrm{s},h}-\boldsymbol{\sigma}_{\mathrm{s},I})\cdot\boldsymbol{\nu},\lambda-\lambda_I\rangle_\Gamma\\
&\quad + \underbrace{\widehat{S}((\mathbf{V}_h-\mathbf{V}_I)\cdot\boldsymbol{\nu},\lambda-\lambda_I)_\Gamma}_{=:T_1} - \underbrace{\widehat{S}\,((\mathbf{V}-\mathbf{V}_I)\cdot\boldsymbol{\nu},\lambda_h-\lambda_I)_\Gamma}_{=:T_2}.
\end{aligned}\tag{6.11}$$

Next, by (3.7), (3.8), and Proposition 6.5, we have

$$\begin{aligned}
&- \langle(\boldsymbol{\sigma}_{\mathrm{l},h}-\boldsymbol{\sigma}_{\mathrm{l},I})\cdot\boldsymbol{\nu},\lambda-\lambda_I\rangle_\Gamma + \langle(\boldsymbol{\sigma}_{\mathrm{s},h}-\boldsymbol{\sigma}_{\mathrm{s},I})\cdot\boldsymbol{\nu},\lambda-\lambda_I\rangle_\Gamma\\
&\le \|\boldsymbol{\sigma}_{\mathrm{l},h}-\boldsymbol{\sigma}_{\mathrm{l},I}\|_{H(\mathrm{div},\Omega_\mathrm{l})}\|\lambda-\lambda_I\|_{H_\mathrm{l}^{1/2}(\Gamma)} + \|\boldsymbol{\sigma}_{\mathrm{s},h}-\boldsymbol{\sigma}_{\mathrm{s},I}\|_{H(\mathrm{div},\Omega_\mathrm{s})}\|\lambda-\lambda_I\|_{H_\mathrm{s}^{1/2}(\Gamma)}\\
&\le 2\sqrt{2}\left(\|\boldsymbol{\sigma}_{\mathrm{l},h}-\boldsymbol{\sigma}_{\mathrm{l},I}\|_{L^2(\Omega_\mathrm{l})} + \|\boldsymbol{\sigma}_{\mathrm{s},h}-\boldsymbol{\sigma}_{\mathrm{s},I}\|_{L^2(\Omega_\mathrm{s})} + \Delta t^{-1}\|u_h-u_I\|_{L^2(\Omega)}\right)\|\lambda-\lambda_I\|_{H^{1/2}(\Gamma)},
\end{aligned}$$

which is then further bounded by weighted Young's inequalities and moving terms to the left-hand-side of (6.11). For T_1, if $\widehat{\beta}$ is uniformly bounded with $\widehat{\beta}_+ := \max_{\boldsymbol{\nu}} \widehat{\beta}(\boldsymbol{\nu})$, we can use the simple estimate

$$\widehat{S}((\mathbf{V}_h - \mathbf{V}_I)\cdot\boldsymbol{\nu}, \lambda - \lambda_I)_\Gamma \leq \frac{1}{4}\|\widehat{\beta}^{-1/2}(\boldsymbol{\nu})(\mathbf{V}_h - \mathbf{V}_I)\cdot\boldsymbol{\nu}\|^2_{L^2(\Gamma)} + \widehat{\beta}_+\widehat{S}^2\|\lambda - \lambda_I\|^2_{L^2(\Gamma)},$$

because the first term on the right can be absorbed into the left-hand-side of (6.11). If $\widehat{\beta}_+ = \infty$, then we must use Lemma 6.13. In this case, we get

$$\widehat{S}((\mathbf{V}_h - \mathbf{V}_I)\cdot\boldsymbol{\nu}, \lambda - \lambda_I)_\Gamma \leq \frac{1}{8}\Delta t\widehat{\alpha}\|\nabla_\Gamma(\mathbf{V}_h - \mathbf{V}_I)\|^2_{L^2(\Gamma)} + C\frac{\gamma_0}{\Delta t}\|\lambda - \lambda_I\|^2_{L^2(\Gamma)} + \dots,$$

where again the first term can be absorbed into the left-hand-side of (6.11), but the second term has the constant $\frac{\gamma_0}{\Delta t}$; the remaining terms can be dealt with similarly by weighted Young's inequalities.

To bound T_2, we use Lemma 6.14 and more weighted Young's inequalities to obtain

$$\begin{aligned}\widehat{S}((\mathbf{V} - \mathbf{V}_I)\cdot\boldsymbol{\nu}, \lambda_h - \lambda_I)_\Gamma \leq{}& C\left(\frac{\Delta t}{h^2}\|(\mathbf{V} - \mathbf{V}_I)\cdot\boldsymbol{\nu}\|^2_{L^2(\Gamma)} + \Delta t\|\nabla_\Gamma(\mathbf{V}_I - \mathbf{V})\|^2_{L^2(\Gamma)}\right)\\ &+ \frac{1}{8}\Delta t\widehat{\alpha}\|\nabla_\Gamma(\mathbf{V}_h - \mathbf{V}_I)\|^2_{L^2(\Gamma)} + \dots\end{aligned}$$

The rest then follows by moving terms to the left-hand-side. Note: by Proposition 6.5, we can replace $\|\boldsymbol{\sigma}_{j,h} - \boldsymbol{\sigma}_{j,I}\|_{L^2(\Omega_j)}$ on the left-hand-side of (6.11) by the full $H(\mathrm{div}, \Omega_j)$ norm. □

Corollary 6.10. *Assume the hypothesis of Theorem 6.9. Fix r such that $0 < r \leq \frac{1}{2}$, and assume $\boldsymbol{\sigma}_\mathrm{l} \in H^s(\Omega_\mathrm{l})$, $\boldsymbol{\sigma}_\mathrm{s} \in H^s(\Omega_\mathrm{s})$ for some $r + \frac{1}{2} \leq s \leq 1$ and define $\theta = \frac{s-(r+1/2)}{1-(r+1/2)}$. Moreover, assume $\mathbf{V} \in H^{1+\theta}(\Gamma)$ and $u_\mathrm{l} \in H^\theta(\Omega_\mathrm{l})$, $u_\mathrm{s} \in H^\theta(\Omega_\mathrm{s})$, and $\lambda \in H^{1/2+\theta}(\Gamma)$. Then,*

$$\begin{aligned}&\|\boldsymbol{\sigma}_\mathrm{l} - \boldsymbol{\sigma}_{\mathrm{l},h}\|_{L^2(\Omega_\mathrm{l})} + \|\boldsymbol{\sigma}_\mathrm{s} - \boldsymbol{\sigma}_{\mathrm{s},h}\|_{L^2(\Omega_\mathrm{s})} + \|\widehat{\beta}^{-1/2}(\boldsymbol{\nu})(\mathbf{V} - \mathbf{V}_h)\cdot\boldsymbol{\nu}\|_{L^2(\Gamma)}\\ &\qquad + \Delta t^{1/2}\|\nabla_\Gamma(\mathbf{V} - \mathbf{V}_h)\|_{L^2(\Gamma)}\\ &\qquad \leq Ch^\theta\Big\{\|\boldsymbol{\sigma}_\mathrm{l}\|_{H^s(\Omega_\mathrm{l})} + \|\boldsymbol{\sigma}_\mathrm{s}\|_{H^s(\Omega_\mathrm{s})} + \left[h + \Delta t^{1/2}\right]\|\mathbf{V}\|_{H^{1+\theta}(\Gamma)}\\ &\qquad\quad + \left[1 + \varpi\left(\gamma_0\frac{h}{\Delta t}\right)^{1/2}\right]\|\lambda\|_{H^{1/2+\theta}(\Gamma)}\Big\},\end{aligned} \tag{6.12}$$

where the constant $C > 0$ only depends on the physical constants and the domain geometry. If $\widehat{\beta}$ is unbounded *(i.e. $\widehat{\beta}_-^{-1/2} = 0$), then $\varpi = 1$ and C is independent of $\widehat{\beta}$; otherwise, $\varpi = 0$.*

Proof. Use Proposition 6.5, Lemma 6.8, the triangle inequality, and standard interpolation estimates [11]. □

Corollary 6.11. *Assume the hypothesis of Corollary 6.10. Then,*

$$\|u - u_h\|_{L^2(\Omega)} \leq Ch^\theta\|u\|_{H^\theta(\Omega)} + \Delta t\cdot(\textit{right-hand-side of (6.12)}), \tag{6.13}$$

where the constant $C > 0$ only depends on the physical constants and the domain geometry. If $\widehat{\beta}$ is unbounded *(i.e. $\widehat{\beta}_-^{-1/2} = 0$), then $\varpi = 1$ and C is independent of $\widehat{\beta}$; otherwise, $\varpi = 0$.*

Proof. Similar as before, except most terms on the left-hand-side of (6.10) are dropped. □

Remark 6.12. The above error estimates suggest that the method converges (for a single time step), *without* requiring the true interface to be smooth, *i.e.* the true interface may contain corners or edges (see also Rem. 6.3). This is important if we include anisotropic surface tension.

If $\widehat{\beta}$ is unbounded, then there is a restriction on the time step (for accuracy purposes only) that appears in (6.12): $\Delta t \geq \gamma_0 h$. By (6.3), if Γ interpolates a smooth surface $\widetilde{\Gamma}$, then $\Delta t \geq Ch^3$, where C is proportional to the maximum curvature of $\widetilde{\Gamma}$; a rather mild restriction. If $\widehat{\beta}$ is uniformly bounded, then there is no *additional* time step restriction with regard to accuracy purposes.

6.2.2. Supporting estimates

Lemma 6.13. *Assume the hypothesis of Theorem 6.9. Then,*

$$((\mathbf{V}_h-\mathbf{V}_I)\cdot\boldsymbol{\nu},\lambda-\lambda_I)_\Gamma \le C\sqrt{\gamma_0}\|\lambda-\lambda_I\|_{L^2(\Gamma)}\Big[\|\nabla_\Gamma(\mathbf{V}_h-\mathbf{V}_I)\|_{L^2(\Gamma)}+\|(\mathbf{V}-\mathbf{V}_I)\cdot\boldsymbol{\nu}\|_{L^2(\Gamma)} + \|\boldsymbol{\sigma}_{\mathrm{l},h}-\boldsymbol{\sigma}_{\mathrm{l},I}\|_{L^2(\Omega_\mathrm{l})}+\|\boldsymbol{\sigma}_{\mathrm{s},h}-\boldsymbol{\sigma}_{\mathrm{s},I}\|_{L^2(\Omega_\mathrm{s})}+\Delta t^{-1}\|u_h-u_I\|_{L^2(\Omega)}\Big].$$

Proof. Using the L^2 projection property of λ_I, we have

$$((\mathbf{V}_h-\mathbf{V}_I)\cdot\boldsymbol{\nu},\lambda-\lambda_I)_\Gamma=((\mathbf{V}_h-\mathbf{V}_I)\cdot\boldsymbol{\nu}-\mu,\lambda-\lambda_I)_\Gamma\le\|\lambda-\lambda_I\|_{L^2(\Gamma)}\|(\mathbf{V}_h-\mathbf{V}_I)\cdot\boldsymbol{\nu}-\mu\|_{L^2(\Gamma)},$$

for all $\mu\in\mathbb{M}_h$. Next, choose

$$\mu(\mathbf{x}):=\sum_i(\mathbf{V}_h-\mathbf{V}_I)(\mathbf{x}_i)\cdot\boldsymbol{\nu}_\gamma(\mathbf{x}_i)\phi_i(\mathbf{x}),$$

where $\boldsymbol{\nu}_\gamma$ is taken from Definition 6.1, $\{\mathbf{x}_i\}$ are the vertices of Γ, and $\{\phi_i\}$ are the piecewise linear basis functions of $\mathbb{M}_h$. Hence, on a particular face F of Γ, we have by (6.2)

$$(\mathbf{V}_h-\mathbf{V}_I)\cdot\boldsymbol{\nu}-\mu=\sum_{i=1}^3(\boldsymbol{\nu}|_F-\boldsymbol{\nu}_\gamma(\mathbf{x}_i))\cdot(\mathbf{V}_h-\mathbf{V}_I)(\mathbf{x}_i)\phi_i\le\sqrt{2\gamma_0}\sum_{i=1}^3|\mathbf{V}_h-\mathbf{V}_I|(\mathbf{x}_i)\phi_i,$$

which implies that $\|(\mathbf{V}_h-\mathbf{V}_I)\cdot\boldsymbol{\nu}-\mu\|_{L^2(\Gamma)}\le C_0\sqrt{\gamma_0}\|\mathbf{V}_h-\mathbf{V}_I\|_{L^2(\Gamma)}$.

Next, we bound $\|\mathbf{V}_h-\mathbf{V}_I\|_{L^2(\Gamma)}$ by something more convenient because a similar term does not appear on the left-hand-side of (6.10) when $\widehat{\beta}\to\infty$. By the discrete version of Proposition 4.4 [16],

$$\|\mathbf{V}_h-\mathbf{V}_I\|^2_{L^2(\Gamma)}\le C_1\left(\|\nabla_\Gamma(\mathbf{V}_h-\mathbf{V}_I)\|^2_{L^2(\Gamma)}+\|(\mathbf{V}_h-\mathbf{V}_I)\cdot\boldsymbol{\nu}\|^2_{H_h^{-1/2}(\Gamma)}\right),\tag{6.14}$$

so we must bound $|\langle(\mathbf{V}_h-\mathbf{V}_I)\cdot\boldsymbol{\nu},\mu\rangle_\Gamma|$. Taking the difference of (4.6) and (5.2) gives for all $\mu\in\mathbb{M}_h$

$$\begin{aligned}\widehat{S}\langle(\mathbf{V}_h-\mathbf{V}_I)\cdot\boldsymbol{\nu},\mu\rangle_\Gamma&=\widehat{S}\langle(\mathbf{V}_h-\mathbf{V})\cdot\boldsymbol{\nu},\mu\rangle_\Gamma+\widehat{S}\langle(\mathbf{V}-\mathbf{V}_I)\cdot\boldsymbol{\nu},\mu\rangle_\Gamma\\&=\langle(\boldsymbol{\sigma}_{\mathrm{l},h}-\boldsymbol{\sigma}_\mathrm{l})\cdot\boldsymbol{\nu},\mu\rangle_\Gamma-\langle(\boldsymbol{\sigma}_{\mathrm{s},h}-\boldsymbol{\sigma}_\mathrm{s})\cdot\boldsymbol{\nu},\mu\rangle_\Gamma+\widehat{S}\langle(\mathbf{V}-\mathbf{V}_I)\cdot\boldsymbol{\nu},\mu\rangle_\Gamma\\&=\langle(\boldsymbol{\sigma}_{\mathrm{l},h}-\boldsymbol{\sigma}_{\mathrm{l},I})\cdot\boldsymbol{\nu},\mu\rangle_\Gamma-\langle(\boldsymbol{\sigma}_{\mathrm{s},h}-\boldsymbol{\sigma}_{\mathrm{s},I})\cdot\boldsymbol{\nu},\mu\rangle_\Gamma+\widehat{S}\langle(\mathbf{V}-\mathbf{V}_I)\cdot\boldsymbol{\nu},\mu\rangle_\Gamma,\end{aligned}$$

where we used (6.4). Using discrete Schwarz on $\langle(\boldsymbol{\sigma}_{\mathrm{s},h}-\boldsymbol{\sigma}_{\mathrm{s},I})\cdot\boldsymbol{\nu},\mu\rangle_\Gamma$ yields

$$\begin{aligned}\langle(\boldsymbol{\sigma}_{\mathrm{s},h}-\boldsymbol{\sigma}_{\mathrm{s},I})\cdot\boldsymbol{\nu},\mu\rangle_\Gamma&\le\|(\boldsymbol{\sigma}_{\mathrm{s},h}-\boldsymbol{\sigma}_{\mathrm{s},I})\|_{H(\mathrm{div},\Omega_\mathrm{s})}\|\mu\|_{H^{1/2}_{\mathrm{s},h}(\Gamma)}\\&\le\left(\|\boldsymbol{\sigma}_{\mathrm{s},h}-\boldsymbol{\sigma}_{\mathrm{s},I}\|_{L^2(\Omega_\mathrm{s})}+\Delta t^{-1}\|u_{\mathrm{s},h}-u_{\mathrm{s},I}\|_{L^2(\Omega_\mathrm{s})}\right)\|\mu\|_{H^{1/2}_{\mathrm{s},h}(\Gamma)},\end{aligned}$$

where we used Proposition 6.5. A similar result holds for $\langle(\boldsymbol{\sigma}_{\mathrm{l},h}-\boldsymbol{\sigma}_{\mathrm{l},I})\cdot\boldsymbol{\nu},\mu\rangle_\Gamma$.

For $\langle(\mathbf{V}-\mathbf{V}_I)\cdot\boldsymbol{\nu},\mu\rangle_\Gamma$, we need to use the fact that $\|\mu\|_{L^2(\Gamma)}\le C_2\|\mu\|_{H_h^{1/2}(\Gamma)}$ for a constant $C_2>0$ independent of h. This follows by [28,29,43], where they show the existence of stable liftings of the normal trace for discrete $H(\mathrm{div})$ spaces such as Raviart–Thomas and Brezzi–Douglas–Marini; proofs are given in two dimensions, but the results also hold in three dimensions. So, combining this with (5.5) and (5.7) gives the bound. Therefore,

$$\langle(\mathbf{V}-\mathbf{V}_I)\cdot\boldsymbol{\nu},\mu\rangle_\Gamma\le\|(\mathbf{V}-\mathbf{V}_I)\cdot\boldsymbol{\nu}\|_{L^2(\Gamma)}\|\mu\|_{L^2(\Gamma)}\le C_2\|(\mathbf{V}-\mathbf{V}_I)\cdot\boldsymbol{\nu}\|_{L^2(\Gamma)}\|\mu\|_{H_h^{1/2}(\Gamma)},\quad\forall\mu\in\mathbb{M}_h.$$

Bringing everything together, we have

$$\begin{aligned}\|(\mathbf{V}_h-\mathbf{V}_I)\cdot\boldsymbol{\nu}\|_{H_h^{-1/2}(\Gamma)}&=\sup_{\mu_h\in\mathbb{M}_h}\frac{\langle(\mathbf{V}_h-\mathbf{V}_I)\cdot\boldsymbol{\nu},\mu_h\rangle_{\Gamma_h}}{\|\mu_h\|_{H_h^{1/2}(\Gamma_h)}}\\&\le C_3\Big(\|\boldsymbol{\sigma}_{\mathrm{l},h}-\boldsymbol{\sigma}_{\mathrm{l},I}\|^2_{L^2(\Omega_\mathrm{l})}+\|\boldsymbol{\sigma}_{\mathrm{s},h}-\boldsymbol{\sigma}_{\mathrm{s},I}\|^2_{L^2(\Omega_\mathrm{s})}\\&\quad+\Delta t^{-2}\|u_h-u_I\|^2_{L^2(\Omega)}+\|(\mathbf{V}-\mathbf{V}_I)\cdot\boldsymbol{\nu}\|^2_{L^2(\Gamma)}\Big)^{1/2},\end{aligned}$$

and combining with (6.14) gives the assertion. □

Lemma 6.14. *Assume the hypothesis of Theorem 6.9. Then,*

$$\begin{aligned}\widehat{S}((\mathbf{V}-\mathbf{V}_I)\cdot\boldsymbol{\nu},\lambda_h-\lambda_I)_\Gamma \leq\, & C\|(\mathbf{V}-\mathbf{V}_I)\cdot\boldsymbol{\nu}\|_{L^2(\Gamma)} \\ & \times\Big[\|\widehat{\beta}^{-1/2}(\boldsymbol{\nu})(\mathbf{V}_h-\mathbf{V}_I)\cdot\boldsymbol{\nu}\|_{L^2(\Gamma)}+\|\widehat{\beta}^{-1/2}(\boldsymbol{\nu})(\mathbf{V}_I-\mathbf{V})\cdot\boldsymbol{\nu}\|_{L^2(\Gamma)} \\ & +\Delta t\widehat{\alpha}h^{-1}\left\{\|\nabla_\Gamma(\mathbf{V}_h-\mathbf{V}_I)\|_{L^2(\Gamma)}+\|\nabla_\Gamma(\mathbf{V}_I-\mathbf{V})\|_{L^2(\Gamma)}\right\}+\widehat{S}\|\lambda_I-\lambda\|_{L^2(\Gamma)}\Big].\end{aligned}$$

Proof. We start with $((\mathbf{V}-\mathbf{V}_I)\cdot\boldsymbol{\nu},\lambda_h-\lambda_I)_\Gamma \leq \|(\mathbf{V}-\mathbf{V}_I)\cdot\boldsymbol{\nu}\|_{L^2(\Gamma)}\|\lambda_h-\lambda_I\|_{L^2(\Gamma)}$, and seek a bound for $\|\lambda_h-\lambda_I\|_{L^2(\Gamma)}$. From the error equations, we get

$$\begin{aligned}&(\widehat{\beta}^{-1}(\boldsymbol{\nu})(\mathbf{V}_h-\mathbf{V}_I)\cdot\boldsymbol{\nu},\mathbf{Y}\cdot\boldsymbol{\nu})_\Gamma+\Delta t\widehat{\alpha}(\nabla_\Gamma(\mathbf{V}_h-\mathbf{V}_I),\nabla_\Gamma\mathbf{Y})_\Gamma \\ &+(\widehat{\beta}^{-1}(\boldsymbol{\nu})(\mathbf{V}_I-\mathbf{V})\cdot\boldsymbol{\nu},\mathbf{Y}\cdot\boldsymbol{\nu})_\Gamma+\Delta t\widehat{\alpha}(\nabla_\Gamma(\mathbf{V}_I-\mathbf{V}),\nabla_\Gamma\mathbf{Y})_\Gamma \\ &\qquad+\widehat{S}(\mathbf{Y}\cdot\boldsymbol{\nu},\lambda_I-\lambda)_\Gamma=\widehat{S}(\mathbf{Y}\cdot\boldsymbol{\nu},\lambda_I-\lambda_h)_\Gamma,\quad\text{for all }\mathbf{Y}\in\mathbb{Y}_h.\end{aligned}\tag{6.15}$$

Next, set $\mu_h:=\lambda_I-\lambda_h$ and use $\boldsymbol{\nu}_\gamma$ from Definition 6.1 to choose $\mathbf{Y}$:

$$\mathbf{Y}(\mathbf{x}):=\sum_i\mu_h(\mathbf{x}_i)\boldsymbol{\nu}_\gamma(\mathbf{x}_i)\phi_i(\mathbf{x}),\ \text{where }\phi_i\text{ are piecewise linear basis functions of }\mathbb{M}_h\text{ and }\mathbb{Y}_h.$$

Then, since $\boldsymbol{\nu}_\gamma(\mathbf{x}_i)\cdot\boldsymbol{\nu}=1-\gamma$, over a single face F of Γ we have

$$\begin{aligned}\int_F\mu_h\mathbf{Y}\cdot\boldsymbol{\nu}&=\int_F\mu_h\sum_{i=1}^3\mu_h(\mathbf{x}_i)\boldsymbol{\nu}_\gamma(\mathbf{x}_i)\cdot\boldsymbol{\nu}\phi_i(\mathbf{x})=\|\mu_h\|^2_{L^2(F)}-\int_F\mu_h\sum_{i=1}^3\mu_h(\mathbf{x}_i)\gamma(\mathbf{x}_i)\phi_i(\mathbf{x}) \\ &\geq\|\mu_h\|^2_{L^2(F)}-\|\mu_h\|_{L^2(F)}\|I_h(\mu_h\gamma)\|_{L^2(F)},\end{aligned}$$

where $I_h:C^0\to\mathbb{M}_h$ is the nodal interpolant on F. For piecewise linear basis functions, we have

$$\|I_h(\mu_h\gamma)\|^2_{L^2(F)}\leq\frac{|F|}{4}\sum_{i=1}^3(\mu_h(\mathbf{x}_i)\gamma(\mathbf{x}_i))^2\leq\gamma_0^2\frac{|F|}{4}\sum_{i=1}^3(\mu_h(\mathbf{x}_i))^2\leq\gamma_0^2 6\|\mu_h\|^2_{L^2(F)}.$$

So combining with the previous inequality gives $\int_F\mu_h\mathbf{Y}\cdot\boldsymbol{\nu}\geq(1-\gamma_0\sqrt{6})\|\mu_h\|^2_{L^2(F)}\geq\frac{1}{2}\|\mu_h\|^2_{L^2(F)}$, which implies $(\mathbf{Y}\cdot\boldsymbol{\nu},\lambda_I-\lambda_h)_\Gamma\geq\frac{1}{2}\|\lambda_I-\lambda_h\|^2_{L^2(\Gamma)}$. Moreover, we have an inverse estimate

$$\|\mathbf{Y}\|_{L^2(\Gamma)}\leq C_1\|\lambda_I-\lambda_h\|_{L^2(\Gamma)},\qquad\|\nabla_\Gamma\mathbf{Y}\|_{L^2(\Gamma)}\leq C_1h^{-1}\|\lambda_I-\lambda_h\|_{L^2(\Gamma)}.$$

Taking all this together, from (6.15), we get

$$\begin{aligned}\widehat{S}\|\lambda_I-\lambda_h\|_{L^2(\Gamma)}\leq C_2\big[&\|\widehat{\beta}^{-1/2}(\boldsymbol{\nu})(\mathbf{V}_h-\mathbf{V}_I)\cdot\boldsymbol{\nu}\|_{L^2(\Gamma)}+\|\widehat{\beta}^{-1/2}(\boldsymbol{\nu})(\mathbf{V}_I-\mathbf{V})\cdot\boldsymbol{\nu}\|_{L^2(\Gamma)} \\ &+\Delta t\widehat{\alpha}h^{-1}\left\{\|\nabla_\Gamma(\mathbf{V}_h-\mathbf{V}_I)\|_{L^2(\Gamma)}+\|\nabla_\Gamma(\mathbf{V}_I-\mathbf{V})\|_{L^2(\Gamma)}\right\} \\ &+\widehat{S}\|\lambda_I-\lambda\|_{L^2(\Gamma)}\big],\end{aligned}$$

which proves the inequality. □

6.3. Multiplier error estimate

We have an error estimate for $\lambda-\lambda_h$ in the discrete $H^{1/2}(\Gamma)$ norm by the next theorem and corollary.

Theorem 6.15. *Assume the hypothesis of Theorem 6.9. Then,*

$$\|\lambda_I - \lambda_h\|_{H_h^{1/2}(\Gamma)} \leq C\Big[\|\lambda - \lambda_I\|_{H^{1/2}(\Gamma)} + \|u - u_h\|_{L^2(\Omega)} + \|\boldsymbol{\sigma}_{\mathrm{l}} - \boldsymbol{\sigma}_{\mathrm{l},h}\|_{L^2(\Omega_{\mathrm{l}})} + \|\boldsymbol{\sigma}_{\mathrm{s}} - \boldsymbol{\sigma}_{\mathrm{s},h}\|_{L^2(\Omega_{\mathrm{s}})} + \|\widehat{\beta}^{-1/2}(\boldsymbol{\nu})(\mathbf{V} - \mathbf{V}_h)\cdot\boldsymbol{\nu}\|_{L^2(\Gamma)} + \Delta t^{1/2}\|\nabla_\Gamma(\mathbf{V} - \mathbf{V}_h)\|_{L^2(\Gamma)}\Big]. \tag{6.16}$$

where the constant $C > 0$ only depends on the physical constants and the domain geometry.

Proof. Beginning as we did in the proof of Theorem 6.9, we have for all $(\boldsymbol{\eta}_{\mathrm{l}}, \boldsymbol{\eta}_{\mathrm{s}}, \mathbf{Y})$ in $\mathbb{Z}_h$:

$$\begin{aligned} &b((\boldsymbol{\eta}_{\mathrm{l}},\boldsymbol{\eta}_{\mathrm{s}}, \mathbf{Y}), (0, 0, \lambda_I - \lambda_h)) \\ &\quad = b((\boldsymbol{\eta}_{\mathrm{l}}, \boldsymbol{\eta}_{\mathrm{s}}, \mathbf{Y}), (u_{\mathrm{l},h} - u_{\mathrm{l}}, u_{\mathrm{s},h} - u_{\mathrm{s}}, \lambda_I - \lambda)) + b((\boldsymbol{\eta}_{\mathrm{l}}, \boldsymbol{\eta}_{\mathrm{s}}, \mathbf{Y}), (u_{\mathrm{l}} - u_{\mathrm{l},h}, u_{\mathrm{s}} - u_{\mathrm{s},h}, \lambda - \lambda_h)) \\ &\quad = b((\boldsymbol{\eta}_{\mathrm{l}}, \boldsymbol{\eta}_{\mathrm{s}}, \mathbf{Y}), (u_{\mathrm{l},h} - u_{\mathrm{l}}, u_{\mathrm{s},h} - u_{\mathrm{s}}, \lambda_I - \lambda)) - a((\boldsymbol{\eta}_{\mathrm{l}}, \boldsymbol{\eta}_{\mathrm{s}}, \mathbf{Y}), (\boldsymbol{\sigma}_{\mathrm{l}} - \boldsymbol{\sigma}_{\mathrm{l},h}, \boldsymbol{\sigma}_{\mathrm{s}} - \boldsymbol{\sigma}_{\mathrm{s},h}, \mathbf{V} - \mathbf{V}_h)), \end{aligned}$$

which then yields

$$\begin{aligned} b((\boldsymbol{\eta}_{\mathrm{l}}, \boldsymbol{\eta}_{\mathrm{s}}, \mathbf{Y}), (0, 0, \lambda_I - \lambda_h)) \leq C\|(\boldsymbol{\eta}_{\mathrm{l}}, \boldsymbol{\eta}_{\mathrm{s}}, \mathbf{Y})\|_{\mathbb{Z}_h}\Big[&\|u - u_h\|_{L^2(\Omega)} + \|\lambda - \lambda_I\|_{H_h^{1/2}(\Gamma)} \\ &+ \|\boldsymbol{\sigma}_{\mathrm{l}} - \boldsymbol{\sigma}_{\mathrm{l},h}\|_{L^2(\Omega_{\mathrm{l}})} + \|\boldsymbol{\sigma}_{\mathrm{s}} - \boldsymbol{\sigma}_{\mathrm{s},h}\|_{L^2(\Omega_{\mathrm{s}})} \\ &+ \|\widehat{\beta}^{-1/2}(\boldsymbol{\nu})(\mathbf{V} - \mathbf{V}_h)\cdot\boldsymbol{\nu}\|_{L^2(\Gamma)} + \Delta t^{1/2}\|\nabla_\Gamma(\mathbf{V} - \mathbf{V}_h)\|_{L^2(\Gamma)}\Big]. \end{aligned}$$

Finally, use $\|\lambda - \lambda_I\|_{H_h^{1/2}(\Gamma)} \leq \|\lambda - \lambda_I\|_{H^{1/2}(\Gamma)}$ (see (5.5), (5.7)), divide through by $\|(\boldsymbol{\eta}_{\mathrm{l}}, \boldsymbol{\eta}_{\mathrm{s}}, \mathbf{Y})\|_{\mathbb{Z}_h}$, take the supremum, and use the discrete inf-sup condition in ([16], Lem. 9). □

Corollary 6.16. *Assume the hypothesis of Theorem 6.9 and Corollary 6.10. Then,*

$$\begin{aligned} \|\lambda - \lambda_h\|_{H_h^{1/2}(\Gamma)} \leq\, &Ch^\theta\|u\|_{H^\theta(\Omega)} \\ &+ C(1 + \Delta t)h^\theta\Big\{\|\boldsymbol{\sigma}_{\mathrm{l}}\|_{H^s(\Omega_{\mathrm{l}})} + \|\boldsymbol{\sigma}_{\mathrm{s}}\|_{H^s(\Omega_{\mathrm{s}})} + \left[h + \Delta t^{1/2}\right]\|\mathbf{V}\|_{H^{1+\theta}(\Gamma)} \\ &+ \left[1 + \varpi\left(\gamma_0\frac{h}{\Delta t}\right)^{1/2}\right]\|\lambda\|_{H^{1/2+\theta}(\Gamma)}\Big\}, \end{aligned} \tag{6.17}$$

with the same conditions on $C > 0$ and ϖ as in Theorem 6.9.

Proof. Combine Theorem 6.15 with Corollary 6.10, Corollary 6.11, the triangle inequality, and standard interpolation estimates. □

7. Implementation details

7.1. Discretization and initialization

The method begins by approximating the bulk domains Ω, $\Omega_{\mathrm{s}}(0)$, $\Omega_{\mathrm{l}}(0)$ by triangulations Ω_h^0, $\Omega_{\mathrm{s},h}^0$, $\Omega_{\mathrm{l},h}^0$ respectively such that $\Gamma(0)$ is approximated by $\Gamma_h^0 = \overline{\Omega_{\mathrm{l},h}^0} \cap \overline{\Omega_{\mathrm{s},h}^0}$ which is an embedded polygonal curve contained in the edges of the mesh of Ω_h^0. This procedure is done in FELICITY [62, 66] using the mesh generation tool TIGER [64]. For the examples in this paper, Ω_h^0 is a triangulation of the square $(-L, L)^2$.

To generate a conforming mesh, TIGER requires the following: a parametrization of Γ in the form of a closed polygon, the parameter L, and the number of points N along one edge of Ω_h. With this, TIGER creates a mesh of Ω_h with an embedded curve Γ_h that interpolates Γ. Moreover, the generated mesh is *robust*, *i.e.* there are rigorous (and reasonable!) bounds on the angles of the triangles [64]. Note: TIGER can also generate robust tetrahedral meshes of three dimensional domains.

Next, initial and boundary data is interpolated into the appropriate finite element spaces using FELICITY. We also define the initial "mapped" temperatures to be $\overline{u_{\mathrm{s},h}}^0 := u^0_{\mathrm{s},h}$ and $\overline{u_{\mathrm{l},h}}^0 := u^0_{\mathrm{l},h}$. For the examples in Section 8.2, we set $u^0_{\mathrm{s},h}$ to a constant and $u^0_{\mathrm{l},h}$ is determined by solving the Laplace equation over $\Omega^0_{\mathrm{l},h}$ with boundary data $u_{\mathrm{D}}\big|_{\partial\Omega^0_h}$ and $u^0_{\mathrm{s},h}\big|_{\Gamma^0_h}$. The time interval $[0,T]$ is discretized into M time steps uniformly spaced by Δt.

7.2. Algorithm

The algorithm is as follows. Setting $i := 0$, we iterate the following procedure for a constant M number of time-steps.

(1) Solve (5.1) and (5.2) for $(\boldsymbol{\sigma}^{i+1}_{\mathrm{l},h}, \boldsymbol{\sigma}^{i+1}_{\mathrm{s},h}, u^{i+1}_{\mathrm{l},h}, u^{i+1}_{\mathrm{s},h}, \lambda^{i+1}_h, \mathbf{V}^{i+1}_h) \in \mathbb{V}^i_{\mathrm{l},h}(0) \times \mathbb{V}^i_{\mathrm{s},h} \times \mathbb{Q}^i_{\mathrm{l},h} \times \mathbb{Q}^i_{\mathrm{s},h} \times \mathbb{M}^i_h \times \mathbb{Y}^i_h$.

(2) Extend interface velocity on Γ^i_h to the entire domain Ω_h. This is done using the harmonic extension described in Section 4.1.2 and the finite element space given in Remark 5.1.
Note that the error estimate (6.12) implies that $\mathbf{V}^{i+1}_h$ converges to $\mathbf{V}^{i+1}$ on the interface. Moreover, this implies that the discrete harmonic extension converges to the continuous harmonic extension, *i.e.* $\mathbf{V}^{i+1}_h$ converges to $\mathbf{V}^{i+1}$ in the bulk.

(3) Update domain using the extended velocity field (see (4.3)). In addition, we map the previous temperatures $u^i_{j,h}$ to $\overline{u_{j,h}}^i$ (for $j = \mathrm{l}, \mathrm{s}$) using (5.3). Recall Remark 4.2, and note that a discrete version of Remark 4.2 is that Δt is controlled by $\nabla \mathbf{V}^{i+1}_h$, where $\mathbf{V}^{i+1}_h$ is the extended velocity. Since $\mathbf{V}^{i+1}_h$ converges to $\mathbf{V}^{i+1}$ as $h \to 0$, we have that Δt actually depends on $\nabla \mathbf{V}^{i+1}$. Hence, Δt does *not* depend on the mesh size, which is confirmed by our numerical experiments.

(4) Re-mesh if needed (Sect. 7.3).

(5) Set $i := i + 1$. Repeat.

7.3. Re-meshing

After the mesh is deformed in step (3) of the algorithm, the mesh is checked for quality. The minimum angle α_0 of all triangles in $\mathcal{T}^i_h$ is measured and if $\alpha_0 < \alpha_{\mathrm{TOL}}$ then a re-mesh is performed. Otherwise, we go to step (5) and repeat the iteration loop. For all simulations, we chose $\alpha_{\mathrm{TOL}} = 5°$. Note: the measured angles have a "sign", *i.e.* if a triangle gets inverted then all of its angles become negative. Thus, our criteria checks for mesh inversion also, though this never happened.

The re-mesh procedure is performed in the following way. Given the interface mesh Γ^i_h, which is a closed curve, it is straightforward to determine what points are inside the curve and what points are outside. This is all that is needed by TIGER [64]; in essence, one can think of Γ^i_h as the zero-level set of a hypothetical level set function. The new mesh (of Ω_h) that is generated has a conforming interface $\widetilde{\Gamma}^i_h$ that interpolates Γ^i_h in a piecewise linear fashion. TIGER also delivers which triangles in Ω_h are inside and outside of $\widetilde{\Gamma}^i_h$, which immediately defines $\widetilde{\Omega_{\mathrm{s},h}}^i$ and $\widetilde{\Omega_{\mathrm{l},h}}^i$. We then interpolate $\overline{u_{\mathrm{s},h}}^i$, $\overline{u_{\mathrm{s},h}}^i$ from $\Omega^i_{\mathrm{s},h}$, $\Omega^i_{\mathrm{l},h}$ to $\widetilde{\Omega_{\mathrm{s},h}}^i$, $\widetilde{\Omega_{\mathrm{l},h}}^i$. Lastly, we move to step (5) and define the new domains as $\Omega^{i+1}_{\mathrm{s},h} := \widetilde{\Omega_{\mathrm{s},h}}^i$, $\Omega^{i+1}_{\mathrm{l},h} := \widetilde{\Omega_{\mathrm{l},h}}^i$, $\Gamma^{i+1}_h := \widetilde{\Gamma}^i_h$.

For the examples in this paper the mesh topology was regenerated up to *three* times in some examples. The computational time for each re-mesh procedure depends on the mesh size, *i.e.* re-mesh time increases for finer meshes. However, the actual re-mesh time is approximately %10 of the time needed to solve the linear system (5.1), (5.2) for *one* time-step (see Sect. 8.2.1). So it is quite *negligible*.

Remark 7.1. It is sometimes useful to pre-warp (or pre-compress) the initial mesh to avoid extra re-meshing steps (see Sect. 8.2.2 for an example).

8. Numerical results

All simulations were implemented in the package FELICITY [62]. The linear systems are solved by MATLAB's "backslash" command. Alternatively, one can use an iterative procedure such as Uzawa's algorithm; (see [24], Sect. 7) for an example in a related problem. Each numerical example was computed on a Dell Optiplex 9020 workstation with Intel(R) Core(TM) i7-4790 CPU @ 3.60GHz and 16 GB of memory.

8.1. Convergence test

8.1.1. Exact Solution

We apply our method to an isotropic surface tension example ($\widehat{\alpha} = \widehat{\alpha}_0$ and $\widehat{\beta} = \widehat{\beta}_0$) with a known exact solution. Define

$$r(t) = \left(r_0^2 + t\right)^{1/2}, \qquad w(t) = -\frac{\zeta\left(d - \frac{1}{2}\right)}{r(t)}, \qquad v(s) = -\frac{\mathrm{e}^{1/4}}{2}\int_1^s \frac{\mathrm{e}^{-1/4z^2}}{z^{d-1}}\mathrm{d}z,$$

and define

$$f(\mathbf{x}, t) = w'(t) = \frac{\zeta\left(d - \frac{1}{2}\right)}{2r^3(t)},$$

and

$$u(\mathbf{x}, t) = \begin{cases} w(t) & \text{for } |\mathbf{x}| \leq r(t), \\ w(t) + v\left(\dfrac{|\mathbf{x}|}{r(t)}\right) & \text{for } |\mathbf{x}| > r(t). \end{cases}$$

When $\widehat{K_{\mathrm{l}}} = 1, \widehat{K_{\mathrm{s}}}, \widehat{S} = 1$, and $\widehat{\alpha}_0 = \widehat{\beta}_0 = \zeta$, u is the exact solution to (2.2), (2.3) (with inhomogeneous boundary data). In this case, the interface $\Gamma(t)$ is a circle centered at the origin with radius $r(t)$.

8.1.2. Results

We test the convergence of our algorithm when $d = 2$, $\Omega = (-1, 1)^2$, $r_0 = 0.25$, $\zeta = 0.01$, and $T = 0.5$. We measure convergence using the following errors:

$$\begin{aligned} \|e_u\|_{L_2,\infty} &= \max_{1\leq i\leq M} \|u_h^i - \Pi_h u(t_i)\|_{L_2(\Omega)}, \\ \|e_u\|_{\infty,\infty} &= \max_{1\leq i\leq M} \left[\max_{\tau\in\mathcal{T}_h^i} \left|(u_h^i - \Pi_h u(t_i))\big|_\tau\right|\right], \\ \|e_{\mathbf{X}}\|_{\infty,\infty} &= \max_{1\leq i\leq M} \left[\max_{\mathbf{p}\in\mathcal{V}_h^i} \left|\sum_{k=1}^{2} |p_k - x_k^i|\right|\right], \end{aligned}$$

where $\Pi_h u(t)$ is the piecewise constant interpolant of $u(\cdot, t)$, and $\mathcal{V}_h^i$ is the set of vertices of the surface triangulation of Γ_h^i, and x^i is the point on Γ_h^i nearest to $\mathbf{p}$ which is collinear with $\mathbf{p}$ and the origin.

Next, define $N_j = 2^j$ where j is the mesh refinement level, and Ω_h is subdivided into $4N_j^2$ triangles. We then set $\Delta t_j = T/M_j$ where $M_j = \lceil 2TN_j^2 \rceil = N_j^2 = 4^j$. Note: $\Delta x_j \approx 2^{1-j}$ and $\Delta t_j = 0.5(4^{-j})$. Convergence errors are listed in Table 3.

Plots of the expanding circle solution are shown in Figures 2, 3, 4. For this experiment, the mesh was regenerated *once* for mesh levels $j = 3, 5, 6$, and 7. The mesh was never regenerated for mesh levels $j = 2$ and $j = 4$. Figure 4 depicts a snapshot of this mesh immediately before and after the re-mesh; this shows that the interface is well-captured by the re-meshing procedure.

TABLE 3. Errors for convergence experiment. The estimated orders of convergence are: $\|e_u\|_{L_2,\infty} \approx O(\Delta x^2)$, $\|e_u\|_{\infty,\infty} \approx O(\Delta x^{5/3})$, $\|e_{\mathbf{X}}\|_{\infty,\infty} \approx O(\Delta x^2)$. The simulation time for this experiment ranged from ≈ 2 seconds for level 2 up to ≈ 7 hours for level 7.

j	$\|e_u\|_{L_2,\infty}$	$\|e_u\|_{\infty,\infty}$	$\|e_{\mathbf{X}}\|_{\infty,\infty}$
2	1.8425×10^{-1}	1.8724×10^{-1}	2.5861×10^{-1}
3	6.4940×10^{-2}	9.9472×10^{-2}	9.8479×10^{-2}
4	1.9307×10^{-2}	3.6761×10^{-2}	2.4667×10^{-2}
5	5.0535×10^{-3}	1.0785×10^{-2}	6.5075×10^{-3}
6	1.2764×10^{-3}	2.8786×10^{-3}	1.6575×10^{-3}
7	3.2038×10^{-4}	8.9851×10^{-4}	4.1744×10^{-4}

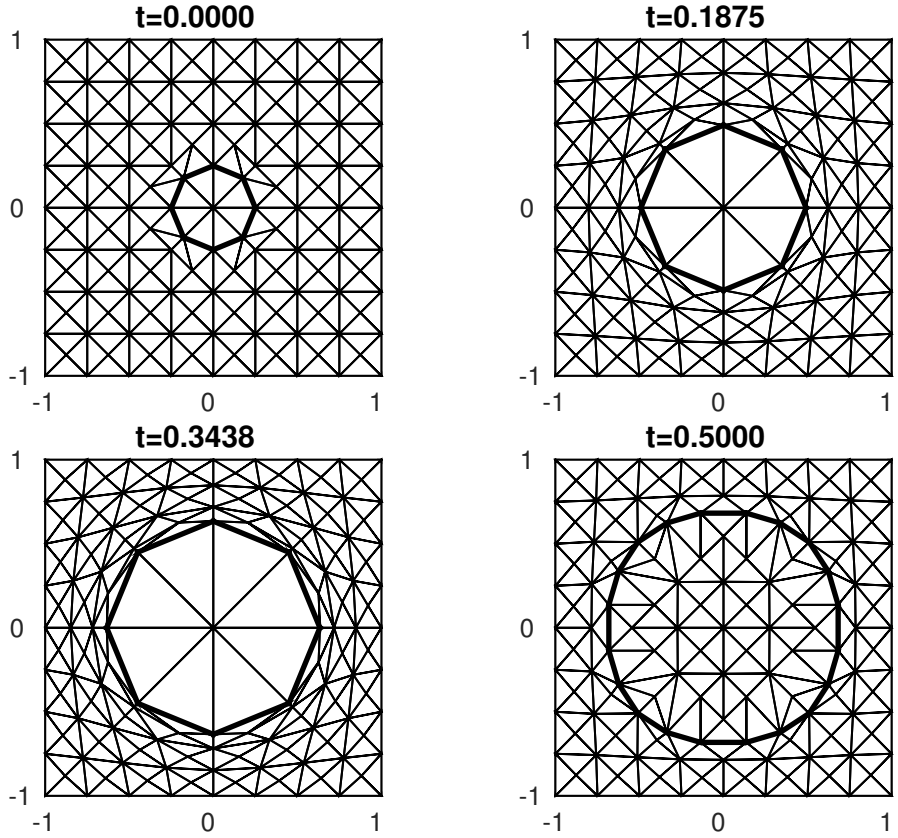

FIGURE 2. Snapshot of mesh for Section 8.1.2 at various time levels when $j = 3$ and $T = 0.5$.

8.2. Numerical examples

In this section we report some results on the application of our algorithm for problems with unknown solutions. For all simulations, the Dirichlet boundary is the entire outer boundary, *i.e.* $\partial_{\mathrm{D}}\Omega \equiv \partial\Omega$ with $u_{\mathrm{D}} = -0.5$. The initial temperature is $u_{\mathrm{s},0} := 0$ in Ω_{s} and $u_{\mathrm{l},0}$ is a smooth function between 0 and -0.5 in Ω_{l}. We set the material parameters $\widehat{K_{\mathrm{l}}} = 1, \widehat{K_{\mathrm{s}}} = 1, \widehat{S} = 2$, $\widehat{\alpha}_0 = 0.005$, and $\widehat{\beta}_0 = 0.01$. We also set $f = 0$.

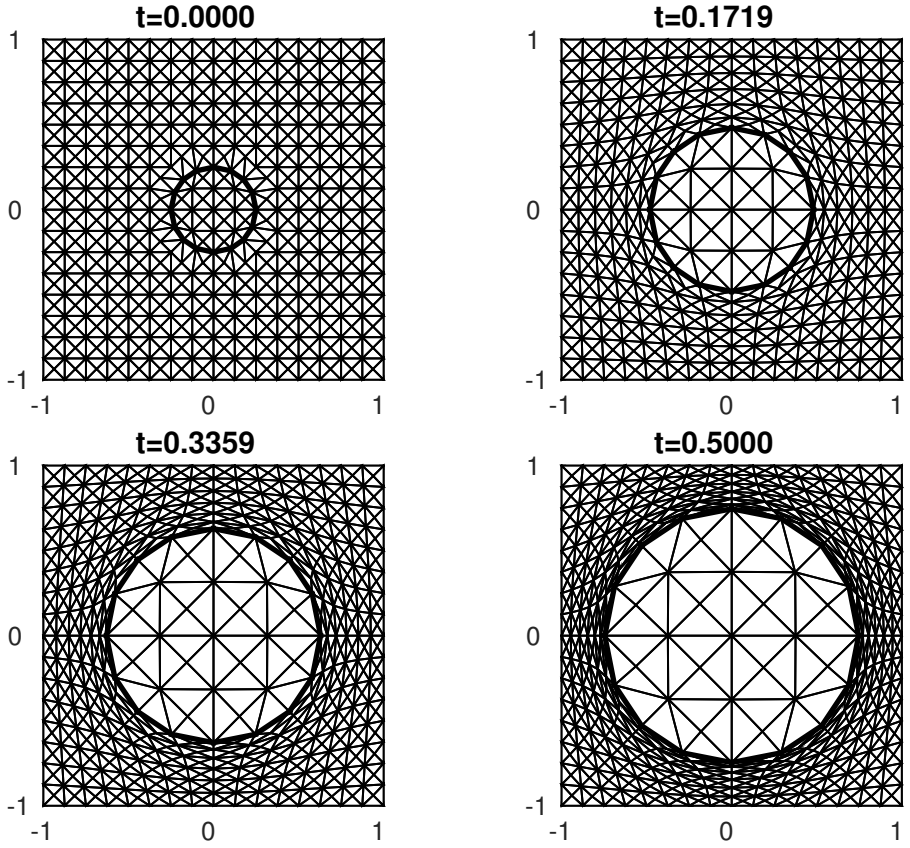

FIGURE 3. Snapshot of mesh for Section 8.1.2 at various time levels when $j = 4$ and $T = 0.5$.

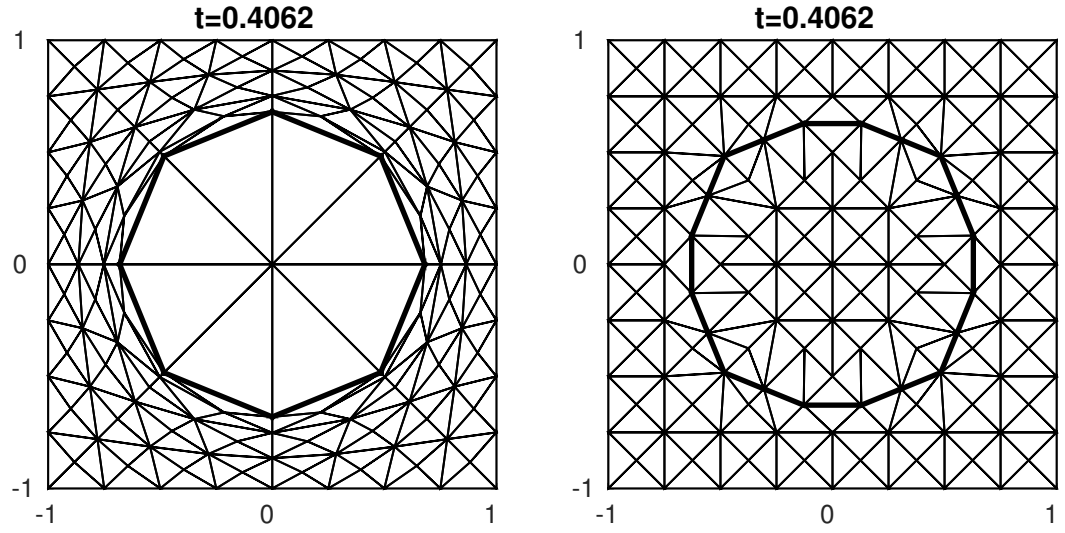

FIGURE 4. Snapshot of mesh for Section 8.1.2 with $j = 3$ immediately before and after a re-mesh.

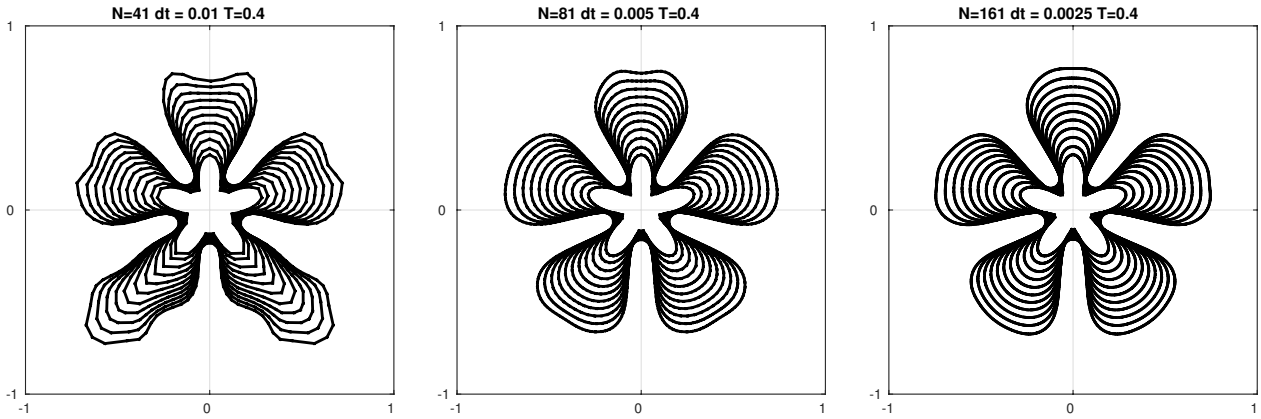

FIGURE 5. Deformation of Γ for Section 8.2.1 for different mesh sizes. Several time-lapses are shown to illustrate the evolution with an initial star shaped interface.

We show the deformation of Γ as well as some snapshots of the mesh (restricted to Ω_s) throughout the simulation. We also show mesh snapshots before and after a re-mesh occurs.

8.2.1. Isotropic surface energy

In this section, we assume the surface tension coefficient $\widehat{\alpha}$ is constant (isotropic). We set $\Omega = (-1,1)^2$ and $T = 0.4$. The interface Γ_0 is "star shaped" and parameterized by

$$x(t) = 0.2 + 0.1\sin(10\pi t)\cos(2\pi t), \qquad y(t) = 0.2 + 0.1\sin(10\pi t)\cos(2\pi t), \qquad 0 \le t \le 1.$$

We run this example with mesh parameter $N = 41, 81, 161$ and $\Delta t = 0.01$. The wall time to compute these simulations ranged from ≈ 30 sec with $N = 41$ to ≈ 20 min with $N = 161$. Note that the initial mesh is *not* pre-warped. For this example, the mesh was regenerated *twice* for all mesh levels. To verify the efficiency of the re-mesh procedure mentioned in Section 7.3, we present the linear system solve time (for one time-step) and the corresponding re-mesh time:

$$\begin{aligned} N = 41: &\quad \text{solve time} \approx 0.08 \text{ seconds}; \quad \text{re-mesh time} \approx 0.02 \text{ seconds}. \\ N = 81: &\quad \text{solve time} \approx 0.80 \text{ seconds}; \quad \text{re-mesh time} \approx 0.06 \text{ seconds}. \\ N = 161: &\quad \text{solve time} \approx 3.50 \text{ seconds}; \quad \text{re-mesh time} \approx 0.25 \text{ seconds}. \end{aligned}$$

Figure 5 shows the overall evolution of the interface.

Figures 6, 7, and 8 show a close-up of the mesh of Ω_s for different mesh sizes.

Figures 9, 10, 11 show the effect of re-meshing on the interface Γ. Again, it is well-captured by the re-meshing procedure.

8.2.2. Anisotropic surface energy

In this section, we consider anisotropic surface energy, *i.e.* we take $\widehat{\alpha} = \widehat{\alpha}(\boldsymbol{\nu}) = \widehat{\alpha}_0 f(\boldsymbol{\nu})$ where

$$f(\boldsymbol{\nu}) := \sum_{j=1}^{J} (\boldsymbol{\nu}^T G_j \boldsymbol{\nu})^{1/2}$$

with $G_j = R_j^T D_j R_j$. The matrices are defined as follows.

- $R_j = R(\theta_j) = \begin{pmatrix} \cos(\theta) & \sin(\theta) \\ -\sin(\theta) & \cos(\theta) \end{pmatrix}$ is a rotation matrix which defines the "direction" of the anisotropy

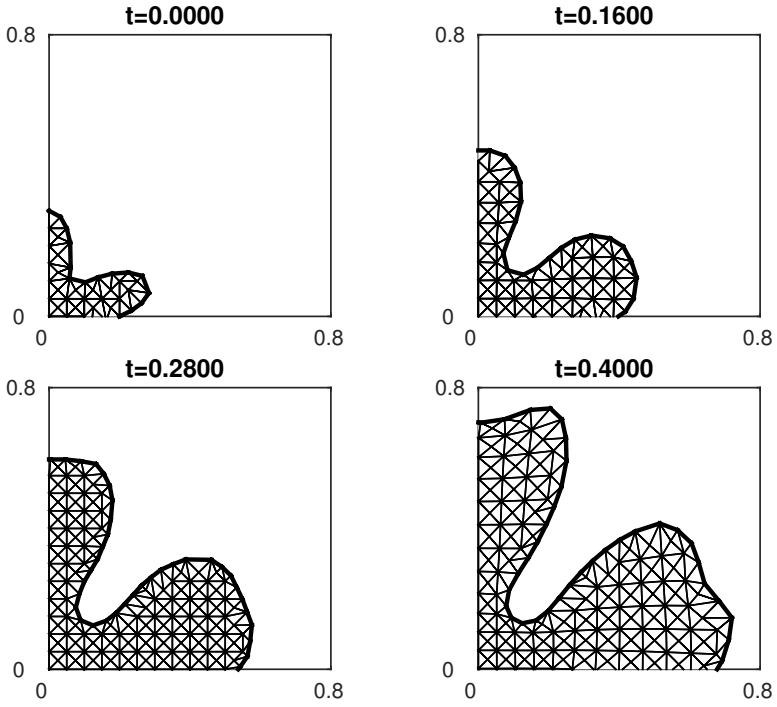

FIGURE 6. Deformation of the mesh for Section 8.2.1 restricted to Ω_s with $N = 41$.

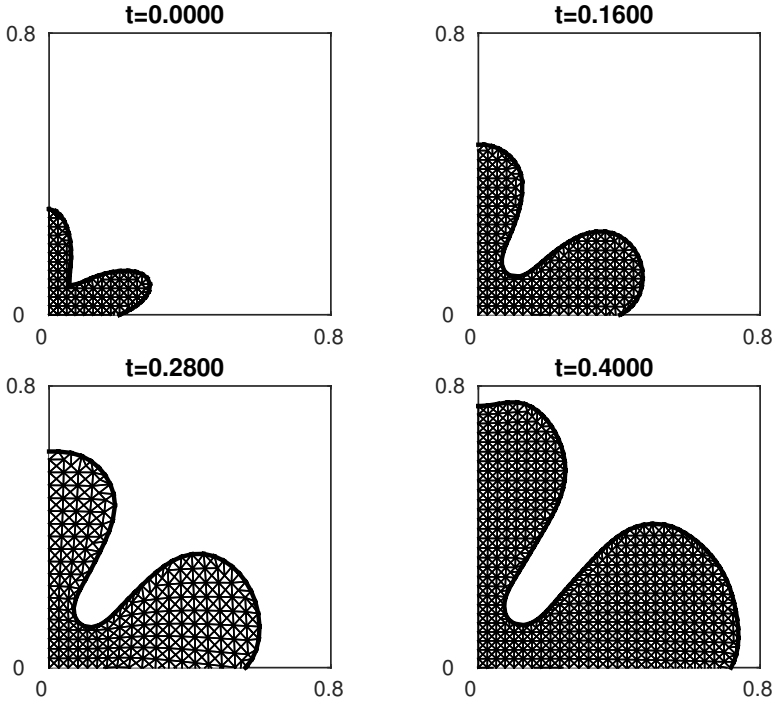

FIGURE 7. Deformation of the mesh for Section 8.2.1 restricted to Ω_s with $N = 81$.

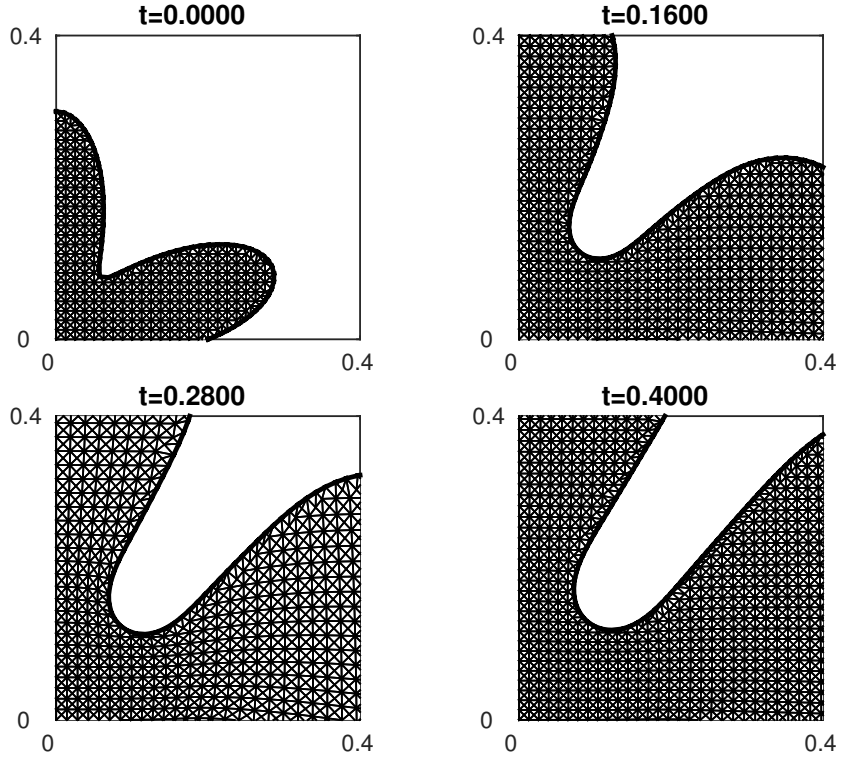

FIGURE 8. Deformation of the mesh for Section 8.2.1 restricted to Ω_s with $N = 161$.

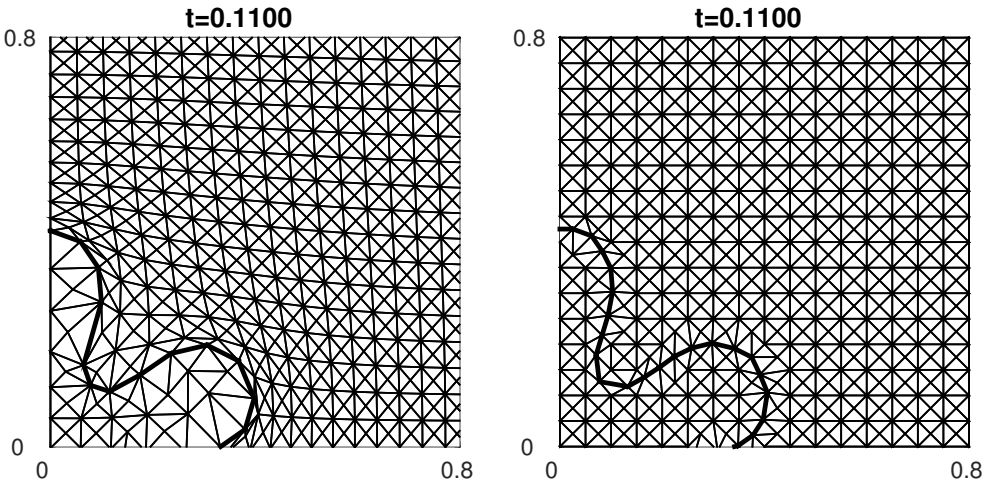

FIGURE 9. Snapshot of mesh for Section 8.2.1 immediately before and after a re-mesh when $N = 41$.

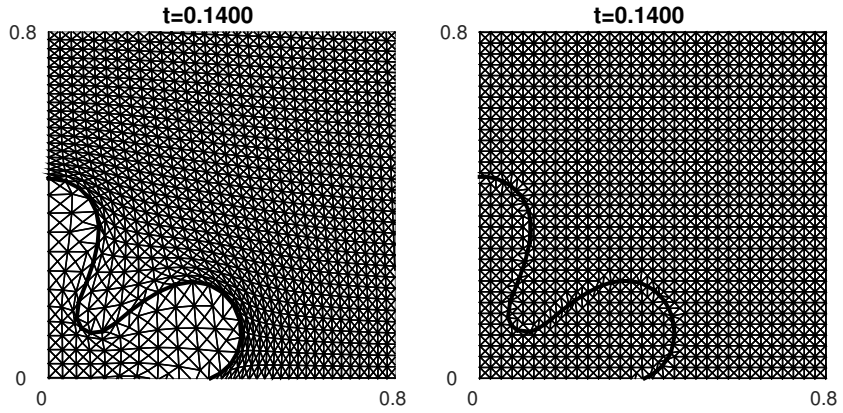

FIGURE 10. Snapshot of mesh for Section 8.2.1 immediately before and after a re-mesh when $N = 81$.

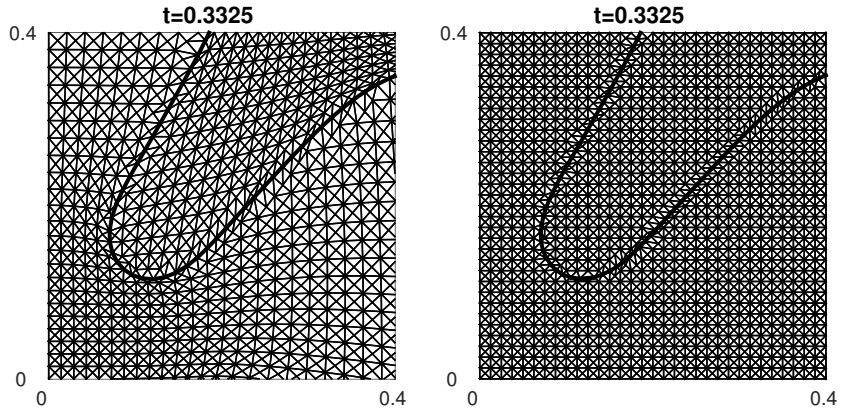

FIGURE 11. Snapshot of mesh for Section 8.2.1 immediately before and after a re-mesh when $N = 161$.

- $G_j = \begin{pmatrix} 1 & 0 \\ 0 & \epsilon_j^2 \end{pmatrix}$ is a diagonal matrix which defines the "strength" of the anisotropy

Implementing anisotropic surface tension is straightforward, as was shown in [16].

For this example, we use the data $J = 3, \theta_j = \dfrac{j\pi}{3}, \epsilon_j = 0.3, 1 \le j \le 3$. We also set $\widehat{\beta} = \widehat{\beta}_0 f(\boldsymbol{\nu})$, $\Omega = (-2, 2)^2$, and $T = 1$. The initial interface Γ^0 is a circle of radius 0.05 centered at the origin. We run this example with mesh parameter $N = 41, 81, 161$ and $\Delta t = 0.025$. The wall time to compute these simulations ranged from $\approx$ 30 sec with $N = 41$ to $\approx$ 20 min with $N = 161$. Note that the initial mesh *is* pre-warped. For this example, the mesh was regenerated *twice* for $N = 41$ and $N = 81$ and *three* times for $N = 161$. Figure 12 shows the overall evolution of the interface.

Figures 13, 14, and 15 show a close-up of the mesh of Ω_s for different mesh sizes.

Figures 16, 17, 18 show the effect of re-meshing on the interface Γ. Again, it is well-captured by the re-meshing procedure.

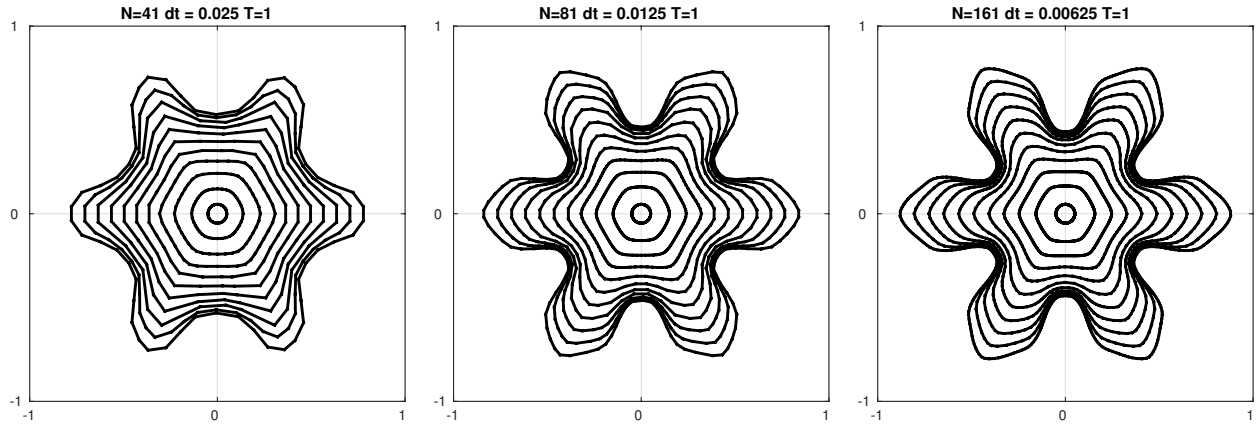

FIGURE 12. Deformation of Γ for Section 8.2.2 for different mesh sizes. Several time-lapses are shown to illustrate the evolution with an initial circular shaped interface. The anisotropic surface tension breaks the initial radial symmetry.

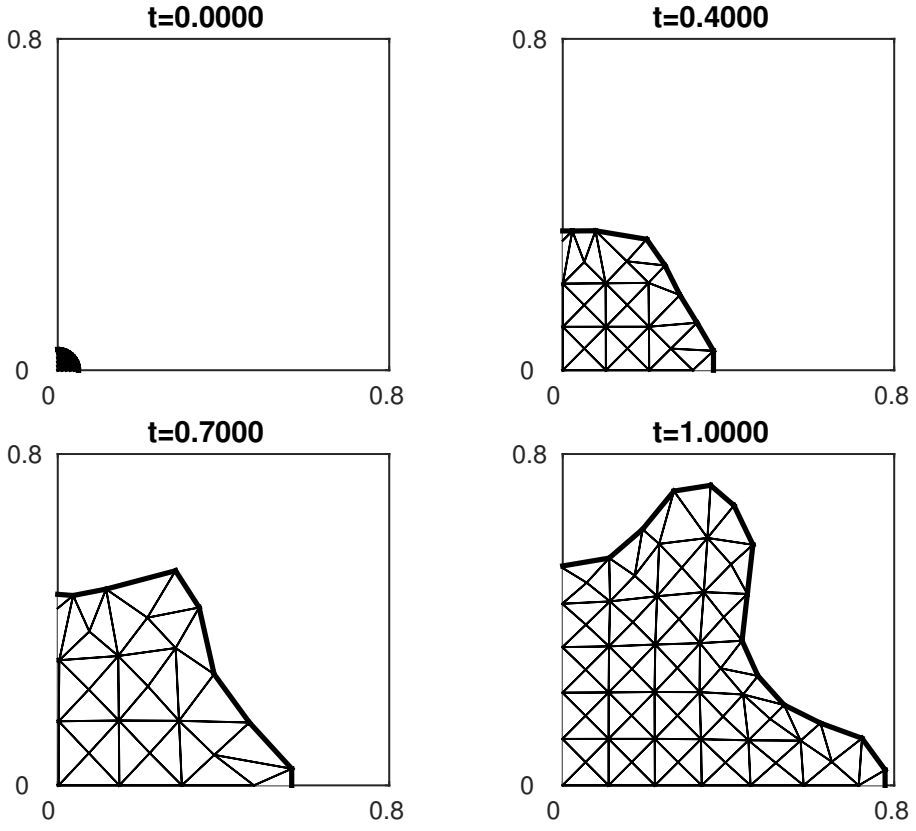

FIGURE 13. Deformation of the mesh for Section 8.2.2 restricted to Ω_s when $N = 41$.

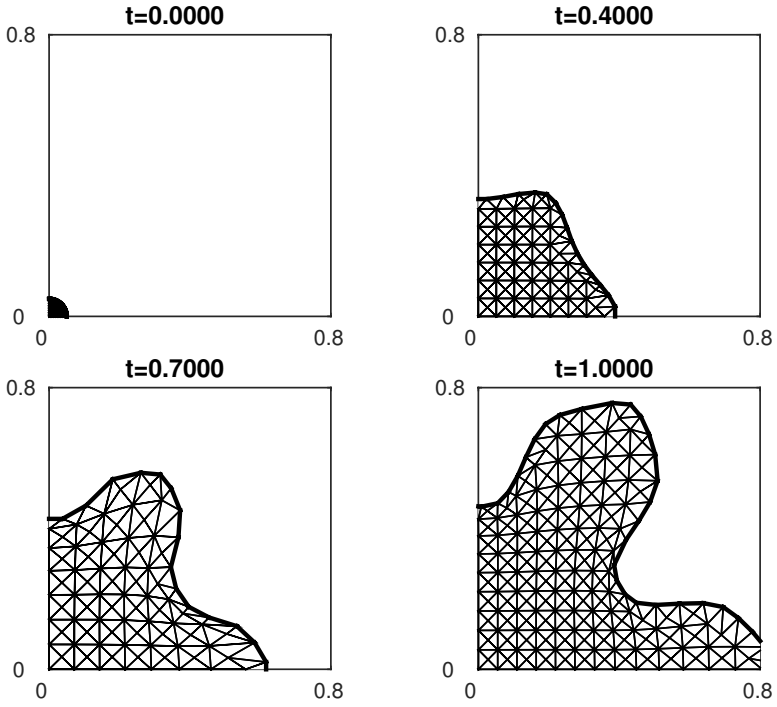

FIGURE 14. Deformation of the mesh for Section 8.2.2 restricted to Ω_s when $N = 81$.

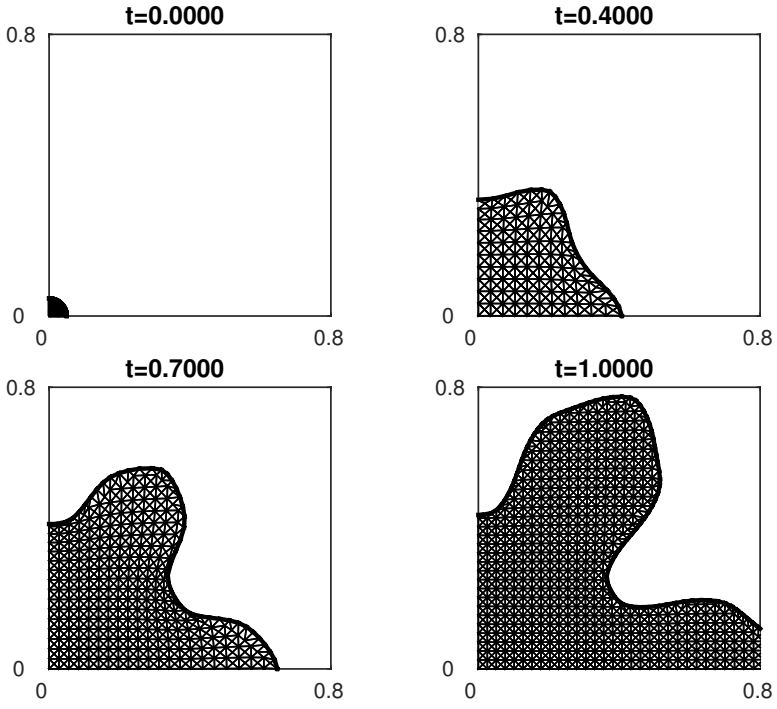

FIGURE 15. Deformation of the mesh for Section 8.2.2 restricted to Ω_s when $N = 161$.

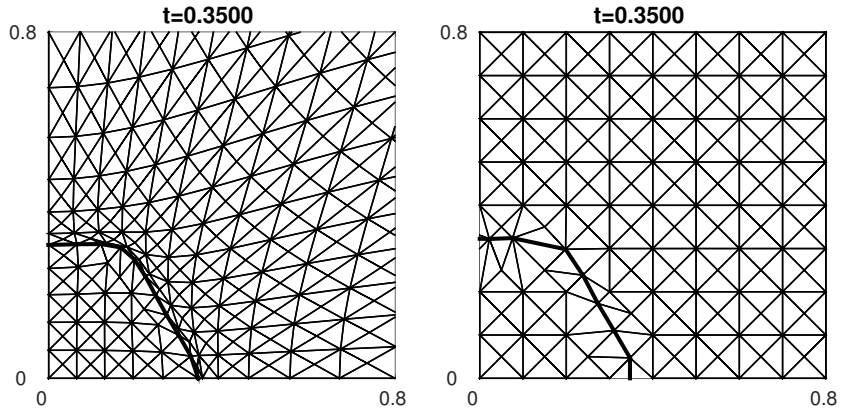

FIGURE 16. Snapshot of mesh for Section 8.2.2 immediately before and after a re-mesh when $N = 41$.

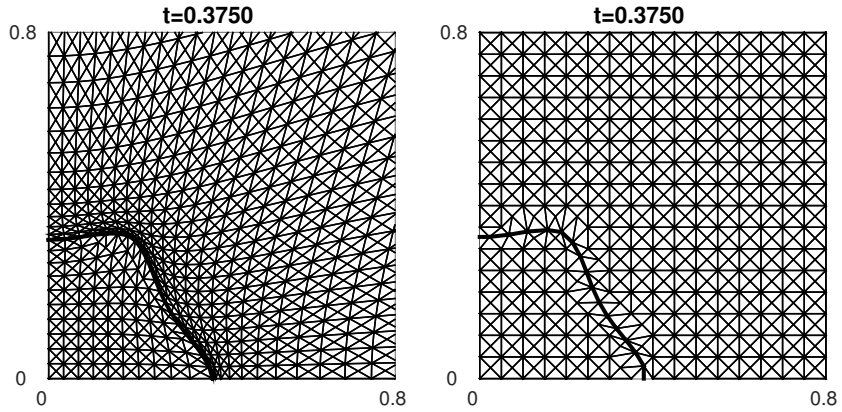

FIGURE 17. Snapshot of mesh for Section 8.2.2 immediately before and after a re-mesh when $N = 81$.

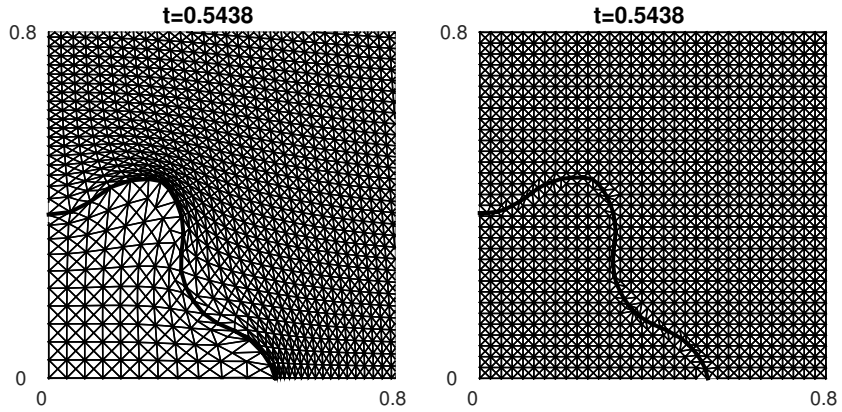

FIGURE 18. Snapshot of mesh for Section 8.2.2 immediately before and after a re-mesh when $N = 161$.

References

[1] R.A. Adams and J.J.F. Fournier, Sobolev Spaces. Vol. 140 of *Pure and Applied Mathematics Series*. Elsevier, 2nd edition (2003).

[2] R. Almgren, Variational algorithms and pattern formation in dendritic solidification. *J. Comput. Phys.* **106** (1993) 337–354.

[3] E. Bänsch, Finite element discretization of the navier-stokes equations with a free capillary surface. *Numer. Math.* **88** (2001) 203–235.

[4] E. Bänsch and K. Deckelnick, Optimal error estimates for the stokes and navier-stokes equations with slip-boundary condition. *ESAIM: M2AN* **33** (1999) 923–938.

[5] E. Bänsch, J. Paul and A. Schmidt, An ale finite element method for a coupled stefan problem and navierstokes equations with free capillary surface. *Int. J. Numer. Methods Fluids* **71** (2013) 1282–1296.

[6] J.W. Barrett, H. Garcke and R. Nürnberg, On stable parametric finite element methods for the stefan problem and the mullins-sekerka problem with applications to dendritic growth. *J. Comput. Phys.* **229** (2010) 6270–6299.

[7] W.J. Boettinger, J.A. Warren, C. Beckermann and A. Karma, Phase-field simulation of solidification. *Annu. Rev. Mat. Res.* **32** (2002) 163–194.

[8] D. Boffi, F. Brezzi and M. Fortin, Mixed Finite Element Methods and Applications. Vol. 44 of *Springer Series in Computational Mathematics*. Springer-Verlag, New York, NY (2013).

[9] D. Boffi and L. Gastaldi, Analysis of finite element approximation of evolution problems in mixed form. *SIAM J. Numer. Anal.* **42** (2005) 1502–1526.

[10] D. Braess, Finite Elements: Theory, Fast Solvers, and Applications in Solid Mechanics. Cambridge University Press, 2nd edition (2001).

[11] S.C. Brenner and L.R. Scott, The Mathematical Theory of Finite Element Methods, vol. 15 of *Texts in Applied Mathematics*. Springer, New York, NY, 3rd edition (2008).

[12] F. Brezzi and M. Fortin, Mixed and Hybrid Finite Element Methods. Springer Verlag, New York, NY (1991).

[13] S. Chen, B. Merriman, S. Osher and P. Smereka, A simple level set method for solving stefan problems. *J. Comput. Phys.* **135** (1997) 8–29.

[14] X. Chen and F. Reitich, Local existence and uniqueness of solutions of the stefan problem with surface tension and kinetic undercooling. *J. Math. Anal. Appl.* **164** (1992) 350–362.

[15] C.H.A. Cheng, D. Coutand and S. Shkoller, Navier-stokes equations interacting with a nonlinear elastic biofluid shell. *SIAM J. Math. Anal.* **39** (2007) 742–800.

[16] C.B. Davis and S.W. Walker, A mixed formulation of the Stefan problem with surface tension. *Int. Free Bound.* **17** (2015) 427–464.

[17] S.H. Davis, Theory of Solidification. Cambridge Monographs on Mechanics. Cambridge University Press (2001).

[18] M.C. Delfour and J.-P. Zolésio, Shapes and Geometries: Analysis, Differential Calculus, and Optimization, volume 4 of *Advances in Design and Control*. SIAM, 2nd edition (2011).

[19] M.P. do Carmo, *Differential Geometry of Curves and Surfaces*. Prentice Hall, Upper Saddle River, New Jersey (1976).

[20] R.R. Duchon, Jean, Évolution d'une interface par capillarité et diffusion de volume. I. Existence locale en temps. *Ann. Inst. Henri Poincaré, (C) Anal. Non Lin.* **1** (1984) 361–378.

[21] G. Dziuk, An algorithm for evolutionary surfaces. *Numer. Math.* **58** (1990) 603–611.

[22] G. Dziuk and C.M. Elliott, Finite element methods for surface pdes. *Acta Numer.* **22** (2013) 289–396.

[23] J. Escher, G. Simonett, N. Alikakos and P. Bates. Classical solutions for hele-shaw models with surface tension. *Adv. Differ. Equ.* **2** (1997) 619–642.

[24] R.S. Falk and S.W. Walker, A mixed finite element method for EWOD that directly computes the position of the moving interface. *SIAM J. Numer. Anal.* **51** (2013) 1016–1040.

[25] M. Fried, A level set based finite element algorithm for the simulation of dendritic growth. *Comput. Vis. Sci.* **7** (2004) 97–110.

[26] A. Friedman and F. Reitich, The Stephan problem with small surface tension. *Trans. Amer. Math. Soc.* **328** (1991) 465–515.

[27] H. Garcke and S. Schaubeck, Existence of weak solutions for the Stephan problem with anisotropic Gibbs–Thomson law. *Adv. Math. Sci. Appl.* **21** (2011) 255–283.

[28] G.N. Gatica, A Simple Introduction to the Mixed Finite Element Method: Theory and Applications. *SpringerBriefs in Mathematics*. Springer (2014).

[29] G.N. Gatica, R. Oyarzúa and F.-J. Sayas, Analysis of fully-mixed finite element methods for the stokes-darcy coupled problem. *Math. Comput.* **80** (2011) 1911–1948.

[30] J.-F. Gerbeau and T. Lelièvre, Generalized navier boundary condition and geometric conservation law for surface tension. *Comput. Methods Appl. Mechanics Eng.* **198** (2009) 644–656.

[31] J.-F. Gerbeau, T. Lelièvre and C.L. Bris, Simulations of MHD flows with moving interfaces. *J. Comput. Phys.* **184** (2003) 163–191.

[32] M.E. Gurtin, Multiphase thermomechanics with interfacial structure 1. heat conduction and the capillary balance law. *Arch. Ration. Mech. Anal.* **104** (1988) 195–221.

[33] M.E. Gurtin, Thermomechanics of Evolving Phase Boundaries in the Plane. *Oxford Mathematical Monographs*. Oxford Science Publication (1993).

[34] G.A. Holzapfel, Nonlinear Solid Mechanics: A Continuum Approach For Engineering. John Wiley and Sons, Inc. (2000).

[35] D. Juric and G. Tryggvason, A front-tracking method for dendritic solidification. *J. Comput. Phys.* **123** (1996) 127 – 148.
[36] R. Kobayashi, A numerical approach to three-dimensional dendritic solidification. *Exp. Math.* **3** (1994) 59–81.
[37] C. Kraus, The degenerate and non-degenerate stefan problem with inhomogeneous and anisotropic gibbsthomson law. *Eur. J. Appl. Math.* **22** (2011) 393–422.
[38] E. Kreyszig, Differential Geometry. Dover (1991).
[39] J.S. Langer, Instabilities and pattern formation in crystal growth. *Rev. Mod. Phys.* **52** (1980) 1–28.
[40] M. Lenoir, Optimal isoparametric finite elements and error estimates for domains involving curved boundaries. *SIAM J. Numer. Anal.* **23** (1986) 562–580.
[41] S. Luckhaus, Solutions for the two-phase stefan problem with the gibbs-thomson law for the melting temperature. In Fundamental Contributions to the Continuum Theory of Evolving Phase Interfaces in Solids, edited by J.M. Ball, D. Kinderlehrer, P. Podio-Guidugli and M. Slemrod. Springer Berlin Heidelberg, (1999) 317–327.
[42] S. Luckhaus and T. Sturzenhecker, Implicit time discretization for the mean curvature flow equation. *Cal. Var. Partial Differ. Equ.* **3** (1995) 253–271.
[43] A. Márquez, S. Meddahi and F.-J. Sayas, Strong coupling of finite element methods for the stokes-darcy problem. *IMA J. Numer. Anal.* **35** (2014) 969–988.
[44] W.W. Mullins and R.F. Sekerka, Morphological stability of a particle growing by diffusion or heat flow. *J. Appl. Phys.* **34** (1963) 323–329.
[45] W. W. Mullins and R.F. Sekerka, Stability of a planar interface during solidification of a dilute binary alloy. *J. Appl. Phys.* **35** (1964) 444–451.
[46] S. Osher and R. Fedkiw, Level Set Methods and Dynamic Implicit Surfaces. Springer-Verlag, New York, NY (2003).
[47] J. Prüss, J. Saal and G. Simonett, Existence of analytic solutions for the classical stefan problem. *Math. Ann.* **338** (2007) 703–755.
[48] J. Prüss and G. Simonett, Stability of equilibria for the stefan problem with surface tension. *SIAM J. Math. Anal.* **40** (2008) 675–698.
[49] J. Prüss, G. Simonett and M. Wilke, On thermodynamically consistent stefan problems with variable surface energy. *Arch. Ration. Mech. Anal.* **220** (2016) 603–638.
[50] J. Prüss, G. Simonett and R. Zacher, Qualitative behavior of solutions for thermodynamically consistent stefan problems with surface tension. *Arch. Ration. Mech. Anal.* **207** (2013) 611–667.
[51] M. Röger, Existence of weak solutions for the mullins–sekerka flow. *SIAM J. Math. Anal.* **37** (2005) 291–301.
[52] A.R. Roosen and J.E. Taylor, Modeling crystal growth in a diffusion field using fully faceted interfaces. *J. Comput. Phys.* **114** (1994) 113–128.
[53] A. Schmidt, Computation of three dimensional dendrites with finite elements. *J. Comput. Phys.* **125** (1996) 293–312.
[54] A. Schmidt, Approximation of crystalline dendrite growth in two space dimensions. *Acta Math. Univ. Comenianae* **67** (1998) 57–68.
[55] A. Schmidt and K.G. Siebert, Design of Adaptive Finite Element Software: The Finite Element Toolbox ALBERTA. Springer, Heidelberg, Germany (2005).
[56] S.A. Sethian, Level Set Methods and Fast Marching Methods, 2nd Edition. Cambridge University Press, New York, NY (1999).
[57] I. Singer-Loginova and H.M. Singer, The phase field technique for modeling multiphase materials. *Rep. Progress Phys.* **71** (2008) 106–501.
[58] L. Tartar, An Introduction to Sobolev Spaces and Interpolation Spaces. Vol. 3 of *Lecture Notes of the Unione Matematica Italiana*. Springer (2007).
[59] R.M. Temam and A.M. Miranville, Mathematical Modeling in Continuum Mechanics. Cambridge University Press, 2nd edition (2005).
[60] A. Visintin, Models of Phase Transitions, vol. 28 of *Progress in Nonlinear Differential Equations*. Birkhäuser, Boston (1996).
[61] V.V. Voronkov, Conditions for formation of mosaic structure on a crystallization front. *Sov. Phys. Solid State* **6** (1965) 2378–2381.
[62] S.W. Walker, FELICITY: Finite ELement Implementation and Computational Interface Tool for You. Available at http://www.mathworks.com/matlabcentral/fileexchange/31141-felicity.
[63] S.W. Walker, *Modeling, Simulating and Controlling the Fluid Dynamics of Electro-Wetting On Dielectric*. Ph.D. thesis, University of Maryland, College Park (2007).
[64] S.W. Walker, Tetrahedralization of isosurfaces with guaranteed-quality by edge rearrangement (TIGER). *SIAM J. Sci. Comput.* **35** (2013) A294–A326.
[65] S.W. Walker, The Shapes of Things: A Practical Guide to Differential Geometry and the Shape Derivative. Vol. 28 of *Advances in Design and Control*. 1st edition. SIAM (2015).
[66] S.W. Walker, FELICITY: A matlab/c++ toolbox for developing finite element methods and simulation modeling. (2017).
[67] S.W. Walker, A. Bonito and R.H. Nochetto, Mixed finite element method for electrowetting on dielectric with contact line pinning. *Int. Free Bound.* **12** (2010) 85–119.